Deep Resources Engineering 2 (2025) 100219

Contents lists available at ScienceDirect

Deep Resources Engineering

journal homepage: www.keaipublishing.com/en/journals/deepre/

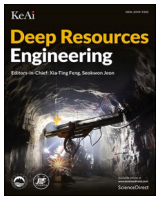

Review

A review of the geological characterization, classification, modeling, and case studies of anisotropic rock masses

Ebrahim Ghorbani [a], Marjan Shahinfar [b], Abbas Taheri [b,*]

[a] Department of Built Environment, Oslo Metropolitan University (OsloMet), Oslo 0166, Norway
[b] The Robert M. Buchan Department of Mining, Queen's University, Kingston K7L3N6, Canada

ARTICLE INFO

Keywords:
Rock mass
Anisotropic rock mass
Rock mass classification
Rock engineering
Underground mining
Deep mining

ABSTRACT

Rock anisotropy caused by inherent structures like bedding, foliation, and micro-fractures directly influences strength, deformability, and stress distribution variations. These directional changes can affect the stability of rock engineering practices, such as underground openings and slopes, and dealing with the anisotropic rock masses (ARMs) is one of the significant challenges. The commonly used conventional classifications are solely based on the isotropic behavior of rock masses and are unsuitable for anisotropic ones. Despite the limitations of these classifications, engineers tend to oversimplify the situation and characterize or design the ARMs, ignoring the impact of anisotropy. This study presents a summary of geological conditions, mechanical behavior, and classification systems of ARMs, as well as a review of numerical modeling techniques that may be applicable in the design phase within such medium. ARM Rating (ARMR), or any other type of alternative classification system that considers the directions in which rocks act instead of just their strength levels, can facilitate improved feasibility analysis for complex geological conditions and supporting systems design in ARMs. Moreover, the failure criteria considering the anisotropic behavior reflect the nonlinear development with long-term dependence on rock strength. Such criteria may be applied to numerical methods, such as the discrete element method (DEM), which offers more or less realistic simulations of ARMs' responses. Nevertheless, establishing standard procedures for the characterization, classification, and design of ARMs, especially in deep underground anisotropic conditions, is in high demand.

1. Introduction

"Rock mass" is a term used for a collection of rock blocks and fragments of varying sizes. The definition considers unaltered and altered material within the rock mass [1–3]. The anisotropy of rock is the directional variability of rocks' physical and mechanical properties due to structural features such as bedding planes, foliation, or fracture alignment [4,5]. Structural features such as mineral alignment and microcrack orientation govern the anisotropy of rocks. Fig. 1 shows the formation of anisotropic-based weakness due to bedding. The planes of weakness reduce the integrity of the rock masses, increasing deformability, porosity, and permeability, especially along the planes. This leads to the rock mass behaving anisotropic [6].

The rock mass consists of intact rock material, discontinuities, weathering zones, and typically filled cavities that may possess anisotropic properties [8,9]. Most rock masses are anisotropic in their strength, deformability, and permeability properties. For discontinuities, while igneous rocks are not prone to strongly directional weaknesses, a weak orientation may exist in some cases, such as granite quarrying [10]. Anisotropic deformation of foliated rock masses under high-stress conditions causes critical engineering issues and has drawn extensive attention globally [11–16].

The foliation causes mechanical anisotropy, and hanging-wall and footwall foliation shear generates up to 30 % - 50 % closure in foliated, high-stress conditions [17]. Researchers have determined that the relative direction of foliation is among the most significant parameters influencing underground structure behavior. Experimental and numerical studies have demonstrated that the dip angle of the layered surrounding rock is crucial in deformation patterns, provided that the dip direction is specified [18–21]. It was revealed that anisotropic deformation in tunnels might cause severe initial support damage, including steel set distortion, spraying concrete cracking, and load-bearing

Peer review under responsibility of Editorial Board of of Deep Resources Engineering.
* Corresponding author.
E-mail addresses: ebrahim.ghorbani@oslomet.no (E. Ghorbani), marjan.shahinfar@queensu.ca (M. Shahinfar), abbas.taheri@queensu.ca (A. Taheri).

https://doi.org/10.1016/j.deepre.2025.100219
Received 15 July 2025; Received in revised form 18 September 2025; Accepted 25 September 2025
Available online 31 October 2025

Nomenclature

3DEC	3D distinct element code
ARMR	Anisotropic rock mass rating
A-BQ	Anisotropic-basic quality
BTS	Brazilian tensile strength
CSMR	Chinese system for rock mass strength
CMRR	Coal mine roof rating
CPA	Critical plane approach
DRMR	Directional rock mass rating
DDA	Discontinuous deformation analysis
DEM	Discrete element method
DFN	Discrete fracture network
EDEM	Expanded DEM
FLAC	Fast lagrangian analysis of continua
FDM	Finite difference method
FEM	Finite element method
GSI	Geological strength index
GBI	Geotechnical blockiness index
GBM	Grain-based model
FDEM	Finite-discrete element method
IRMR	In situ rock mass rating
I-System	Index of ground-structure
MQD	Marble quality designation
MRMR	Mining rock mass rating
MSMR	Modified slope mass rating
M-RMR	Modified rock mass rating
N	Rock mass number
PFC	Particle flow code
PGR	Pegmatitic granite
RFPA	Realistic failure process analysis
RBSN	Rigid-body-spring network
RFDF	Rock fracture dynamics facility
RMCS	Rock mass classification systems
RMi	Rock mass index
Q-System	Rock mass quality
RMQR	Rock mass quality rating
RMR	Rock mass rating

capacity loss, thus leading to deviations in surrounding rock classification [22].

The deformation anisotropy of rock has been studied based on several testing techniques. As shown in Fig. 2, several tests may be conducted on specimens sampled at different orientations to determine the anisotropic properties [23]. The multiple tests are both costly and time-consuming. Also, these methods cannot uniquely determine the directions of anisotropy because such a direction has to be assumed from prior visual observation of the specimens [24]. Isotropic modeling of tunneling and slope stability projects results in inadequate stress distribution and stability prediction, which contributes to unexpected failures or unjustified deformations in layered and fractured rocks [25]. For instance, in borehole stability analysis, isotropic stress models underestimate failure pressures, especially in deep engineering conditions where anisotropic behaviors dominate the stress response and deformation mechanisms [26]. In addition, the assumption of isotropic rock mass behavior cannot reflect strength differences in different directions, giving rise to errors in the excavation support design or fracture extension analysis [27]. These limitations necessitate introducing anisotropic rock properties into engineering design to enhance safety, precision, and efficiency in tunnel, slope, and deep mining excavation engineering [28].

Rockburst incidents in tunnels have occurred in numerous countries, mirroring the existence of many various concepts of the term "rockbursting." Various rockbursting mechanisms have been recognized with a definite distinction between source and damage mechanisms. Fig. 3 illustrates four failure mechanisms common in rock masses during the excavation or tunneling process: strainburst, buckling, ejection, and collapsed arch formation [29]. Fig. 3a shows a strainburst, the sudden failure leading to sharp-edged thin plates which ejected violently and locally from the opening rock surface. Fig. 3b points out buckling, where compressive stresses induce bending and eventual failure of the thin columns of rock. Fig. 3c depicts ejection, where pieces of rock are violently ejected from the tunnel surface at high-stress differentials. Finally, Fig. 3d shows a collapsed arch that results from a failure in the surrounding rock mass, which creates arch instability due to the activity of bedding planes and shear zones. These processes emphasize the need to carefully consider anisotropic mechanical properties and geological characteristics in tunnel and support system design [29].

Fig. 1. A sequence of sedimentary rock layers [7].

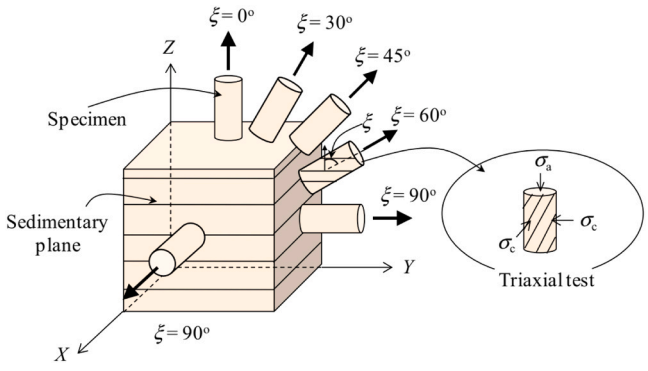

Fig. 2. Conventional method for determining parameters of anisotropic rocks from multiple tests on specimens sampled at different orientations [23].

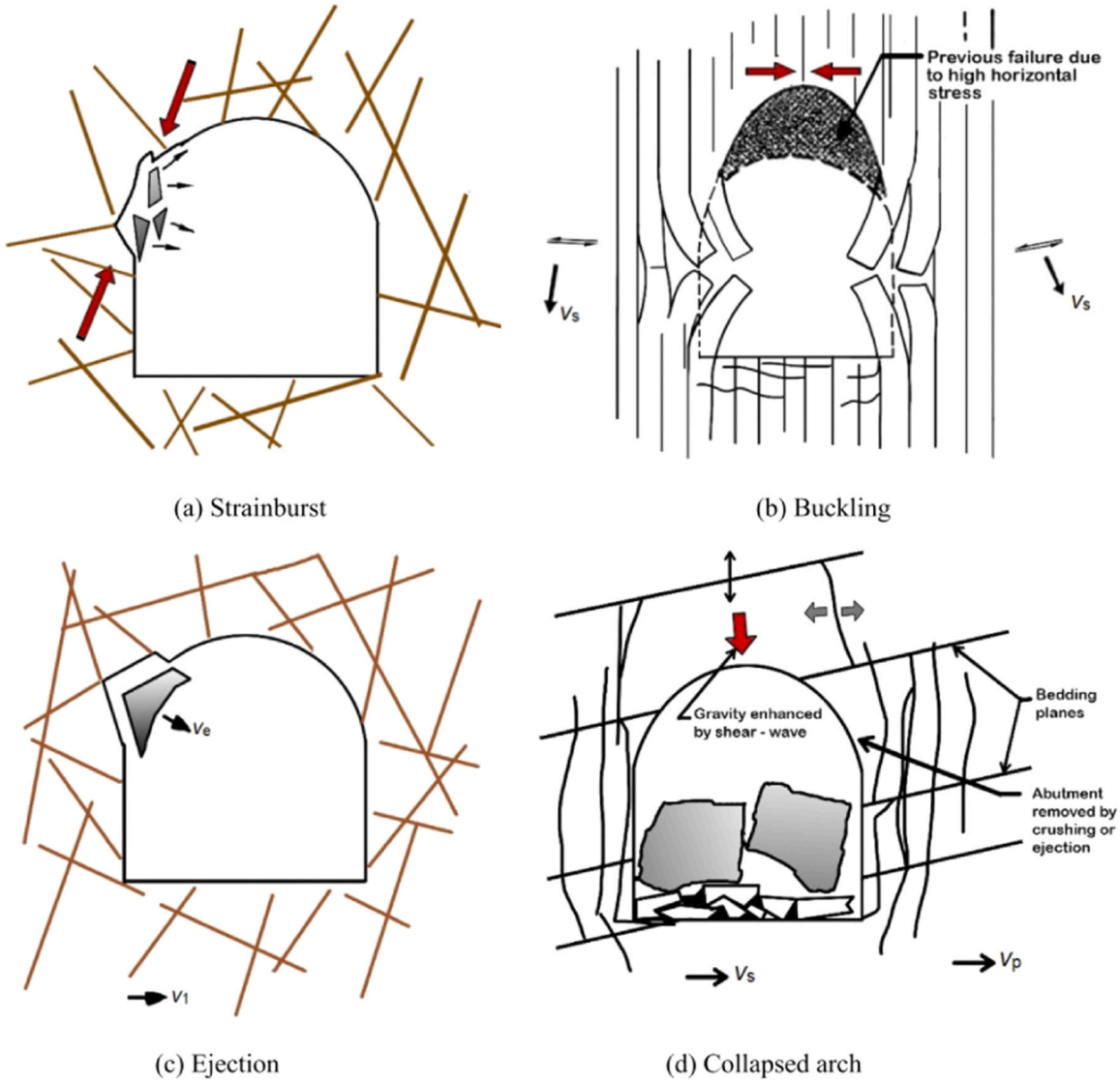

Fig. 3. Failure types in underground openings [29].

Rock physics models are essential for making more refined predictions of stress-dependent elastic moduli and for estimating horizontal stress. For this purpose, an anisotropy template was created to test the elastic modulus changes induced by stress and examine the texture of rocks. The template, which relies on effective medium models of compliant and stiff layers, crack inclusions, and intrinsic and extrinsic anisotropic constituents, enables the examination of stress-dependent stiffness changes. Fig. 4 shows a schematic view of various rock fabrics and their effect on a cross plot of bedding-parallel (C‖) and bedding-perpendicular (C⊥) stiffnesses. The elastic stiffness in each direction is calculated as $C_{XX} = \rho \times V_{XX}$, where ρ is density, V is the wave velocity (P or S), and XX represents ‖ and ⊥ directions. Thomsen anisotropy parameters ε and γ are used to quantify anisotropy in a transversely isotropic medium. In isotropic rocks, the mineral composition and porosity changes control the stiffness along a diagonal direction termed the isotropy line. In contrast, in anisotropic rocks, the mechanical stiffness displays the difference between the two principal directions such that the stiffness measured along the parallel direction is larger than that measured in the perpendicular direction (C‖ > C⊥). Consequently, data points relating to stiffness depart from the isotropy line [30]. Structural features such as fine-scale layering, mineral orientation, and micro-crack orientation induce anisotropic properties in sedimentary, metamorphic, and crystalline rocks [31]. Strength directional dependency can lead to rock stability anisotropy, which is significant in underground structure design or in-situ stress condition assessment [5]. This review paper addresses key aspects of anisotropic rock masses, including geological characteristics, mechanical behavior, characterization, classification systems, design and numerical simulation, and case studies.

This paper attempted to summarize, assess, and review almost 300 publications related to the research and studies of anisotropic rock masses from the early 1950s to the present. The review consisted of the different sections, including geological characteristics (2), laboratory-scale mechanical behavior (3), classification and characterization (4), numerical simulation and design (5), a few case studies (6), and finally reading to the conclusion (7).

2. Geological characteristics of anisotropic rock masses

Anisotropic behavior can be intensity-controlled by flaky and elongated minerals like mica, chlorite, and amphiboles, which influence rock behavior noticeably even at the laboratory scale [32,33]. Understanding the geological environment is crucial when designing an infrastructure project. Most project designs attempt to save on cost and time, and drift towards focusing on borehole investigations without fully considering the general geological history [34]. However, the geological

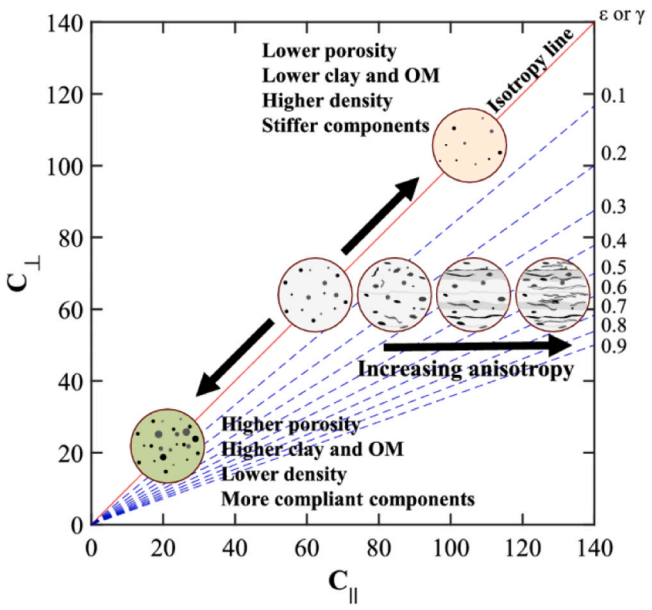

Fig. 4. Schematic rock samples with various features and their respective locations in the elastic stiffness cross plot. The red line marks the isotropy line, while the dashed lines mark increasing amounts of anisotropy [30].

environment controls rock mechanics, and factors such as tectonic stresses, metamorphic histories, and erosion histories profoundly affect rock mass behavior. The rock mass is regulated by the planes of weakness and intact rock, along with geological structures like faults, karst, and saturated zones, which influence its stability. Scanline surveys are based empirically on the accumulation of field rock data and constitute one of the fundamental components of rock-mass quality rating [35,36]. Fig. 5 illustrates various geological features of anisotropic rock masses.

2.1. Metamorphic rocks

Metamorphic rocks result from the alteration or recrystallization of pre-existing igneous, sedimentary, and metamorphic rocks (called protoliths) in response to changes in physical and chemical conditions, the main drivers being temperature, pressure, and the introduction of chemically reactive fluids and gases [41–43]. Metamorphism alters the mineral composition, including the formation of new minerals (garnet, zoisite, kyanite, chlorite, biotite, sericite, staurolite, sillimanite, talc, and andalusite). Temperature sources are the geothermal gradient, the effect of magmatic intrusions, and friction in rock masses of tectonic movements following prograde or retrograde mechanisms. The weight of sediments or crust causes pressure. Typical textures are crystalline, granular, xenoblastic, idioblastic, granoblastic, and porphyroblastic. Structures include gneissic, schistose, and slaty [42,44].

Most foliated metamorphic rocks, such as schist, slate, gneiss, and phyllite, exhibit natural orientations in their flat or elongated minerals or contain a banding phenomenon, resulting in anisotropic mechanical properties. The temperature and pressure conditions contribute to developing preferred orientations of crystalline minerals and platy micas [45]. Evidence of microstructures in micas and related layer-silicates, associated with processes such as dislocation glide, kinking, diffusion-assisted recovery, and dynamic recrystallization, is commonly found in foliated rocks deformed at various crustal depths [46–50]. For example, Fig. 6 illustrates two examples of anisotropic features in metamorphic rock. Fig. 6a depicts a field image of the shear zone in marble, highlighting alternating bands and the marked positions of the oriented samples for analysis [51], and Fig. 6b shows a metamorphic folded rock. Nearly 1.1 billion years ago, layers of sedimentary rock were put under tremendous heat and pressure during the emergence of the Grenville Mountains, Canada. Today, differential weathering of the softer marble and harder silicate-rich layers has further emphasized the folding that formed during that mountain building. Fig. 7 illustrates texture anisotropy in a metamorphic slate, highlighting the layering and intersecting planar fabric [52]. As low-grade metamorphic rocks, slates exhibit extreme anisotropy due to the alignment of phyllosilicate minerals like mica and chlorite, influenced by tectonic stresses (Fig. 7) [53]. This anisotropy also affects the elastic properties of rocks and seismic wave behavior [54].

The classification of metamorphic rocks begins with determining the presence of foliation; if present, its type aids in identification, while non-foliated rocks are classified by their physical properties. The rock's mineral composition influences foliation, and diagrams are often used to illustrate the relationships between foliation types, protoliths, and rock names [55]. It is essential to return to geological fundamentals to understand anisotropy characteristics. Fig. 8 provides a schematic for developing metamorphic rock types and associated fabric evolution.

2.2. Sedimentary rocks

Stratified sedimentary rocks, such as mudstones, siltstones, sandstones, and limestones, are anisotropic due to bedding planes. Anisotropy stems from sedimentation processes where strata or minerals of varying grain sizes are deposited [52]. Fissility, a widespread phenomenon in sedimentary rocks, refers to settling grains in parallel planes, and the rock splits along the planes [56]. Sedimentary anisotropy is typical in siltstones, claystones, and mudstones. Sandstones and some limestones are also slightly anisotropic due to the presence of bedding planes [57–62]. Fig. 9a [63] and Fig. 9b [64] show some examples of anisotropy in sedimentary rock masses. Fig. 9c illustrates the detailed geological characteristics of the Nakatsu formation at a test site. The cavern, located at a depth of GL-50 m, lies entirely within this formation, which consists of mudstone interspersed with sand layers of varying thickness (0.5–15 cm). These sand layers are composed of fine to medium sand and scoria particles (1–5 mm) that are insufficiently cemented. Such features significantly influence the mechanical properties of the rock mass. Additionally, the figure highlights the presence of thin, discontinuous layers of carbonaceous material or tuffaceous mudstone within the formation [65]. Fig. 10 shows the structural and mineral orientation of various layers of siltstones (the parallel orientation of detrital phyllosilicates and siderite minerals). Together, these figures emphasize the role of bedding, laminations, and mineral alignment in producing anisotropic behaviors in sedimentary rocks [66].

2.3. Igneous rocks

Igneous rocks can also be anisotropic due to flow structures, including porous rhyolites, which may develop anisotropic features due to weathering [67]. While igneous rocks generally have minimal fabric anisotropy, some exceptions are present. In some instances, anisotropy is observed because of layering due to the flow of lava as highly viscous masses before final solidification, for example, in rocks such as granite [68]. Studies suggest that weathering affects different orientations of rock structures unevenly, causing variations in compressive strength based on the direction of applied stress [67,69,70]. In igneous rocks, the anisotropy of magnetic susceptibility relies on the magnetite grains' irregular shape and magnetic interactions between them. These grains routinely crystallize after magma flow, and the flow-oriented silicate framework provides a preferred direction to the grains, promoting anisotropy [51,70,71]. Fig. 11 highlights the anisotropic and heterogeneous characteristics of the rock mass at the ONKALO site, emphasizing its structural variability and orientation-dependent features. The insets offer a detailed view of laboratory specimens ($8 \times 8 \times 8$ cm^3) assessed under true-triaxial stress conditions at the Rock Fracture Dynamics Facility (RFDF) at the University of Toronto. They include pegmatitic granite (PGR) and veined gneiss (VGN) samples, which, to some degree,

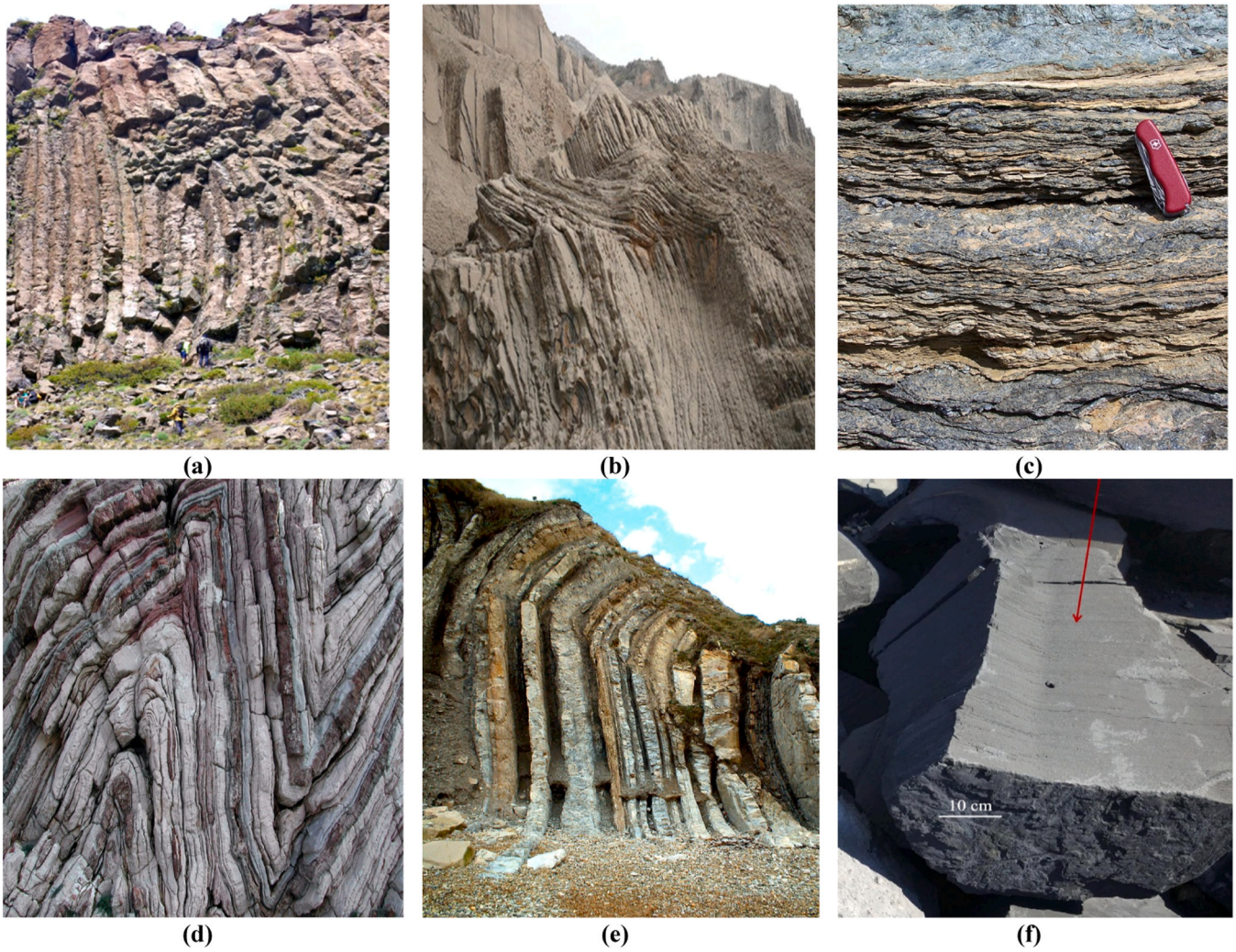

Fig. 5. Various geological features of anisotropic rock masses: (a) columnar jointed [37]; (b) bedding [7]; (c) foliated texture in mica-schist formation [38]; (d) limestone and chert layers [38]; (e) vertical limestone bedding [39]; and (f) shale outcrops with visible bedding planes [40].

capture the anisotropic and heterogeneous features of the field scale and controlled laboratory conditions [72].

2.4. *Effect of secondary structures*

Understanding secondary structures such as fault planes, shear zones, folds, and joint systems is necessary to clarify rocks' mechanical behavior and stability, especially anisotropic ones. These features form post-rock formations due to tectonic forces such as compression, tension, or shearing. Fault planes are primary examples of secondary structures resulting from tectonic deformation, reducing the shear strength of rock masses and creating potential slip surfaces that can destabilize slopes and underground excavations. Joint systems are usually fractures with no significant displacement and are produced by stress release or tectonic forces, concentrating stress and allowing water infiltration that weakens rock masses [25,73–75]. Shear zones and faults also control stress redistribution in rock masses. Reactivation of pre-existing faults due to tectonic stresses creates zones of localized deformation that may undoubtedly lead to instability in tunnels or slopes [76–79]. Folds are secondary structures due to compressional forces in the tectonic environment. They change the orientation of rock layers that may facilitate the formation of zones of weakness and thereby control the stress distribution and failure patterns [80–84]. The geometry and characteristics of jointed rock masses are influenced by numerous factors, including fracture intensity, fracture length, and block size distribution (BSD) [85–87]. Some typical blocks formed by joints are shown in Fig. 12. The variations in the sizes and shapes of the rock blocks make this parameter very complicated [88].

The level of complexity of geotechnical conditions is a principal factor for assessing and managing underground structures. Fig. 13 presents a detailed matrix to determine complexity levels, classified as minor, moderate, and significant complexity. The matrix addresses block size, anisotropy, stress/strength conditions, and deformation behaviors. For instance, a mining site exhibiting a depth exceeding 500 m and a uniaxial compressive strength (UCS) that does not exceed 100 MPa poses considerable geotechnical challenges. The rock mass is extensively jointed, displaying a blocky configuration with superior joint surface characteristics, resulting in a Geological Strength Index (GSI) exceeding seventy. Moreover, the rock demonstrates significant non-linearity, as evidenced in coarse-grained metamorphic formations where the m_i approximates twenty. Additionally, the anisotropic characteristics of the rock mass are distinctly evident, defined by pronounced foliation and highly anisotropic behavior [89].

Isotropic rocks have stress-induced bursts with homogeneous crack development, and anisotropic rocks have structural bursts controlled by inherent discontinuities. These anisotropic properties control stress distribution, producing different types [90–92]. Anisotropic rock masses possess varying geological properties based on structural composition, mineral orientation, and geological evolution. These characteristics were considered in this section, as well as their implications on the

Fig. 6. Examples of anisotropic features in metamorphic rock: (a) field photograph of a shear zone in marble characterized by alternating bands, with the position of the oriented samples marked [51] and (b) folded rock from the Grenville Mountains, Ontario (Geological Museum of Queen's University in Kingston, Canada).

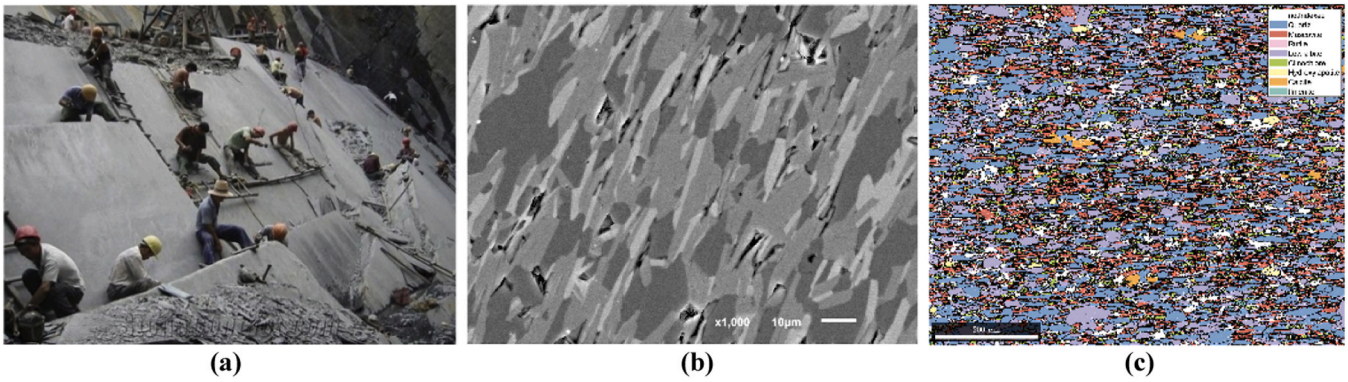

Fig. 7. Anisotropic structure of the slate: (a) slate outcrop in one of the Valdeorras quarries (Spain), illustrating the compositional and structural heterogeneities with high-quality slates restricted to local areas; (b) SEM image of slate displaying aligned platy minerals, indicating anisotropy (scale: 10 μm); and (c) EBSD map highlighting mineral phases like quartz and muscovite, with strong textural alignment (scale: 200 μm) [53].

behavior of rocks. The anisotropic nature of metamorphic, sedimentary, and igneous rocks and the role played by secondary structures such as faults, folds, and shear zones in controlling rock mass stability were also explained.

3. Lab-scale mechanical behavior

The anisotropy of the rock also has a profound influence on the geomechanical properties of the rock. Rock anisotropy can result from the presence of cleavage, foliation, bedding planes, schistosity, joints, micro- or macro-fissures, or any other directional or planar feature brought about by variations in mineral composition, grain size, crystal size, fabric, porosity, and weathering [7,93–96].

Directional strength is a variation in the strength characteristics of rock masses in different directions due to anisotropy. For example, the strength of schistose rocks in a direction parallel to foliation planes is usually lower than that in a direction normal to such planes [2,97–100]. Their internal structures control the strength and deformability of anisotropic rock masses. Rocks with prominent bedding planes or foliation exhibit anisotropic mechanical behavior depending on the loading angle with respect to these planes. Deformation modulus (E_t) and UCS are the essential parameters for assessing rock behavior [59,101–104].

Texture	Characteristics	Protolith	Rock Name	
Foliated (Increasing Temperature and Pressure)	Fine-grained rock tends to split in parallel fragments (known as slaty cleavage)	Shale	Slate	
	It contains shiny muscovite (light) or biotite (dark) micas, which may see other minerals. Has a schistose pattern of foliation	Shale	Schist	
	It contains alternating bands of light- and dark-colored minerals (usually biotite or amphibole), called gneissic banding	Shale or Igneous Rock	Gneiss	
Possibly Foliated	Most of the minerals in this rock are amphiboles, which may be aligned to form a foliation.	Mafic or Ultramafic Rock	Amphibolite	
Non-Foliated	Equigranular grains of quartz, which have a hardness of 7	Sandstone or Siltstone	Quartzite	
	Equigranular grains of calcite or dolomite, which has a hardness of 4 and reacts to acid	Limestone or Dolostone	Marble	
	It contains mainly carbon, is a low-density rock, and has a shiny appearance	Bituminous Coal	Anthracite Coal	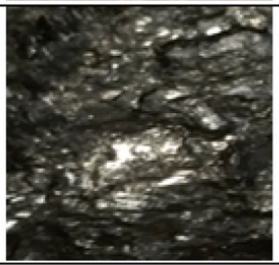

Fig. 8. Summary chart of metamorphic rocks, including the names of some of the possible sedimentary rock and igneous rock protoliths for each metamorphic rock [55].

Fig. 9. Examples of anisotropy in sedimentary rock masses: (a) scanning electron microphotograph of a shale [63]; (b) anisotropy due to bedding in sedimentary rocks in a tunnel face exposure [64]; and (c) mudstone with inter-bedded sand layers [65].

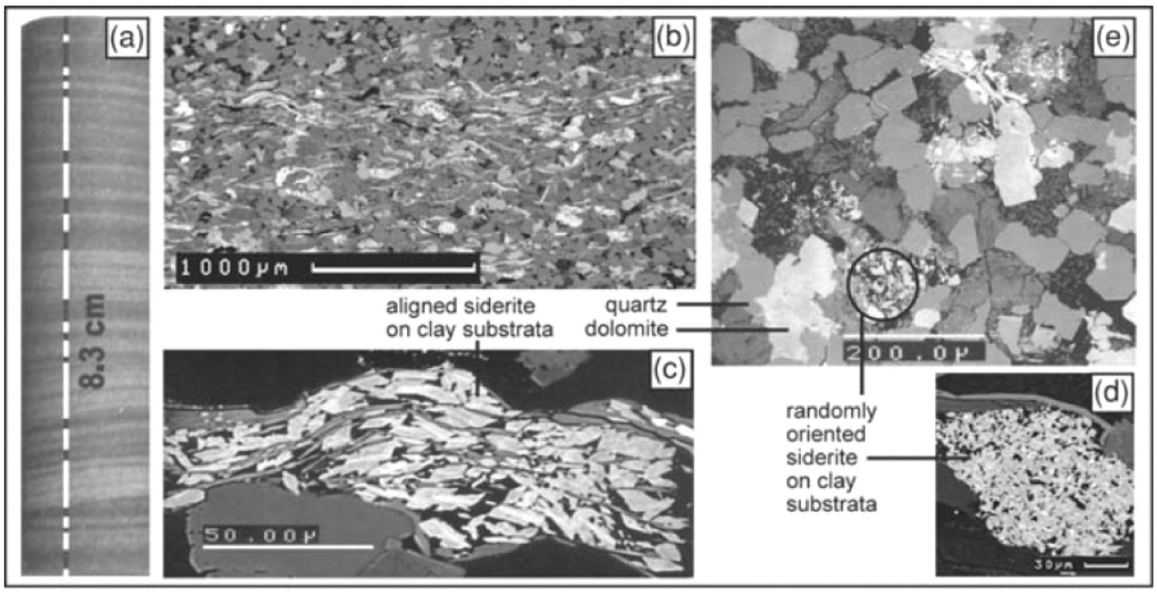

Fig. 10. Structure and variation in mineral alignment across different layers of Siltstone: (a) alternating dark mud-rich and light sand-rich layers; (b) bedding-parallel alignment of detrital phyllosilicates and authigenic clays in mud-rich layers; (c) rhombohedral siderite minerals, with 50 % aligned parallel to mica; and (d) random orientation of the remaining siderite minerals [66].

In laboratory tests, the presence of joints significantly affects the strength characteristics of the rock as a mass. With a single joint, the rock strength highly depends on the joint's orientation relative to the loading direction. A single joint reduces compressive strength, especially when the load is parallel to the joint plane, as the rock can slip along the joint under stress. The presence of two or more joints also reduces the overall rock strength since multiple planes of weakness permit failure at lower stresses. Jaeger and Cook mentioned that the orientation of the applied load relative to the joints strongly influences the failure mechanism, where rock masses exhibit complex failure modes when loaded in multi-jointed systems [105]. These behaviors are essential for attempting to capture the structural stability of rock masses in real engineering settings, where joint networks are ubiquitous [105]. The definition of the angle of anisotropy, β, the angle between the weakness plane and the loading direction, is shown in Fig. 14. Its variation can lead to one of the different types of anisotropies: U-shape, shoulder-shape, wavy-shape, and U-shoulder-shape, as depicted in Fig. 15. To understand and figure out the status of rock masses in rock engineering toward their characterization, determining the mechanical characteristics is the basis and prerequisite for the next steps such as analytical and numerical analyses. These characteristics would be more crucial when anisotropy, as a microstructural property, is studied, requiring more attention than macro-structural analyses, including joints or discontinuities. The most important mechanical characteristics of anisotropic rocks are presented in the following sections.

3.1. Behavior under compression

The primary property of rock is its strength. Different methods over the decades have been employed to point out the strength of anisotropic rocks. More specifically, the compressive strength of such rocks has been studied by different researchers using UCS or triaxial compressive strength (TCS) tests.

The classic examples of determining the UCS of anisotropic rocks were related to the shales and slates investigated by different researchers [107,108], the tests on gneisses and schists [109], on Idaho Springs Gneisses, as seen in Fig. 16b [110], quarzitic and carbonaceous phyllite, Barnsley hard coal, and Penrhyn Slate illustrated in Fig. 16c-f [106]. They concluded that the UCS in anisotropic rocks has a nonlinear relationship with the anisotropy angle. Evert Hoek showed this conclusion, where the experiments had been done on a South African slate, explaining that the dashed line demonstrates the impact of a weakness plane oriented at $\beta = 90^\circ$ or 0° for compressive tests, as shown in Fig. 16a [108]. It shows that the value of UCS has reduced almost fourfold due to the weakness plane, emphasizing the influence of anisotropy on rock mass behavior.

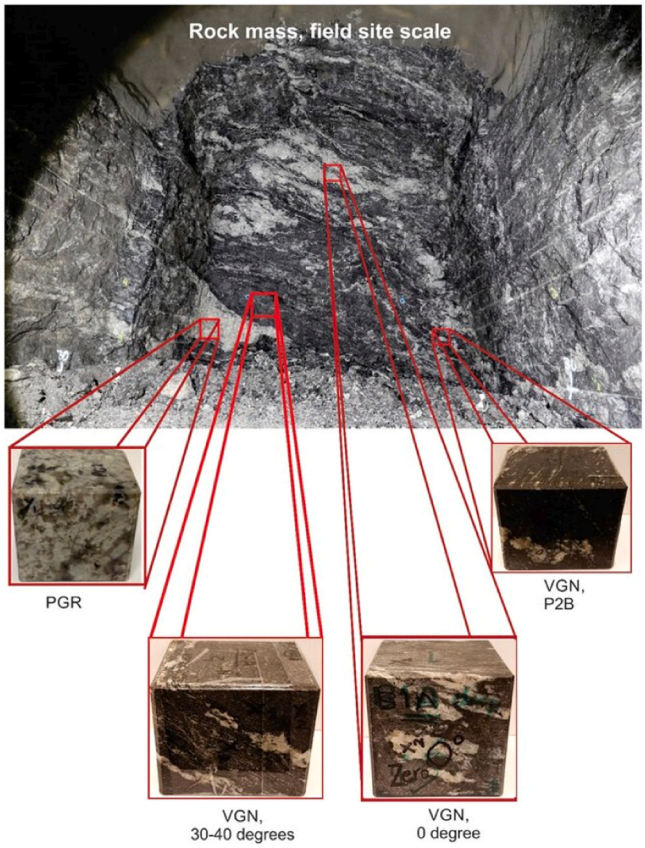

Fig. 11. Anisotropic and heterogeneous features of the ONKALO rock mass, with insets showing PGR and VGN specimens tested under true-triaxial stress at the RFDF, University of Toronto [72].

Triaxial compressive strength is another experiment that determines the strength of rock mass in conditions close to reality. This test was done on chlorite and graphite schist [111], diatomite [112], and coal [113]. These investigations indicate that compressive failure occurs when β is between 0 and 90 degrees, and its magnitude is at its lowest when the angle is between 20 and 40 degrees. A similar observation has been reported by Behrestaghi et al. [114] that for all confining pressures, the highest strength in schists occurred at $\beta = 90°$. The minimum occurred at $\beta = 30°$, which was then shifted to $\beta = 45°$, as shown in Fig. 16g-k for four different rocks. Saroglou et al. [115] conducted an experimental campaign to study the influence of foliation on various parameters of Greek gneiss. They figured out that the minimum strength tool was placed at the inclination of planes of weakness with the principal stress, β, around 30°, as seen in Fig. 16l. Based on TCS test results on the impact of weak planes on confined pressure, Saroglou et al. mentioned the Hoek and Brown isotropic criterion [2] should be used with high care, using it by considering lower values of UCS since the UCS and the parameter m_i may be changed because of foliation in metamorphic rocks [115]. These results were reported by Goshtasbi et al. [116], who, based on TCS tests on slate rocks of the Sanandaj-Sirjan zone in Iran, concluded that the anisotropy type was U-shaped. The maximum and minimum strengths demonstrated at $\beta = 90°$ and $\beta = 30°$, respectively, are represented in Fig. 16m.

In addition, it is shown that TCS in meta-sedimentary rocks has higher values when the bedding planes are perpendicular rather than in a parallel direction [117]. To evaluate the effect of different β (= 0°, 15°, 30°, 45°, 60°, 75°, and 90°) on the mechanical behavior of 140 metamorphic rock samples collected from different locations of the Hamedan Province in Iran under different confined pressures, Fereidooni et al. [94] undertook an experimental program. They found that the maximum principal stress increases with increasing confining pressure, and its variations are the greatest at $\beta = 0°$. Their findings of minimum strength values were the same as those mentioned earlier ($\beta = 90°$).

In contrast, in the condition without confining pressure, the minimum values of UCS occurred at $\beta = 15–30°$, as demonstrated in Fig. 16n-q. It states that when the confining pressure increases, the β associated with the minimum UCS increases. Song et al. [118] studied the coal anisotropy by emphasizing the influence of specimen size via conducting UCS tests with four different sample diameters and different bedding orientations corresponding to loading direction $\beta = 0°$, 15°, 30°, 45°, 60°, and 90°. They concluded that the strength anisotropy declines when the sample size increases, and the highest decline occurs when $\beta = 0°$. An empirical equation for the samples' diameters and UCS has been introduced, and a cosine function can be applied for the anisotropy angle and UCS of coal in varied sizes. This illustrates that the coal anisotropy will not experience changes when the sample diameters exceed a critical value.

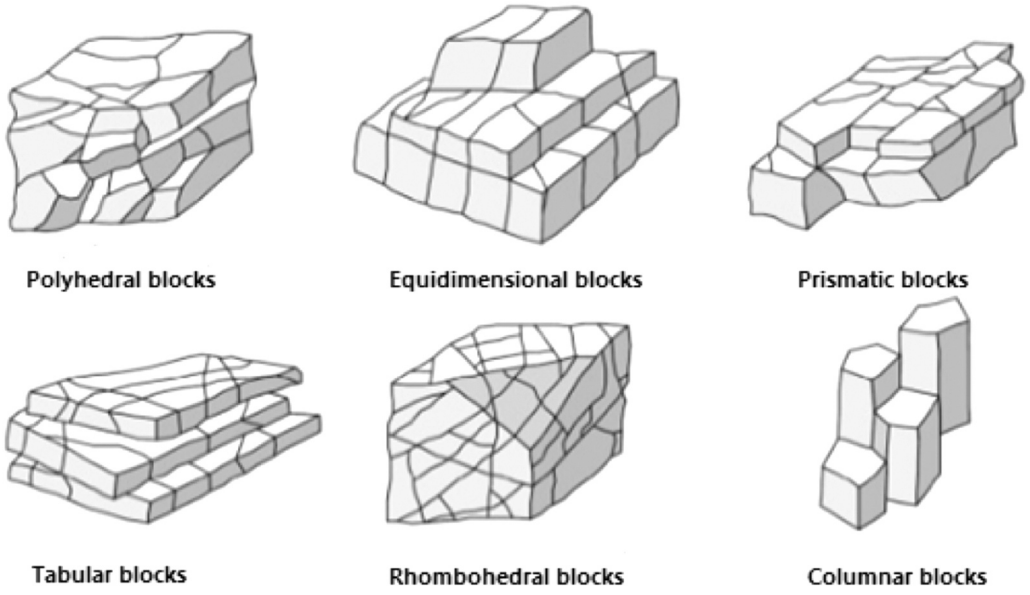

Fig. 12. Block shapes of rock masses, including the joint sets [88].

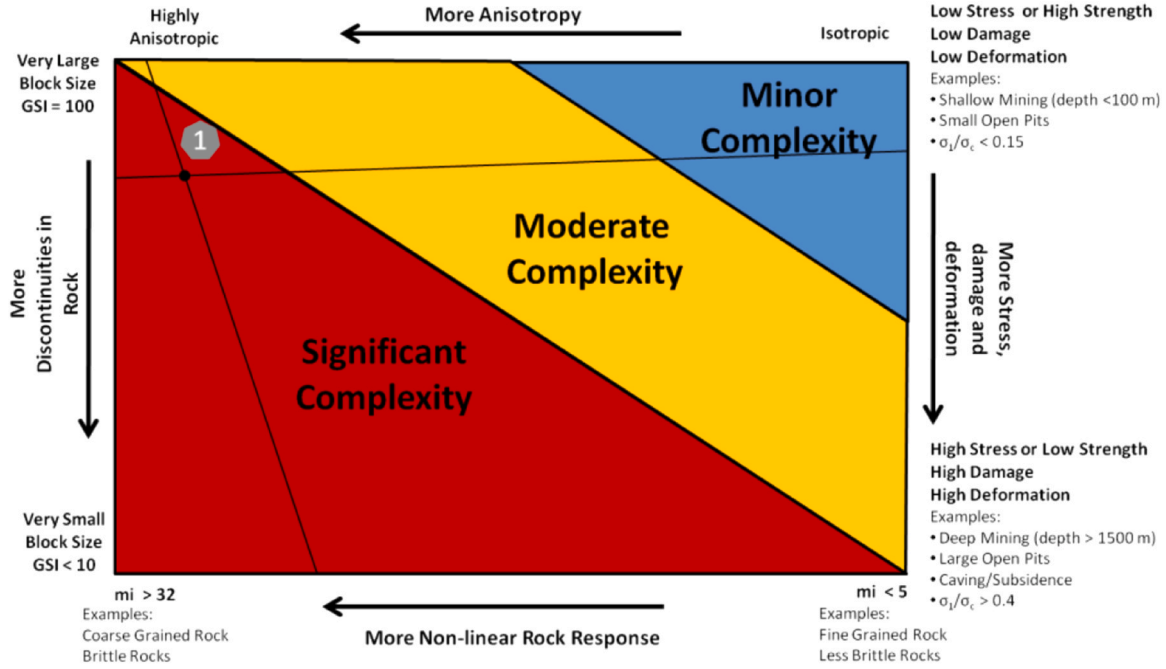

Fig. 13. A matrix for evaluating the degree of complexity involved in various geotechnical conditions (see example for clarification on how to use) [89].

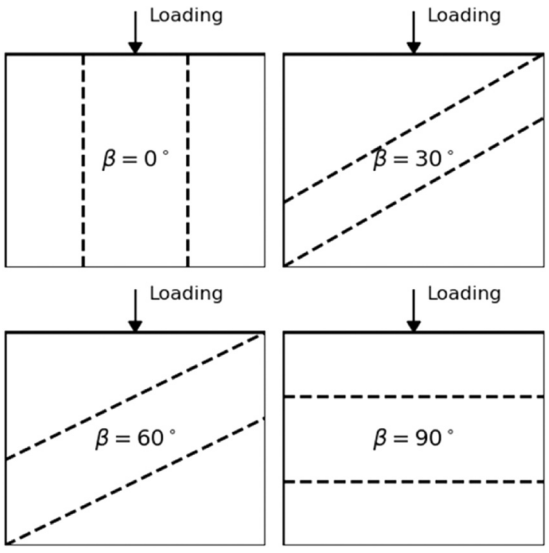

Fig. 14. Definition of β, the angle between the weakness plane and loading direction.

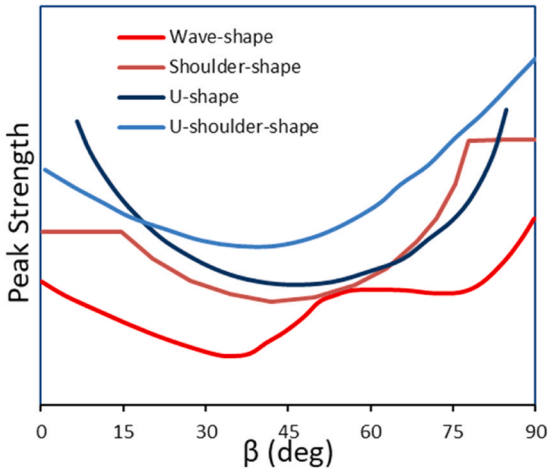

Fig. 15. Different anisotropy shapes based on the variation of β [106].

More details of the compressive behavior of these types of rock masses are provided in Table 1 and Fig. 16. It can be concluded that in most cases, the lowest compressive strength in rocks occurs between β = 30° and β = 45° and the highest value takes place at β = 0° and β = 90°, in both uniaxial and triaxial condition. It demonstrates that shear failure most likely would occur in anisotropic rock mass along a foliation or plane of weakness with an angle of 30–45 degrees, recommending the big picture for selecting the excavation's alignment concerning the foliation and suitable supporting systems. On the contrary, the maximum UCS at β = 0° or β = 90° tells the practitioners this fact that rock may not fail or slide on the foliation with such orientations, suggesting the most appropriate trending for construction to have the highest rock's capacity against compression loading as well as minimizing potential shear failure along the foliation.

3.2. *Deformability properties*

To investigate deformability in anisotropic rocks according to the variation of β, the studies on three schists, including Graywake schist I, Graywake schist II [119], represented in Fig. 17a-b, and Hast schist [120], as shown in Fig. 17d, Barnsley hard coal, as demonstrated in Fig. 17c [113], diatomite [112], three shales, consisting of Moszczenica shale, Borynia shale, and Wilchwy silty shale [121], depicted in Fig. 17e have been undertaken. Their findings showed that first, the two types of U-shaped and irregular-shaped (see Fig. 17) are the dominant anisotropies, then the highest E_t occurs at β = 0° and the lowest one at β = 30–60°, followed by an increase at β equals to 75°.

By calculation of the secant modulus of the strain-stress curve at different anisotropy angles, Fereidooni et al. [94] reported similar findings that the maximum value of E_t took place at β= 0° and added that the deformability modulus values increased with the increase of confining pressure, and by a continuation of such increase, the minimum point associated with E_t changed to the larger β values. They also mentioned that by increasing confining pressure, highly foliated rocks

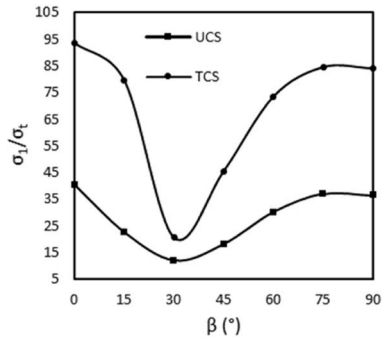

(a) slate [108]

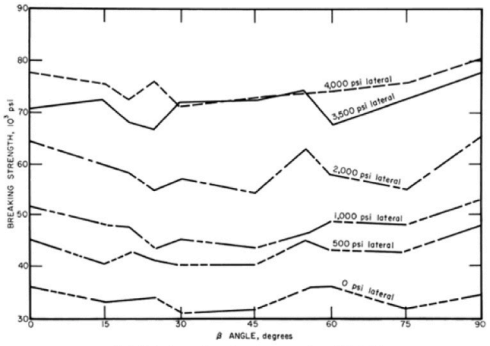

(b) Idaho Springs gneiss [110]

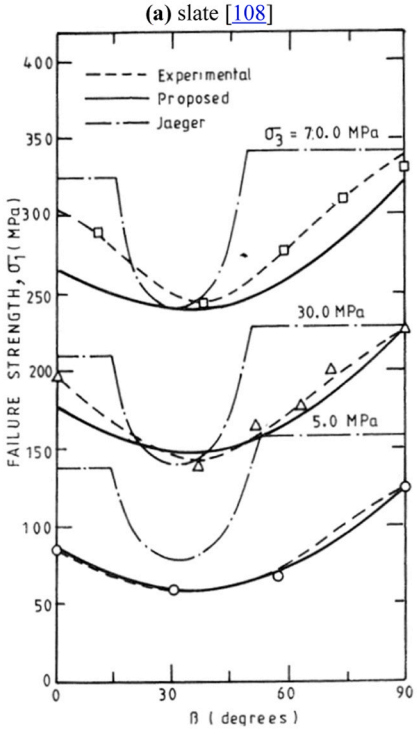

(c) quarzitic phyllite [106]

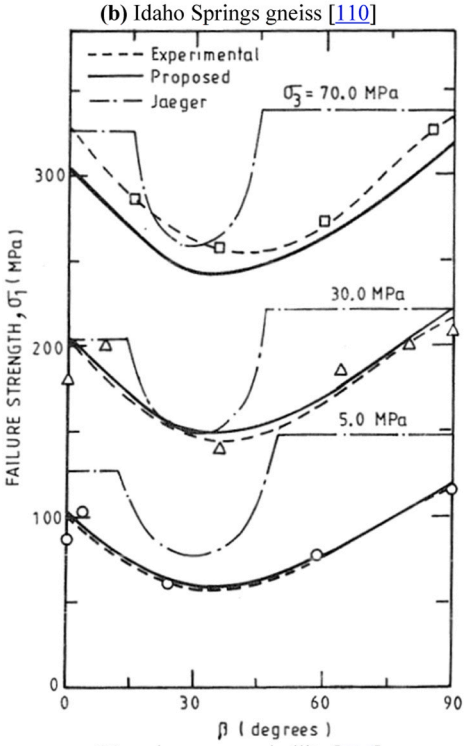

(d) carbonaceous phyllite [106]

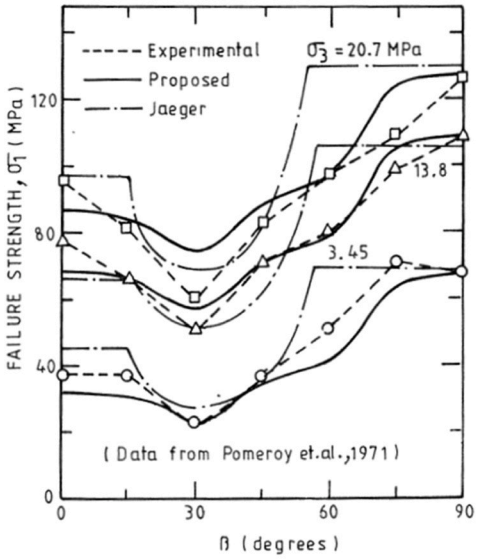

(e) Barnsley hard coal [106]

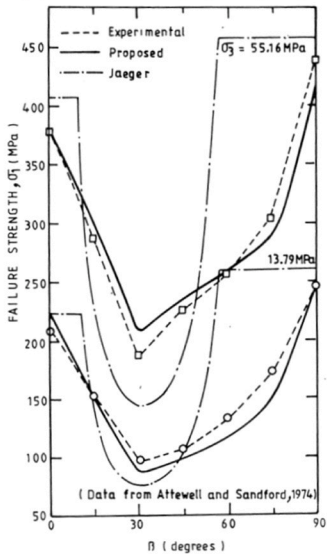

(f) Penrhyn slate [106]

Fig. 16. Anisotropic rock compressive behavior with the variation of β illustrated by the different researchers.

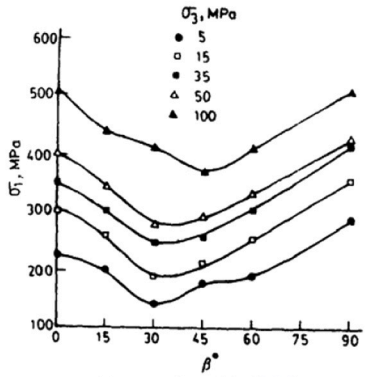

(g) quartzite schist [114]

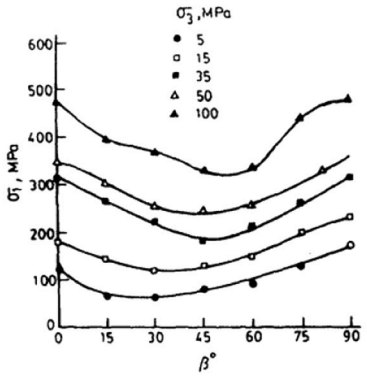

(h) chlorite schist [114]

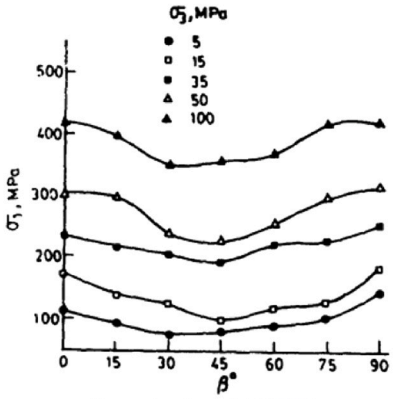

(j) quartz mica schist [114]

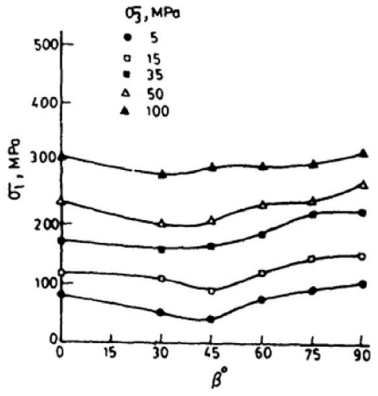

(k) biotite schist [114]

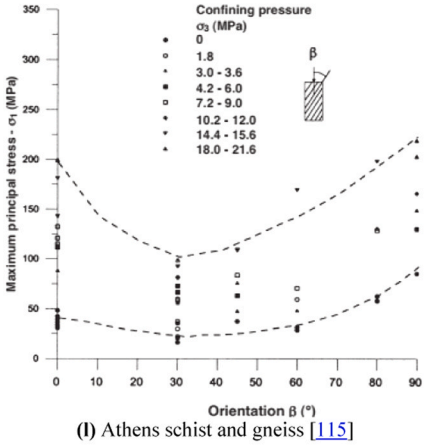

(l) Athens schist and gneiss [115]

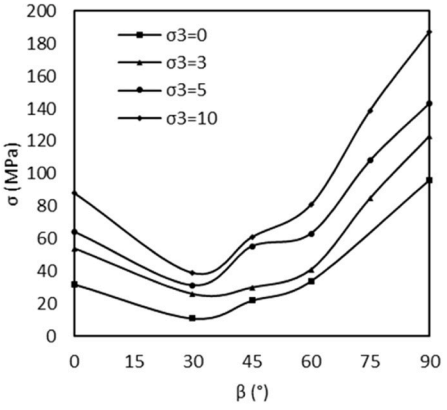

(m) slate [116]

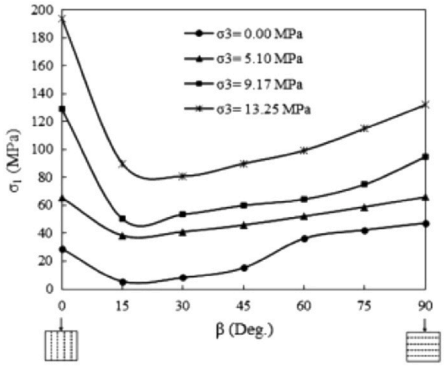

(n) phyllite [94]

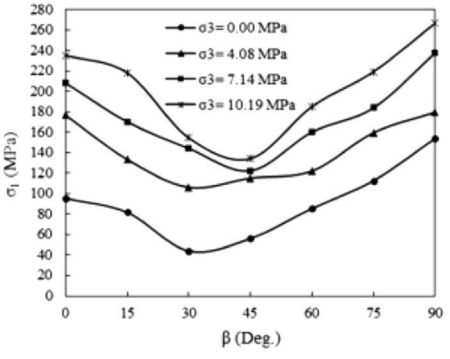

(o) sillimanite garnet hornfels [94]

Fig. 16. (*continued*).

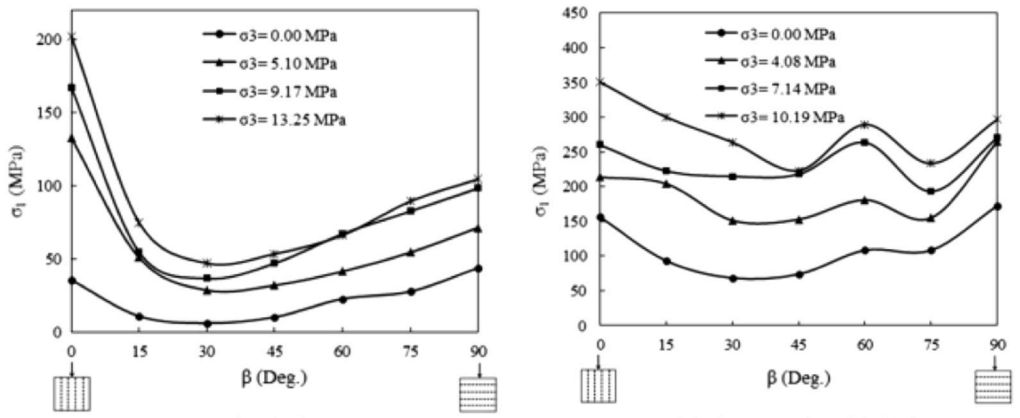

(p) slate [94] **(q)** andalusite garnet hornfels [94]

Fig. 16. (*continued*).

experienced more changes in the modulus values at $\beta = 0^{\circ}$. They came to the opposite conclusion about how E_t changes with confining pressure compared to Behrestaghi et al. [114], who mentioned that deformability behavior is similar to UCS and doesn't depend on confining pressure, based on studies done on schists.

Even though the findings mentioned above have been proven by other studies, which ascertained that the value of E_t increases according to the confining pressure in schist [18], illustrated in Fig. 17l-m, shale [122], gneiss, schist, and marble [123], and sandstone (see Fig. 17n) [124]. In a study by Villalobos et al. [125], the effect of anisotropy on elastic properties, such as the elasticity modulus and Poisson's ratio, was assessed by undertaking triaxial compressive tests with the confining pressures up to 20 MPa and varying β on the foliated phyllite samples, as shown in Fig. 17o. Their findings showed that the elasticity modulus values increase with increased confining pressure. On the other hand, as the values of β changed from 0° to 90°, the values of β first decreased until $\beta = 45^{\circ}$ and then increased until $\beta = 90^{\circ}$, showing a U-shaped curve. Additionally, they concluded that confining pressure variation does not change the Poisson's ratio, while increasing the β values results in a decrease in an almost linear fashion.

More details and the anisotropy shape for different anisotropic rock masses through the E_t standpoint were summarized in Table 2 and Fig. 17, respectively. It can be concluded that the lowest values of the deformability behavior of anisotropic rock masses under uniaxial and triaxial compression conditions occur at β less than 50. At the same time, the highest magnitude takes place at β equals 0 or 90 degrees. Additionally, the impact of confining pressure shows that E_t first decreases and then increases with an increase in β. In most cases, the overall trend of the E_t anisotropy shape decreases as the angle increases, indicating an improvement in the structure's load-bearing capacity, a decrease in the inward convergence of the tunnels' walls or roof, and a reduction in the need for ground support. On the other hand, this kind of reduction may also have adverse effects, such as brittle failures due to rapid crack propagation in the high-stress redistribution, higher stress concentration

Table 1
Studies on determining the compressive strength of different anisotropic rock masses.

Rock type	β	Confining pressure	UCS — TCS at β		Results	Anisotropy shape (UCS—TCS)	Ref.
	(Degree)	(MPa)	Lowest	Highest			
Slate	0, 15, 30, 45, 60, 90	0, 9.2, 10.3, 17.7, 19.2, 34.9, 38.2, 40.3, 46.0, 46.3, 48.8, 49.2, 50.6, 58.1, 65.7	30 — 30	0 — 0	Fig. 16a	U-shaped — Shoulder-shape	[108]
Idaho Springs Gneiss	0, 15, 20, 25, 30, 45, 55, 60, 75, 90	0, 3.45, 6.9, 13.8, 24.15, 27.6	30 or 45 — 25–55	0 — 90	Fig. 16b	Wave-shape	[110]
Quarzitic Phyllite	0, 15, 30, 45, 60, 75, 90	0, 5, 30, 70	30 — 30	90 — 90	Fig. 16c	U-shaped — Shoulder-shape	[106]
Carbonaceous Phyllite			30 — 30	90 — 90	Fig. 16d		
Barnsley hard coal			30 —30	90 — 90	Fig. 16e		
Penrhyn Slate			30 — 30	90 — 90	Fig. 16f		
Quartzite schist	0, 15, 30, 45, 60, 75, 90	0, 5, 15, 35, 50, 100	30 — 30	90 — 0 or 90	Fig. 16g	Wave-shape — U-shape	[114]
Chlorite schist			30 — 30–45	90 — 0 or 90	Fig. 16h	U-shape	
Quartz mica schist			30 — 45	90 — 0 or 90	Fig. 16j	U-shape — Wave-shape	
Biotite schist			30 — 45	90 — 90	Fig. 16k	U-shape — Wave-shape	
Athens schist and gneiss	0, 15, 30, 45, 60, 75, 90	7 cases between 0 and 21.6	30 — 30	90 — 90	Fig. 16l	U-shape	[115]
Slate	0, 30, 45, 60, 75, 90	0, 3, 5, 10	30 — 30	90 — 90	Fig. 16m	U-shape	[116]
Phyllite	0, 15, 30, 45, 60, 75, 90	0, 5.1. 9.17, 13.25	15 — 15–30	90 — 0	Fig. 16n	Semi-U-shape	[94]
Sillimanite garnet hornfels		0, 4.08, 7.14, 10.19	30 — 45	90 — 90	Fig. 16o	Semi-U-shape	
Slate		0, 5.1. 9.17, 13.25	30 — 30	90 — 0	Fig. 16p	Semi-U-shape	
Andalusite garnet hornfels		0, 4.08, 7.14, 10.19	30 — 45	0 — 0 or 90	Fig. 16q	Semi-U-shape — Wave-shape	

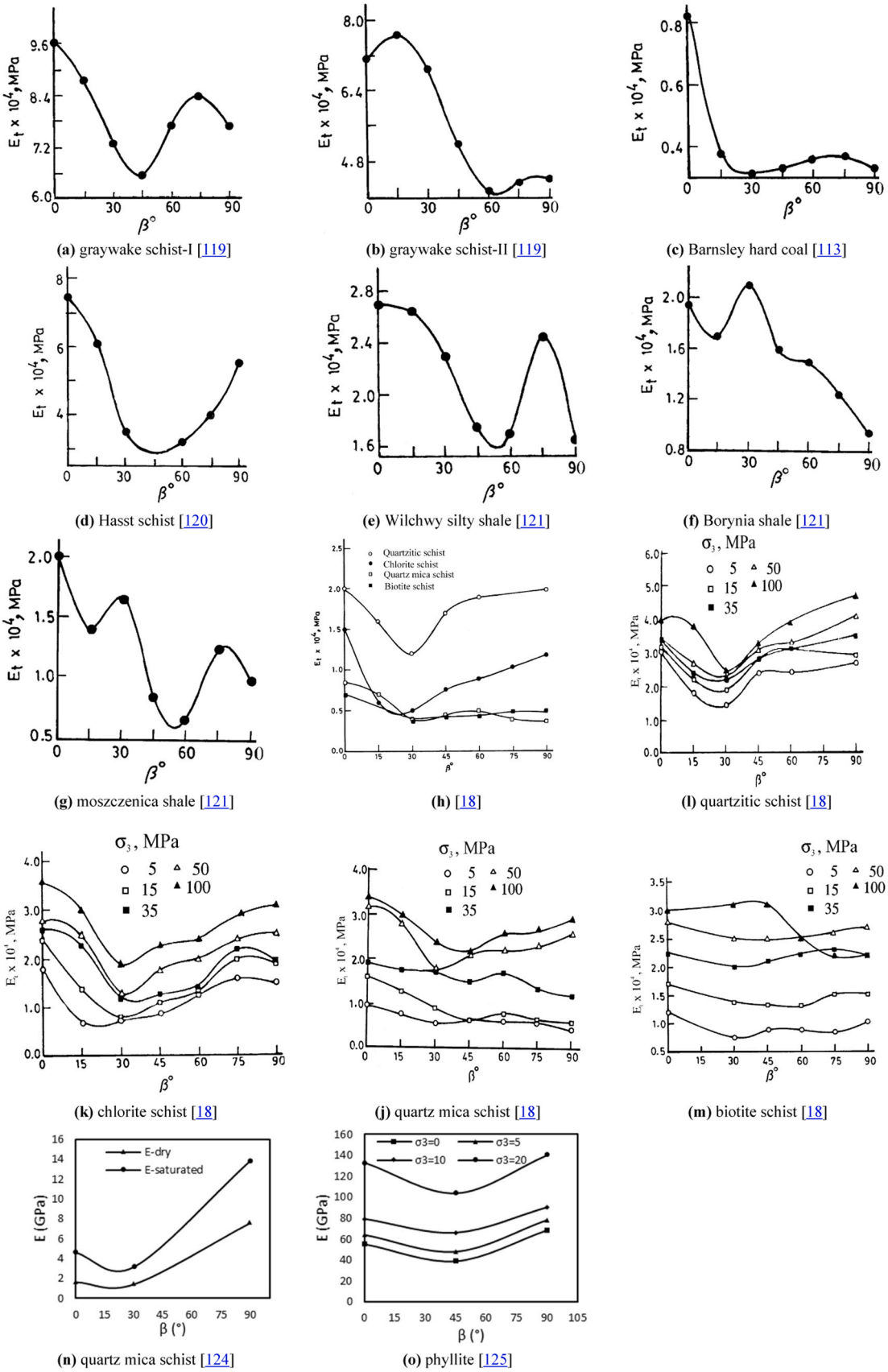

Fig. 17. Anisotropic rock mass deformability behavior with the variation of β illustrated by the different researchers.

Table 2
Studies on determining deformability behavior (E_t) of different anisotropic rock masses from the standpoint of modulus of elasticity.

Rock type	β	Confining pressure	E_t at β (UTC)		Results	Anisotropy shape	Ref.
	(Degree)	(MPa)	Lowest	Highest			
Graywake schist-I	0, 15, 30, 45, 75, 90	0	45 — -	0 — -	Fig. 17a	Wave-shaped	[119]
Graywake schist-II			60 — -	15 — -	Fig. 17b	Wave-shaped	
Barnsley hard coal	0, 15, 30, 45, 75, 90	0	30 — -	0 — -	Fig. 17c	Declining wave-shaped	[113]
Hasst schist	0, 15, 30, 60, 75, 90	0	45 — -	0 — -	Fig. 17d	U-shaped	[120]
Wilchwy silty shale	0, 15, 30, 45, 60, 75, 90	0	50 — -	0 — -	Fig. 17e	Wave-shaped	[121]
Borynia shale			90 — -	30 — -	Fig. 17f	Wave-shaped	
Moszczenica shale			50 — -	0 — -	Fig. 17g	Wave-shaped	
Quartzitic schist	0, 15, 30, 45, 60, 75, 90	0, 5, 15, 35, 50, 100	30 — 30	0 and 90 — 90	Fig. 17h-l	Wave-shaped — U- & Wave-shaped	[18]
Chlorite schist	0, 15, 30, 45, 60, 75, 90		20 — 30	0 — 0	Fig. 17k	U-shaped	
Quartz mica schist	0, 15, 30, 45, 60, 75, 90		30 — 45	0 — 0 and 90	Fig. 17j	Wave-shaped	
Biotite schist	0, 15, 30, 45, 60, 75, 90		30—30 and 45	0 — 0	Fig. 17m	Wave-shaped	
Quartz mica schist	0, 30, 90	0	30 — -	90 — -	Fig. 17n	U-shoulder-shape	[124]
Phyllite	0, 45, 90	0, 5, 10, 20	45 — 45	90 — 90	Fig. 17o	U-shoulder-shape	[125]

around excavation walls, and a rising risk of rock burst due to reduced ductility.

3.3. Behavior under tension

The attempts to measure and consider the tensile strength (TS) of rocks, remarkably anisotropic ones, were made when the influence of schistosity on the Brazilian tensile strength (BTS) was assessed for metamorphic rocks [126,127]. After that, various researchers were employed to study the anisotropy of BTS from different points of view, as demonstrated in Fig. 18 (a, e, g, l, and j) [128–131].

Barla and Innaurato [128] conducted indirect tensile testing on two rock types of granitoid gneiss and serpentinous schist to study the influence of anisotropy on the tensile strength in both parallel and perpendicular loading directions and different values of β. It was reported that maximum values of tensile strength took place at $\beta = 0^\circ$ for both rock types, whereas the minimum values occurred at $\beta = 60^\circ$ for schist and at $\beta = 75^\circ$ for the gneiss, represented in Fig. 18a-b. Additionally, a polynomial fitting curve showed the highest degree of approximation. In another study, Ma et al. [131] conducted Brazilian tests to assess the anisotropic tensile strength of Longmaxi Shale-I and Jixi Coal. They reported for the Longmaxi Shale-I case, the samples experienced tensile failure when $0^\circ < \beta < 24^\circ$ (intact rock) and $76^\circ < \beta < 90^\circ$ (along the bedding), whereas for the Jixi Coal case, tensile failure occurred at $0^\circ < \beta < 23^\circ$ or $76^\circ < \beta < 90^\circ$; their results can be seen in Fig. 18k. Furthermore, Kundu et al. [132] undertook Brazilian tensile strength tests on two lineated mylonitic and crenulated schist to study the effect of anisotropy in dry and saturated conditions. They stated that tensile strength is a function of β. The minimum value occurred at the angle between 20° and 30° for the dry quartz–mica schist, while for the saturated quartz–mica schist, the angle for minimum strength is 45°, which is somewhat the same as previously mentioned findings, shown in Fig. 18h-l.

In addition, the effect of water on the tensile strength has been reported with a significant reduction toward higher values of the anisotropy angle. Meanwhile, such reduction was not evident for the dry–quartz–mica schist, which was speculated due to the lower mica content (16.4 %) compared to 37 % in saturated quartz–mica schist. The anisotropy angles (0° and 90°, respectively), in which the highest and lowest tensile strengths occurred, have been proven by the study conducted by Alencar et al. [133]. Also, the maximum and minimum values of BTS for limestone samples were reported at $\beta = 70^\circ$ and $\beta = 20^\circ$, respectively, as seen in Fig. 18m [134]. There are several pieces of research considering anisotropies for tensile strength [135,136] on layered sandstone or evaluating transversely isotropic rock using diametrical compression through the impact of layering orientation on the loading direction [97,137–139]. They have mostly focused on fracturing in reservoirs not related to mining or rock engineering applications, which most likely contain these microstructural characteristics.

More details on the studies to determine the tensile strength of anisotropic rocks are presented in Table 3 and Fig. 18. Since reports have shown various anisotropic shapes and different minimum and maximum values under variable confining pressure values, it appears that the tensile strength of anisotropic rock masses lacks a general trend. However, it should be mentioned that the wave shape can be seen as the major anisotropy shape for the tensile strength of anisotropic rocks.

3.4. Behavior under shear

In an experimental study, Ghazvinian et al. [140] conducted shearing tests on green schistose rock samples to study the effect of schistosity dip ($\alpha = 0^\circ$, 15°, 30°, 45°, 60°, 75°, 90°) and strike ($\gamma = 30^\circ$, 40°, 50°) on shear strength with different β angles ($\beta = 0^\circ$, 30°, 45°, 60°, 90°). Fig. 14 shows the testing configuration. The results show that shearing happened across weak planes of schistosity at $\alpha = 0^\circ$ and $\alpha = 15^\circ$; at $\alpha = 30^\circ$, however, confining pressures had less impact. They mentioned that the shear strength increases with the increase in β values, showing a U-shaped curve as shown in Fig. 19a. It should be noted that by increasing the α values from 45°, the failure plane changed from shearing at the schistosity plane to a predetermined plane ($\alpha = 45^\circ$) and sliding at the schistosity at $\alpha = 90^\circ$. In addition, it was found that splitting happens along the weak planes and that the shearing mode changed from solitary sliding to shearing and tensile splitting of the weak planes along their strike direction for values of β greater than 45. Similar findings by Ghazvinian et al. [140] have been reported by Wang et al. [141] and Liu et al. [142], represented in Fig. 19b-c, respectively.

A few cases (Table 4) indicate that the shear behavior of anisotropic rock masses lacks a defined anisotropic shape, underscoring the necessity for further research to gain a deeper understanding of the behavior of these rocks under shear. The rare studies related to the shear behavior show the need for in-depth research, especially considering true triaxial shear tests to study the multi-dimensional coupling disturbance associated with structural planes [143,144].

4. Anisotropic rock mass classification and characterization

Anisotropic rock mass characterization is critical for developing safe and efficient engineering structures in geotechnically demanding situations. It is imperative to recognize that the successful application of rock mass classification systems (RMCSs) necessitates site-specific validation, particularly in contexts involving anisotropic, jointed, or weak rock masses, where conditions exhibit considerable variability [145,146].

RMCSs have progressed from load-based approaches like Terzaghi's classification to more complete classifications like RMR (Rock Mass Rating), Q-System (Rock Mass Quality), and ARMR (Anisotropic Rock

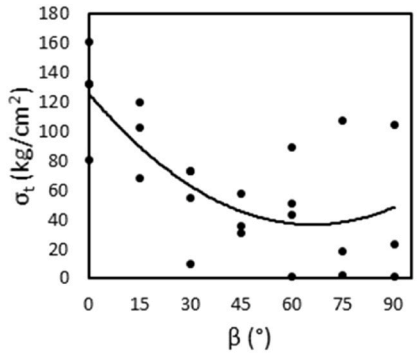

(a) granitoidic gneiss; decreasing trend [128]

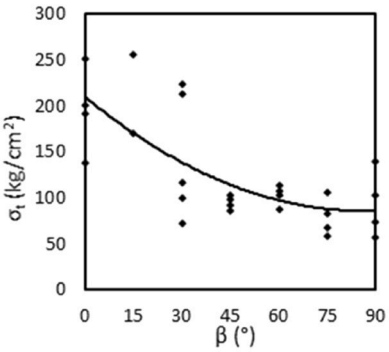

(b) serpentinous schist; decreasing trend [128]

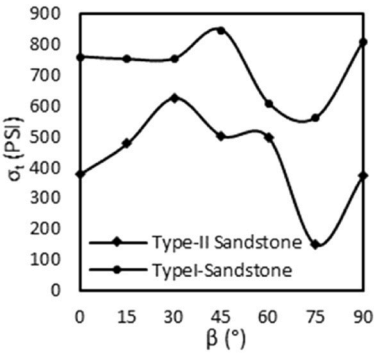

(c) sandstone; first increasing, then decreasing, and again increasing trend [137]

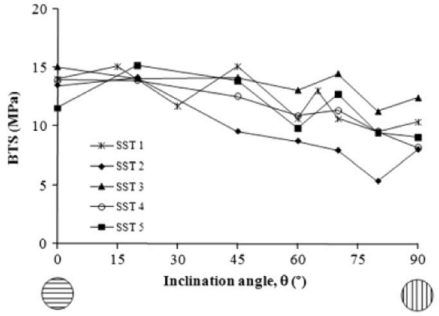

(d) sandstone; decreasing trend [135]

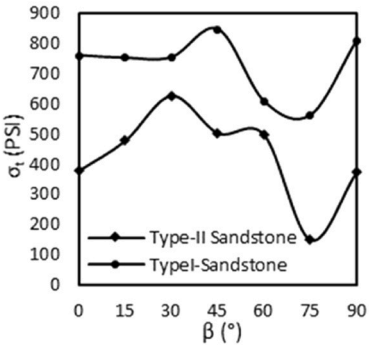

(e) shale; varying trend [129]

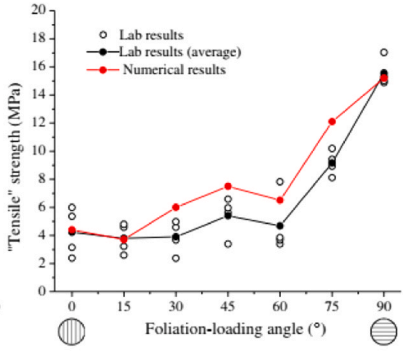

(f) shale; increasing trend [97]

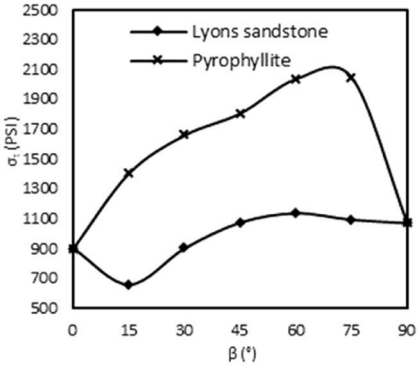

(g) increasing trend [130]

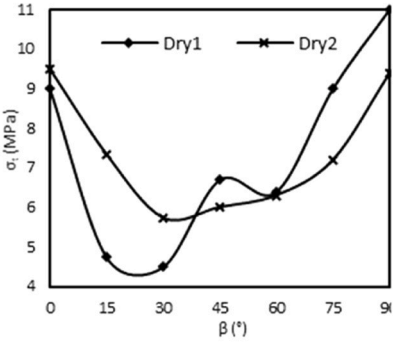

(h) quartz–mica schist; first decreasing, then increasing trend [132]

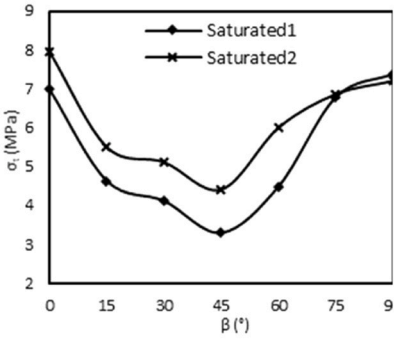

(l) quartz–mica schist; first decreasing, then increasing trend [132]

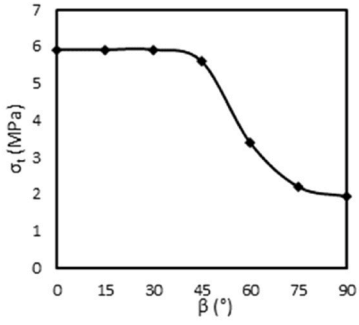

(j) shale; decreasing trend after β = 45° [131]

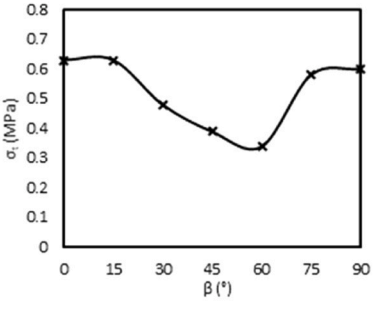

(k) coal; first decreasing, then increasing trend [131]

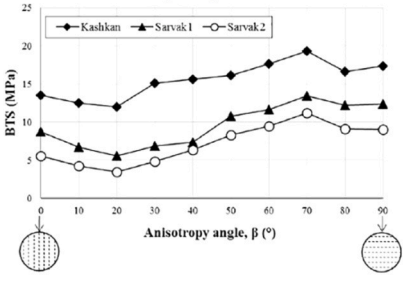

(m) increasing trend from β = 45° to β = 80° [134]

Fig. 18. Anisotropic rock mass tensile behavior with the variation of β illustrated by the different researchers.

Table 3
Studies on determining the tensile strength of different anisotropic rock masses.

Rock type	β	TS at β		Results	Anisotropy shape	Ref.
	(Degree)	Lowest	Highest			
Granitoidic gneiss	0, 15, 30, 45, 60, 75, 90	60	0	Fig. 18a	Semi-U-shape	[128]
Serpentinous schist		75	0	Fig. 18b		
Sandstone	0, 15, 30, 45, 60, 75, 90	75	45 and 30	Fig. 18c	Wave-shape	[137]
Sandstone	0, 15, 30, 45, 60, 75, 90	80	0	Fig. 18d	Wave-shape	[135]
Shale	0, 15, 30, 45, 60, 75, 90	15	60	Fig. 18e	Wave-shape	[129]
Slate	0, 15, 30, 45, 60, 75, 90	30	75	Fig. 18f	Semi-U-shape	[97]
Sandstone	0, 15, 30, 45, 60, 75, 90	15	60	Fig. 18g	U-shoulder-shape	[130]
Pyrophyllite		0	75			
Dry quartz–mica schist	0, 15, 30, 45, 60, 75, 90	20–30	90	Fig. 18h	Wave-shape	[132]
Saturated quartz–mica schist		45	0	Fig. 18l		
Shale	0, 15, 30, 45, 60, 75, 90	75	15	Fig. 18j	Shoulder-shape	[131]
Coal		60	0	Fig. 18k		
Layered sedimentary	0–90 with a step of 10	20	70	Fig. 18m	Wave-shape	[134]
Limestone1						
Limestone2						

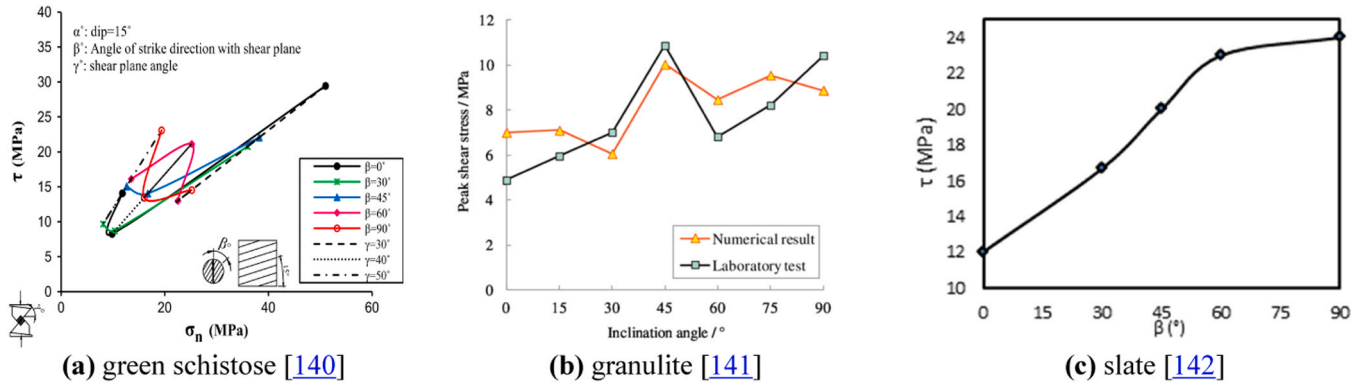

Fig. 19. Anisotropic rock mass shear behavior (shear strength) with the variation of β, illustrated by the different researchers.

Table 4
Studies on shear strength (SS) of different anisotropic rock masses.

Rock type	β	SS at β		Results	Anisotropy shape	Ref.
	(Degree)	Lowest	Highest			
Green schistose	0, 30, 45, 60, 75, 90	0	90	Fig. 19a	Wave-shape	[140]
Granulite	0, 15, 30, 45, 60, 75, 90	0	90	Fig. 19b	Wave-shape	[141]
Slate	0, 15, 30, 45, 60, 75, 90	0	90	Fig. 19c	Semi- shoulder-shape	[142]

Mass Rating), which take into consideration rock strength, environmental, and discontinuity factors. Table 5 represents the chronological evolution of RMCSs, highlighting key developments since 1946. The applications of RMCSs are presented in Fig. 20. This diagram illustrates the integration of empirical and numerical approaches in geotechnical engineering. It demonstrates how RMCSs play a crucial role in the discipline, primarily through various systems, including the Q-system, RMR, Q-slope, SSR, and GSI.

Despite their extensive use, the assumption of isotropy in classification systems such as RMR, Q-system, and GSI limits their usefulness in complex geological environments. Additionally, under anisotropic conditions, GSI has significant limitations. More recent systems, such as ARMR [16] and A-BQ [147]. They are specialized for geological or engineering conditions, with updated considerations for anisotropic behaviour. However, most systems rely heavily on subjective visual observations, which introduce variability, mainly where multiple experts interpret the same features [148]. Although technological advances, e.g., geophysics and remote sensing, have increased the data available for rock mass characterization, no system has fully integrated these tools into its method [149].

Classification systems are widely used in design applications for underground projects, where they help determine the quality of rock masses and the need for support systems. Also, rock mechanics studies have been essential in accurately determining the numerical values associated with these systems. In commonly used rock mass classification methods, such as the RMR and Q systems, up to six parameters are considered to classify a rock mass, providing pragmatic recommendations for excavation support and safety measures. Both of these methods usually consider rock masses to be isotropic in their assumptions, minimizing their capacity to manage complicated anisotropic characteristics [182,183].

Despite their broad adoption, these direct design tools remain dependent on subjective visual assessments, leading to variability in rock mass evaluations when different experts interpret the same geological features [184,185]. An empirical rock slope engineering technique called Q-slope is used to evaluate the stability of rock slopes excavated in the field [145,146]. Q-slope, designed for use in opencast mine benches or road or railway cuttings without reinforcement, enables geotechnical engineers to potentially modify slope angles as rock mass conditions change during construction [178,186]. The SSR (Slope

Table 5
Evolution of rock mass classification systems.

Year	Classification System	Author(s)	Ref.
1946	Rock load classification system	Terzaghi	[150]
1958	Stand-up time classification	Lauffer	[151]
1964	RQD (rock quality designation)	Deere	[152]
1964	Japanese rock mass classification system (Denken system)	Tanaka	[153]
1965	Kiruna factor	Hansagi	[154]
1972	RSR (rock structure rating)	Wickham	[155]
1973	RMR (rock mass rating)	Bieniawski	[156]
1974	Q-System (rock mass quality)	Barton et al.	[157]
1974	IRMR (In situ rock mass rating)	Jakubec and Laubscher	[158]
1977	MRMR (mining RMR)	Laubscher	[159]
1978	SRMC (sydney rock mass classification)	Pells	[160]
1980	RMS (rock mass strength)	Selby	[161]
1984	SMR (slope mass rating)	Romana	[162]
1988	SRMR (slope RMR)	Robertson	[163]
1994	MQD (Marble quality designation)	Chan et al.	[164]
1995	N (Rock Mass number)	Goel et al.	[165]
1995	CMRR (coal mine roof rating)	Molinda & Mark	[166]
1995	CSMR1(Chinese system for SMR)	Chen	[167]
1996	RMi (rock mass index)	Palmström	[168]
1996	M-RMR (modified RMR)	Ünal	[169]
1997	GSI (geological strength index)	Hoek and Brown	[170]
1998	Chinese standard for engineering classification of rock masses	Lin Yunmei	[171]
1999	TSR (total stability rating)	Benumof and Griggs	[172]
2002	SSPC (slope stability probability classification)	Hack	[173]
2006	GBI (geotechnical blockiness Index)	Walker and De Bruyn	[174]
2007	MSMR (modified slope mass rating)	Tomás et al.	[175]
2010	SSR (slope stability rating)	Taheri & Tani	[176]
2014	RMQR (Rock mass quality rating)	Aydan et al.	[177]
2015	Q-slope	Barton and Bar	[178]
2018	SSAM (slope stability assessment methodology)	McQuillan et al.	[179]
2019	ARMR (anisotropic RMR)	Saroglou et al.	[16]
2019	I-System (index of ground-structure)	Bineshian	[180]
2019	A-BQ (anisotropic-basic quality)	Guo et al.	[147]
2021	DRMR (directional RMR)	Maazallahi and Majdi	[181]

Stability Rating) method investigates the stability of rock slopes on a large scale by combining five other parameters with GSI to make it more suitable for jointed rock mass conditions. It provides design charts for proposing stable excavation slopes based on safety factors, facilitating easy implementation in engineering practice. The reliability of SSR has been established by comparing it to other methods in several field cases in different areas to affirm its reliability in field slope stability analysis [176].

Estimating rock mass design parameters can be achieved using the GSI in conjunction with the Hoek-Brown failure criterion. This RMCS application is referred to as an indirect design application. To connect empirical observations with the mechanical characteristics of rock, GSI is a crucial element in the computation of the deformation modulus and strength in numerical modeling [187]. The Q system may be adopted for estimating GSI by appraising the conditions of joints and the volume of rock blocks, which are critical for ascertaining the strength of rock masses [188]. These methodologies evaluate variables, including the density of discontinuities, the dimensions of blocks, and the conditions of joint surfaces, and have been integral to engineering design, particularly in the analysis of slope stability and subsurface structures [156, 189].

The GSI quantification often relies on qualitative evaluations, leading to variability among novice engineers. The empirical approaches for determining GSI values may inadequately represent actual geological conditions, prompting questions regarding their objectivity [190]. Fig. 21a-e shows applications of the GSI chart to exposed faces in a range of rock formations. The original purpose of the GSI chart was to provide a guide for the initial estimation of rock mass properties. It was always assumed that the user would improve the initial estimates with more detailed site investigations, numerical analyses, and back analyses of the tunnel or slope performance to validate or modify them [191]. Fig. 22 superimposes rock types from field studies onto the original qualitative GSI table, revealing a geological trend opposite to the commonly accepted GSI contour lines. None of the proposed GSI quantification methods can be defined as being bias-free since they all primarily rely upon qualitative information that is impacted by subjective interpretation (engineering judgment does not necessarily provide an objective perspective) [190].

Hoek and Brown (H-B) failure criterion, which is the primary method to define rock mass strength using GSI, does not apply to anisotropic rock mass conditions. This limitation may lead to oversimplification of the evaluation and incorrect predictions for complex geological settings such as tunnels or slopes in layered rocks [16]. Fig. 21f illustrates the influence of scale on rock mass anisotropy and, therefore, the application of the H-B failure criterion.

All the quantification methods proposed in the literature build upon the original GSI table and, contrary to expectations, do not truly reflect the role of geology. Besides, relying on qualitative parameters such as block shape and surface conditions introduces subjectivity, particularly in settings where anisotropy is a dominating effect [192]. ARMR offers another alternative that includes anisotropy-associated parameters in rock mass classifications to tackle the limitations of typical classification systems, as presented in Table 6. The system accounts for the influence of anisotropy on both failure and stress mechanisms and, therefore, is

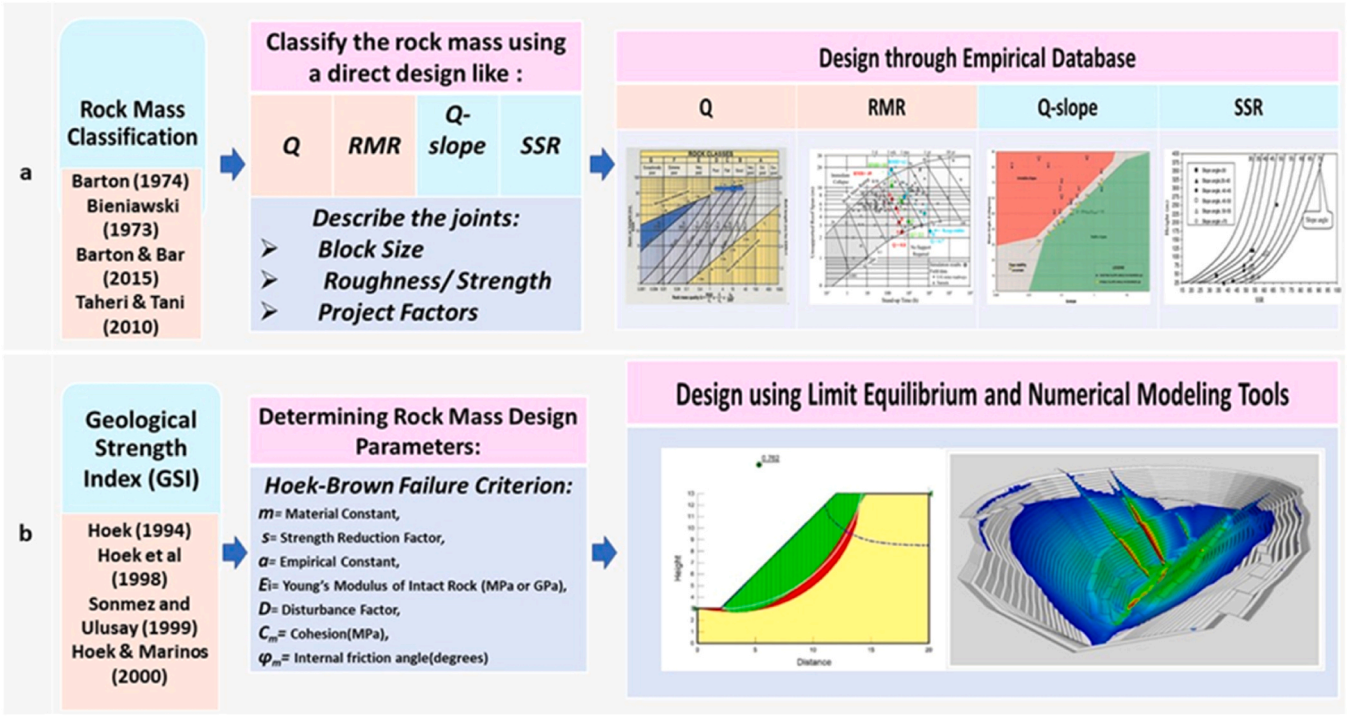

Fig. 20. Application of rock mass classification systems in rock engineering.

more suitable for anisotropic conditions [16]. This is more pronounced for anisotropic blocky rock masses with persistent joints or tectonically disturbed fabric, where traditional GSI may underestimate or incorrectly represent mechanical behaviors [193]. However, its validity for real applications has not been proven yet.

With this classification, which includes anisotropy within the classification of rock masses, it would be possible to use the modified H-B failure criterion for the determination of the strength of anisotropic rock masses without any measurement or correction according to the total value that would be computed for ARMR [16]. This is based on the fact that anisotropy of strength in anisotropic rock masses is associated with (1) intact rock strength anisotropy and (2) the structure anisotropy of rock masses, both of which have been considered in ARMR. This failure criterion is defined as the following equations to determine the anisotropic rock masses' strength [146]:

$$\sigma_1 = \sigma_3 + \sigma_{ci,\beta}\left(k_\beta\left(m_{b,an}\left(\frac{\sigma_3}{\sigma_{ci,\beta}}\right) + s_{an}\right)\right)^a \tag{1}$$

$$m_{b,an} = m_i \exp\left(\frac{ARMR - 100}{28 - 14D}\right) \tag{2}$$

$$s_{an} = \exp\left(\frac{ARMR - 100}{9 - 3D}\right) \tag{3}$$

$$a = 0.5 + \frac{1}{6}\left(e^{-ARMR/15} - e^{-20/3}\right) \tag{4}$$

$$\sigma_{cm,an} = \sigma_{ci,\beta}\left(\frac{\left(m_{b,an} + 4S_{an} - a(m_{b,an} - 8s_{an})\right)\left(m_{b,an}/(4 + s_{an})\right)^{a-1}}{2(1+a)(2+a)}\right) \tag{5}$$

Where σ_1: "major principal stress at failure," σ_3: "minor principal stress at failure," $\sigma_{ci,\beta}$: intact rock UCS at β, the anisotropy orientation, $m_{b,an}$: "reduced value of m_i parameter for anisotropic rock mass," s_{an} and a stand for the constants associated with the anisotropy orientation," m_i: dimensionless H-B material constant for intact rock, D: disturbance factor, and $\sigma_{cm,an}$: strength of the anisotropic rock mass.

5. Anisotropic rock mass simulation and design

5.1. Constitutive models

Anisotropic failure criteria are crucial for accurately estimating the strength of rocks with varying degrees of anisotropy. A "failure criterion" is an equation that explicitly or implicitly defines the maximum principal stress required to cause the rock to "fail." In the case of brittle behavior, this failure is interpreted as the rock breaking along one or more failure planes [194]. A failure criterion for anisotropic rocks should incorporate inherent direction-dependent strength characteristics, providing a comprehensive model that accurately captures both the nonlinearity and the anisotropic nature of their responses [195,196]. Table 7 summarizes failure criteria for continuous and discontinuous materials, which are divided into mathematical and empirical methods. It lists influential researchers and their contributions, showcasing classic and recent advancements [197].

Continuous approaches focus on modeling the gradual failure of materials, accounting for the consistent behavior of anisotropic materials under varying stress or strain conditions. These approaches aim to describe failure as a progressive process, maintaining continuity in the predicted material response without abrupt changes or discontinuities [198]. Pietruszczak and Mroz introduced an approach known as the critical plane approach (CPA) to describe the strength anisotropy of geological materials [199]. While being useful in accounting for the anisotropic condition in rock masses, it requires a well-defined anisotropic strength envelope, which allows CPA to search for orientations to find the weakest plane. Therefore, it can be considered a data-intensive criterion, showing its limitation. The strength criteria for anisotropic rocks developed by previous researchers generally enable the precise prediction of experimental outcomes [2,123,200–202]. These methods often require many triaxial tests to calibrate the failure criterion parameters. A practical criterion should enable accurate strength prediction even with a limited amount of triaxial compression data [198].

The continuous model with equivalent properties may be appropriate for a heavily jointed rock mass without a definite orientation. For a jointed rock mass with a few structural planes with definite directions,

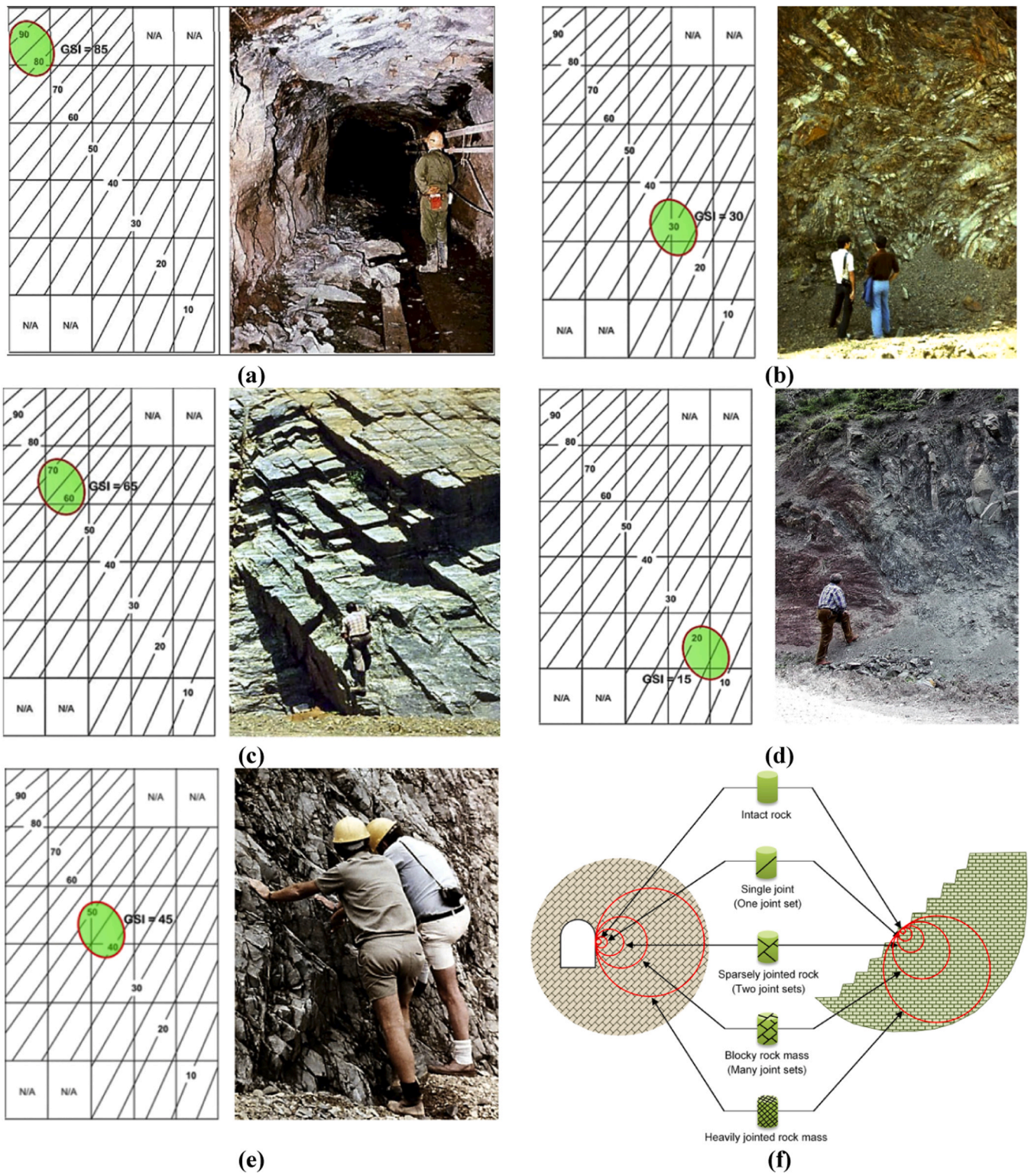

Fig. 21. Applications of the GSI chart to exposed faces in a range of rock formations and scale effects in rock mass characterization: (a) spalling in the sidewalls of a mine tunnel in intact hard rock subjected to anisotropic horizontal stresses [191]; (b) complex folding in a bedded sedimentary deposit [191]; (c) orthogonal jointing in granitic rock on a dam site [191]; (d) tectonically deformed sediments with almost complete loss of structural patterns [191]; (e) interlocking angular Andesite blocks defined by several joint sets, exposed in an open pit mine bench [191]; and (f) effect of scale on rock mass anisotropic conditions [4].

A	1	Sandstone (Massive or bedded, no clayey cement present)
	2	Sandstone (brecciated, no clayey cement present)
B	1	Siltstones, claystone, and clay shales (bedded, foliated, fractured)
	2	Siltstones, claystone, and clay shales (sheared, brecciated)
C	1	Limestone (massive)
	2	Limestone (thin bedded)
	3	Limestone (brecciated)
D	1	Fresh granite
E	1	Sound gneiss
F	1	Strong schist (ex; micaschists)
	2	Weak schists (ex, chloritic schists, phyllites)
	3	Sheared schist
G	1	Ophiolite (massive strong peridotite with widely spaced discontinuities)
	2	Ophiolite (good to fair quality peridotite or compact serpentinite with discontinuities)
	3	Ophiolite (schistose serpentinite)
	4	Ophiolite (poor to very poor-quality sheared serpentinite)

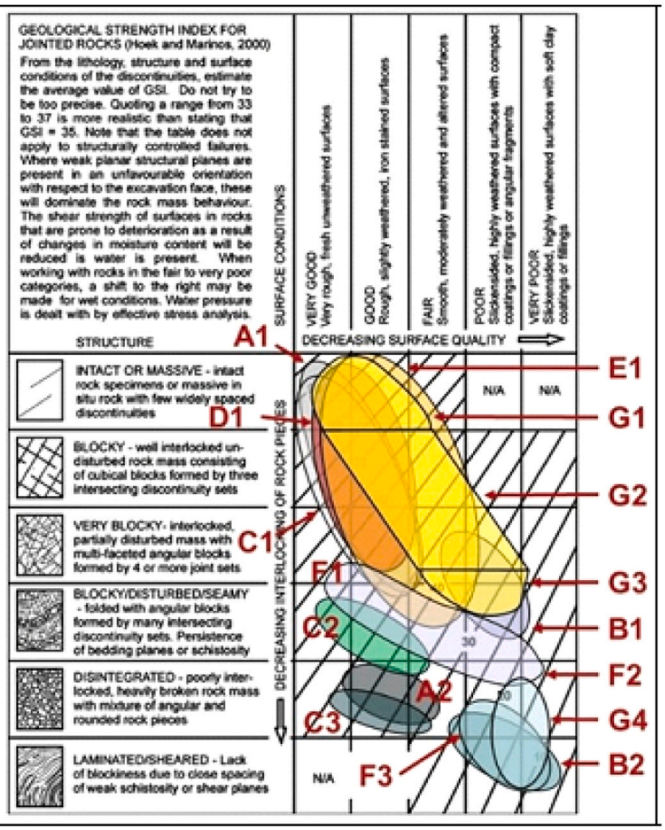

Fig. 22. GSI chart with superimposed geology of different case studies [190].

the discontinuum model or methods to consider the specific discontinuities are necessary. Naturally, a rock mass contains multiple joints and fractures as a discontinuous material. The behavior of a rock mass has been recognized to be significantly affected by the formation of complex discontinuities. These potential instabilities are dominated by the rock matrix's physical and mechanical parameters and its discontinuities [243]. Numerous failure criteria have been developed for assessing anisotropic rocks in recent decades. Jaeger [218] suggested that the cohesion of rocks changes with the orientation angle, while the friction angle remains constant [235]. Hoek and Brown [2] proposed that the strength parameters m_b and s, in their widely adopted failure criterion, vary with the direction of loading and provided expressions for these constants.

5.2. Numerical simulation approaches

Failure (including displacements and stresses) analyses for anisotropic rock masses, as part of stratified/layered rock masses, require taking into account different variables rather than isotropic material modeling methods, as such media can demonstrate a wide range of failures, including squeezing, spalling, wedging, brittle failures, and so on, resulting in more challenging issues compared to isotropic conditions [244]. Two primary methodologies for simulating rock-like materials are continuum and discontinuum modeling. Various methods have been employed to assess the failure mechanism in these materials, ranging from theoretical and numerical modeling to laboratory investigations and field observations.

Theoretical models, such as the "voussoir beam model" [245] and the "clamped beam model" [246] provide examples for assessing the surrounding anisotropic rock masses' failure processes. The analytical and semi-analytical models to evaluate the induced displacements and stresses in the structures being built in anisotropic rock masses include regular [247–249] or arbitrary [250–252] openings and the lining system deformation [253,254]. It should be mentioned that there are not many analytical methods available because the problem related to anisotropic rock masses would be more complex and non-linear due to their inherent directional properties. On the contrary, numerical simulation offers more convenient, time- and cost-effective, and comprehensive insights into the situation where the problem is complex, requiring thorough analyses.

Various numerical simulation methods have been employed over the last decades to investigate the failure processes in anisotropic rock masses, including (1) the Finite element method (FEM), employing Phase2 (RS2 since 2015) [255,256], (2) the Finite difference method (FDM), using 3-dimensional Fast Lagrangian Analysis of Continua (FLAC3D) [15,251,257]; (3) the Discrete element method (DEM) by the 3D distinct element code (3DEC) [258–260], the Universal DEC (UDEC) [261–263], the particle flow code (PFC) [264–266], PFC3D-grain-based model (GBM) simulation [267], and expanded DEM (EDEM) [268]; (4) the Discontinuous deformation analysis method (DDA) [246,269]; (5) the Realistic Failure Process Analysis Method (RFPA) [19,270]; (6) the hybrid finite-discrete element method (FDEM) [271–273], including ELFEN [274]; (7) the Rigid-body-spring network (RBSN) [275]; and (8) the Discrete Fracture Network (DFN) [276,277]. Field observations are generally employed for particular cases, since the condition should be modified based on the project [278]. Therefore, the limited, time-consuming, and expensive nature of their applications hinders the development of a universal model for deep underground excavation [279]. Moreover, observational methods are limited in their ability to monitor entire failure processes, as they can only identify specific failures in anisotropic rock masses, such as bulking, spalling, and slippage. However, these methods can be used to verify or calibrate the theoretical or numerical modeling findings [257,280].

Numerous researchers have employed numerical methods, DEM and FDEM, to simulate so-called fractured, layered, or stratified rock masses. To specifically address the anisotropy effect in the FDEM modeling

Table 6
Anisotropic rock mass rating (ARMR) classification [16].

R_c, Strength anisotropy degree		≤ 1.1	1.1 – 2	2 – 3	3 – 5	≥ 5	
Description		Isotropic	Low	Moderate	High	Very High	
Rating		**20**	**17**	**13**	**8**	**3**	
UCS (MPa)	> 250	100 – 150	50 – 100	25 – 50	5 – 25	1 – 5	< 1
Point load strength (MPa)	> 10	4 – 10	2 – 4	1 – 2	UCS required for low-strength material		
Rating	**15**	**12**	**7**	**4**	**2**	**1**	**0**
Spacing of anisotropic structure (mm)			> 1200	600 – 1200	200 – 600	40 – 200	< 40
Rating			**20**	**15**	**10**	**8**	**5**
RQD %	90 – 100	75 – 90	50 – 75	25 – 50	< 25		
Rating	**15**	**10**	**7**	**4**	**2**		
Condition of anisotropy surfaces	Very rough surfaces, not continuous, no separation, unweathered	Rough surfaces, separation < 1 mm, slightly weathered.	Slightly rough surfaces, separation < 1 mm, highly weathered	Slickensided surfaces or gouge-filled < 5 mm thick or separation 1–5 mm, continuous.		Soft gouge, > 5 mm thick or s separation > 5 mm, continuous.	
Rating	**15**	**10**	**7**	**4**		**0**	
Groundwater	Completely Dry	Damp	Wet	Dripping	Flowing		
Rating	**15**	**10**	**7**	**4**	**0**		
Adjustment of the total rating based on the confining stress range			Low in-situ stress		$\sigma_1/\sigma_c < 0.15$	No change in rating	
			Intermediate in-situ stress		$0.15 \leq \sigma_1/\sigma_c \leq 0.4$	Move one cell towards the left in R_c Rating (+5, +4, or +3)	
			High in-situ stress		$\sigma_1/\sigma_c > 0.4$	Move two cells towards the left in the R_c Rating	
ARMR Rating		**100 – 81**	**80 – 61**	**60 – 41**	**40 – 21**	**< 20**	
Class Number		I	II	III	IV	V	
Description		Massive or isotropic	Slightly anisotropic rock mass	Moderately anisotropic rock mass	Highly anisotropic rock mass	Very highly anisotropic to sheared rock mass	

process, researchers recommend the smeared method (see Fig. 23), which takes into account the relationship between cohesive strength-based variables in the fracture media and the angle, thereby facilitating bedding shear slip and rock matric failure [271–274,281,282]. However, this method has its own limitations, mainly when dealing with support system design issues and determining input parameters, which can be challenging [283]. Deng et al. conducted numerical simulations using FDEM to evaluate the failure mechanism in layered rock masses, considering their anisotropy and the impact of various mechanical parameters [284]. They concluded that the failure in the surrounding rock mass of the underground opening transitions from composite failure to a V-shaped notch failure, followed by spalling in the bedding plane. This phenomenon occurs when the strength of the rock mass, the in-situ stress lateral pressure coefficient, and bedding thickness increase or when the opening span decreases. Additionally, they noted that the impact of the elastic modulus is negligible, whereas the effect of the rock mass layers' dip angle is sophisticated and requires more in-depth analyses.

Table 7
Different failure criteria of anisotropic rock mass [194].

Continuous criteria		**Discontinuous Criteria**	
Mathematical approach	**Empirical approach**	**Mathematical approach**	**Empirical approach**
Von Mises (1928) [203]	Casagrande and Carrillo (1944) [217]	Jaeger (1960) [228]	Walsh and Brace (1964) [229]
Hill (1948) [204]	Jaeger (1960) [218]	Walsh and Brace (1964) [229]	Hoek (1964, 1983) [237,238]
Olszak and Urbanowicz (1956) [205]	McLamore and Gray (1967) [219]	Smith and Gilbert (2007) [230]	Ladanyi and Archambault (1972) [239]
Murrell (1965) [206]	Smith and Cheatham (1980a) [220]	Backers (2010) [231]	Bieniawski (1974) [240]
Goldenblat and Kopnov (1966) [207]	Ramamurthy et al. (1988) [106]	Pramanik and Deb (2015) [232]	Hoek and Brown (1980) [2]
Boehler and Sawczuk (1977) [208]	Ashour (1988) [221]	Asadi and Bagheripour (2015) [197]	Yoshinaka & Yamabe (1981) [241]
Tsai and Wu (1971) [209]	Zhao et al. (1992) [222]	Pei et al. (2018) [233]	Priest (1993) [35]
Pariseau (1981) [210]	Singh (1998) [223]	Pouragha et al.(2019) [234]	Ghosh and Daemen (1993) [242]
Dafalias (1979, 1987) [211]	Tien and Kuo (2001) [224]	Pan et al. (2019) [235]	Bagheripour et al. (2011) [52]
Allirot and Boehler (1979) [112]	Tien et al. (2006) [20]	Zhang et al. (2020) [236]	Mammoliti et al. (2022) [200]
Nova and Sacchi (1979) [212]	Tiwari and Rao (2007) [225]		Shi et al. (2016) [201]
Nova (1980) [213]	Sargolou and Tsiambaos (2008) [123]		Zhang et al. (2022) [202]
Boehler and Raclin (1982) [214]	Zhang and Zhu (2007) [226]		
Cazacu and Cristescu (1999) [215]	Lee et al. (2012) [227]		
Pietruszczak and Mroz (2001) [199]			
Mroz and Maciejewski (2011) [216]			

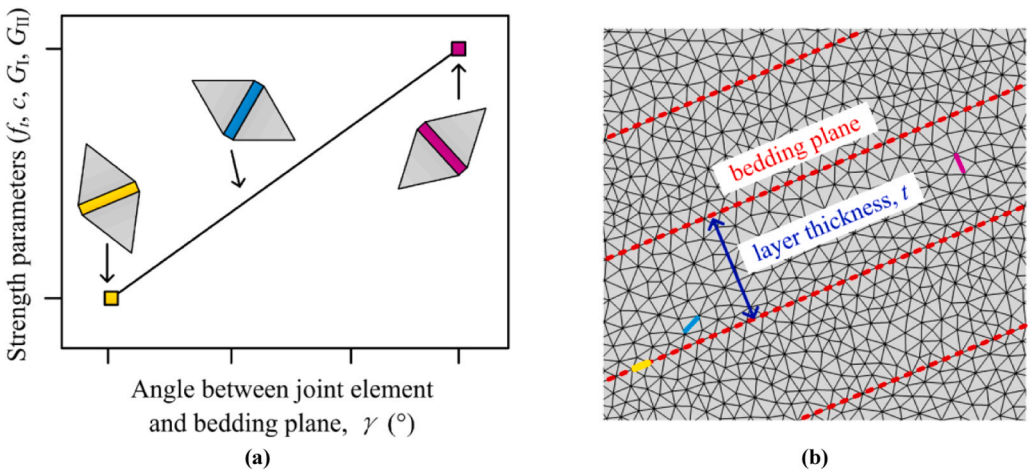

Fig. 23. The smeared method in FDEM [282]: (a) linear variation of strength-based variables with the angle between the joint and weakness plane; and (b) the meshing topology.

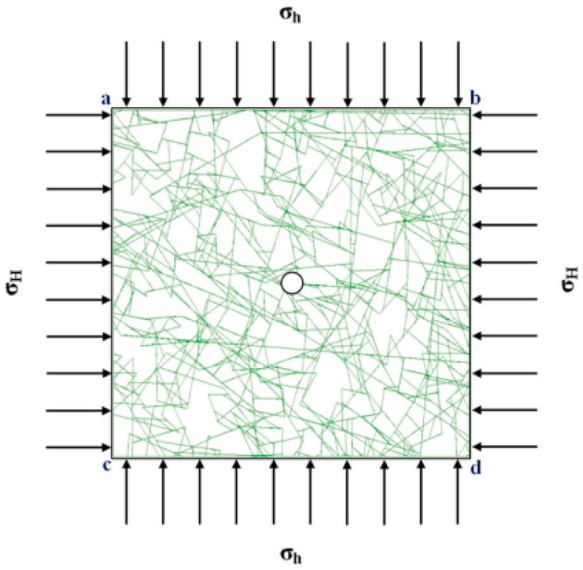

Fig. 24. DFN-DEM model to assess the induced stresses around the opening in fractured rock masses with different anisotropy degrees [276].

Furthermore, DFN is also introduced as a particular method based on DEM, in which large numbers of stochastic simulations are developed based on fracture systems [285]. Noorian-Bidgoli and Jing used DFN to determine the strength and uneven deformation of broken rock masses modeled in UDEC with various confining pressures [277]. They concluded that the strength and deformability of these kinds of media should be focused on the directions of in-situ stresses. Using the usual method of aligning the tunnel's axial direction with the direction of principal stresses might not be sufficient for safety management. Karimi-Khajelangi and Noorian-Bidgoli used a hybrid DFN-DEM numerical model (see Fig. 24) to look at stress levels around a crack in a rock mass with varying degrees of anisotropy, to know how this affected the induced stresses [276]. Their findings demonstrated that irregular joints' anisotropy in the rock mass leads to anisotropy in the induced stresses around the underground opening, a phenomenon not achievable with the Kirsch method.

Every model has its own capabilities and limitations. Both the voussoir and clamped beam models have limitations when explaining the failure processes in deep openings. Additionally, these models are limited to calculating elastoplastic-based deformations, which means they cannot estimate the crack initiation, propagation, and coalescence steps induced by the failure [246]. These restrictions also apply to FEM- and FDM-based simulations, mainly because they rely on continuum-based approaches. Additionally, when using FLAC3D for modeling in the FDM case, it is necessary to calibrate the ubiquitous joint constitutive model before initiating the simulation. This calibration indirectly creates anisotropy in the model [258].

When the discontinuous simulation methods, including UDEC, DDA, and so on, are used to model the anisotropic rock mass condition, the discontinuity or weakness plane is simulated as a "straight, continuous, and regular" element, which leads to different results compared to the actual status of these specific rock masses [269,286]. So, when UDEC is used to model the uneven rock masses, it's hard to model the failure in the rock's matrix, but it's easy to predict failures within the layers, like slippage, tension, and bending [258,287,288]. Different numerical models predict different failure modes, indicating a lack of a comprehensive or universal model for simulating anisotropic rock masses. However, numerical simulation categorizes five specific failure modes for this type of medium [284]: (1) V-shaped notch, (2) weakness plane

Table 8
Influential parameters are used in the design of anisotropic rock masses [284,289].

Parameter	Unit	Parameter	Unit
Bulk density	kg/m^3	Cohesion parallel to weakness plane, c_{min}	MPa
Young's modulus parallel to the weakness plane, E	GPa	Cohesion perpendicular to weakness plane, c_{max}	MPa
Young's modulus perpendicular to the weakness plane, E′	GPa	Type I fracture energy parallel to weakness plane, $G_{I,\ min}$	J/m^2
Poisson's ratio parallel to the weakness plane, ν	-	Type I fracture energy perpendicular to weakness plane, $G_{I,\ max}$	J/m^2
Poisson's ratio perpendicular to the weakness plane, ν'	-	Type II fracture energy parallel to weakness plane, $G_{II,\ min}$	J/m^2
The time step for tunnel excavation simulation, Δt	s	Type II fracture energy perpendicular to weakness plane, $G_{II,\ max}$	J/m^2
Average element size, h	m	Internal friction angle	Deg
Shear modulus, G'	GPa	Sliding friction angle	Deg
Tensile strength parallel to weakness plane, $f_{t,\ min}$	MPa	Normal contact penalty, P_n	GPa
Tensile strength perpendicular to weakness plane, $f_{t,\ max}$	MPa	Tangential contact penalty, Pt	GPa

Table 9
Case Studies of anisotropic rock masses and their geological characterization and design details.

Name; Ref.; Figure	Rock Mass Conditions	Design Data Determination	Design Approach	Remark
Ballarat Gold Mine (Australia) [258] Fig. 25	Interbedded sandstone, siltstone, shale, and quartz rock mass	Intact rock and joint properties have been derived/calibrated by experiment and 3DEC simulations, incorporating a bedding plane with two orthogonal, non-persistent joint sets	FLAC3D has been utilized to simulate the rock mass. Ubiquitous Joint Rock Mass (UJRM) and Subiquitous models were employed to consider the influence of anisotropy on the induced deformation and yielding	While employing the subiquitous model to consider the impact, the properties of the material and weakness planes should be calibrated to prevent misleading interpretations
Westwood Mine (Canada) [290,298] Fig. 26	Strong to weak shaly rocks with time-dependent behavior, plus high anisotropy stemming from foliation	Point load test and UCS to define matrix and foliation properties, and engineering judgment	Utilizing FLAC3D to populate a "buckling scheme" in a continuum medium. Applying the virtual testing on the UJRM specimens and considering the anisotropic behavior through embedding ubiquitous joints, utilizing the Cave Hoek constitutive model with embedded ubiquitous joints	While assessing the buckling effect, the incorporated anisotropy influence exists in the rock mass, the destressing in the simulation process depends on the stress level, not making the stress magnitude equal to zero in "the buckled zone"
CSA Mine (Australia) [291] Fig. 27	Steeply dipping, thinly bedded siltstone	Lab testing was performed to measure UCS, which was loaded perpendicular to the foliation axis; core logging was performed to classify rock mass characteristics using GSI and Q'; back analysis and field observations were utilized to verify the findings	FLAC3D-based simulation through utilizing a strain softening constitutive model and considering strength anisotropy through embedding ubiquitous joints within a continuum model	While parallel and perpendicular excavation with respect to lamination has an almost apparent influence on stability, different orientations need more in-depth investigations to reach a general and consistent idea, instead of varying interpretations
Olkiluoto (Finland) [292] Fig. 28	Migmatites and gneisses rock mass with a well-developed, pervasive foliation and lineation	A database of foliation via "surface mapping of natural outcrops and of two investigation trenches" and pilot-cored drill holes using digital borehole-wall images such as BIPS and OPTV	Developing a rock mechanics foliation (RMF) number (0−3) to characterize the type and intensity variation of foliation in the heterogeneous and anisotropic rocks	Orientation, intensity, and type of foliation are the critical characteristics of foliation for the rock deformability, strength, and excavation disturbed zone (EDZ) analyses
Shirengou Iron Ore Mine (China) [296] Fig. 29	Biotite hornblende plagioclase gneiss, amphibolite plagioclase gneiss, and granitic gneiss, consisting of large-scale discontinuities	Mechanical properties were determined by using the Monte Carlo simulation to assess the DFNs based on probabilistic models and simulating compression tests in the RFPA2D; ShapeMetriX3D was used for the development of a 3D image of the exposed rock mass to determine geological characteristics	The mine was simulated in COMSOL Multiphysics (FEM-based simulation), incorporating the anisotropy of the properties and applying the Hoffman anisotropic strength criterion to examine the damage zone	Joint plane orientation plays a crucial role in the damage zone of anisotropic rock masses
Monte Seco Tunnel (Brazil) [295] Fig. 30	Fractured gneiss with potential rockfall due to the fracture sets and the metamorphic foliation	Geomechanical classification (RMR_{14}, Q, and GSI); fractures and foliations mapping using TLS; laboratory tests to determine intact rock properties; pull-off tests to measure rock mass tensile strength; direct shear tests on the rock mass; Barton-Bandis failure criterion is used for discontinuities	Integrated TLS-DFN-DEM to first map the fracture orientations, trace lengths, and end-point positions in the tunnel using TLS, followed by discontinuity analysis to develop the probability density functions for the diameters and orientations, and then utilizing 3DEC to construct DFNs, which were used to generate the continuous DFNs (C-DFNs); finally, using C-DFNs, the DEM models were populated employing the Coulomb-slip joint model	Further research on the mechanical behavior of interlock structures is recommended
Agnew Gold Mine (Australia) [293] Fig. 31	Sandstone and ultramafic conglomerates, with closely spaced bedding planes	Damage mapping and in-situ stress measurements using acoustic emissions, identification of major fault structures and their impact on stability, convergence monitoring using laser scanning	Combined elastoplastic numerical modeling with damage mapping and convergence monitoring to effectively manage and predict rock mass behavior under stress	Managing accelerated ground deformation at the Agnew Gold Mine requires a multifaceted approach combining damage mapping, numerical modeling, and continuous field monitoring
La Ronde and Lapa mines (Canada) [297] Fig. 32	Foliated rock masses with the presence of prominent structural features	Squeezing index measurement, foliation spacing, and frequency by scan lining, employing the Q-system to assign the joint alteration and a joint roughness number, and strain measurements with the wall-to-wall convergence measures	Numerical modeling using 3DEC and UDEC, simulation of foliation and block deformation, stress redistribution analysis, model calibration with field deformations, integration of empirical squeezing index, and reinforcement strategies	Distinct element modeling provides a better representation of squeezing mechanisms compared to continuum methods; explicit foliation modeling is essential for accurate failure simulation
Sishen Mine (South Africa) [294] Fig. 33	Banded Iron Formation and shale	Persistence measurements from high-density laser scanning and face mapping; structural mapping used for synthetic rock mass modelling	Snowden modified the anisotropic model utilized in the Slide software for slope stability analysis, incorporating rock bridges to refine the analysis	Including rock bridges in the analysis decreased failure probability from 14 % to 4 %, leading to improved slope design.
TBM Tunnels (Northern Norway) [280] Fig. 34	Coarse-grained granitic gneiss with foliation. Strength varied with foliation angles	In-situ stress determination and hydraulic fracturing, UCS, and indirect tensile strength tests on intact rock	2D and 3D elastic and plastic numerical models with RS2/3, FEM-based Numerical simulations with joint elements, and failure depth estimation were measured in the tunnel and compared to predictions from models. The empirical relationships were used to compare observed and predicted failure depths	Strength anisotropy impacts notch formation and brittle failure patterns

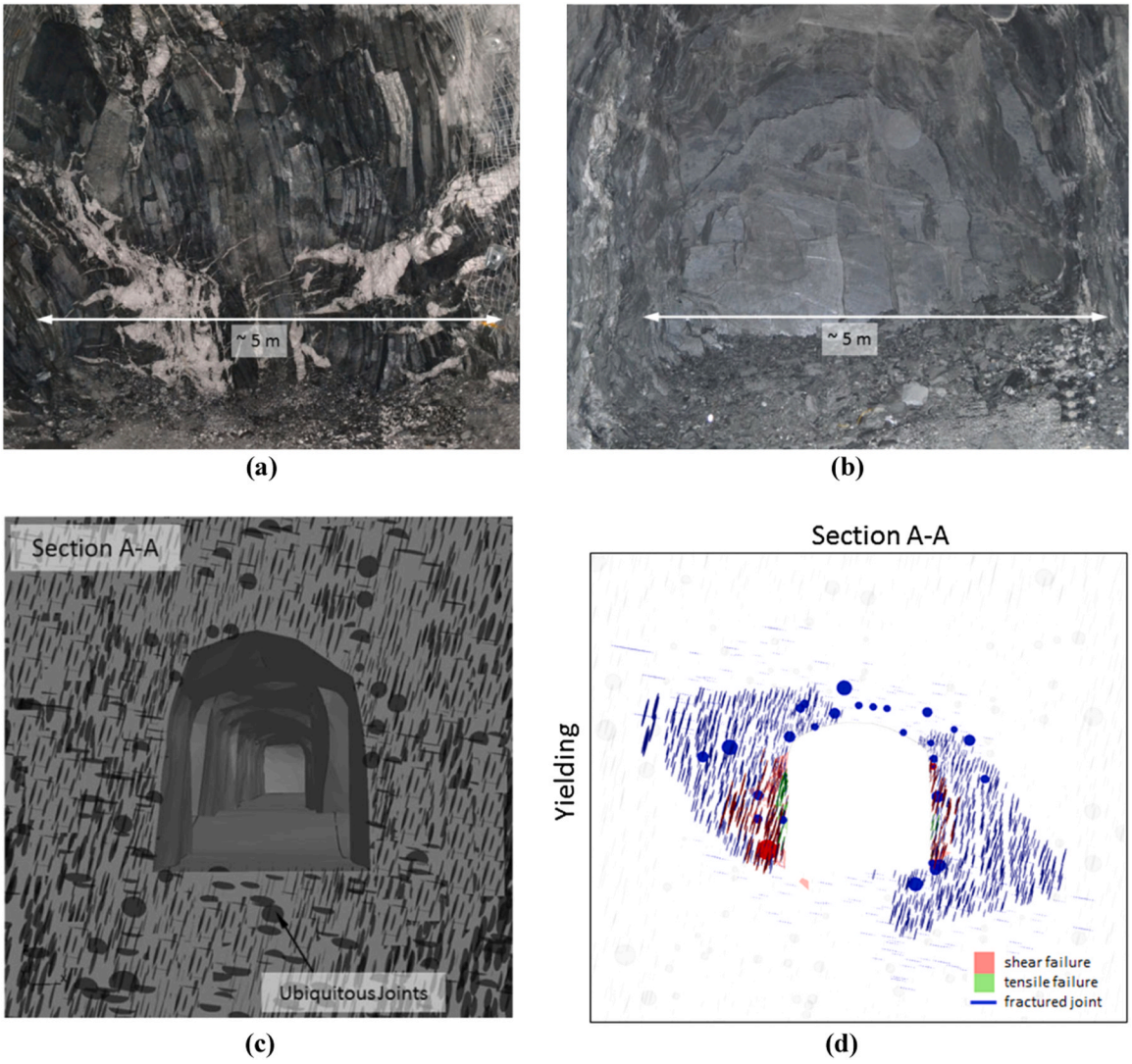

Fig. 25. Anisotropic rock mass at the Ballarat Gold Mine in Australia: (a) parallel bedding to excavation; (b) perpendicular to excavation; (c) FLAC3D model section A-A; and (d) induced yielding at section A-A [258].

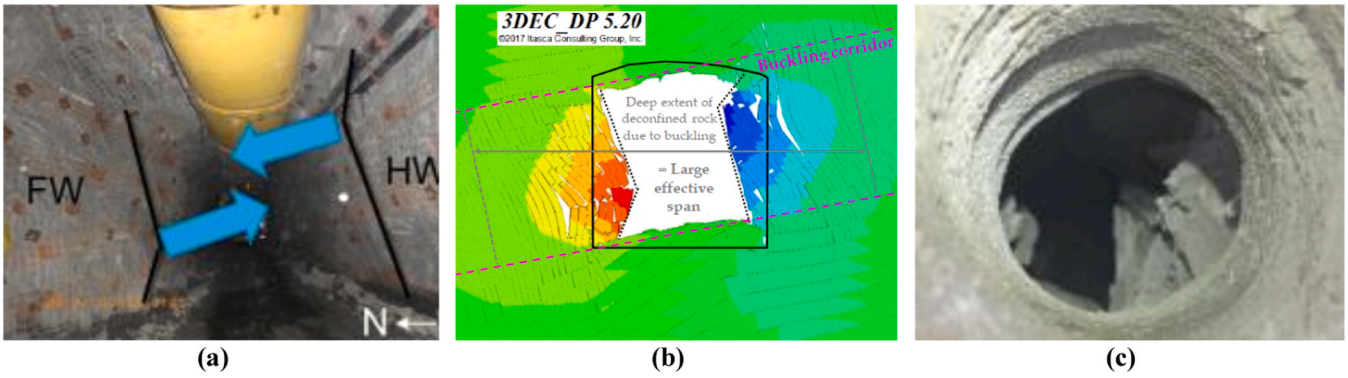

Fig. 26. Anisotropic rock mass at Westwood mine in Canada: (a) an example of buckling; (b) example of DEM model with emergent buckling; and (c) hole squeezing (courtesy of the mine) [290].

Fig. 27. Buckling and tensile fractures in tunnel sidewalls due to anisotropic rock mass aligned with foliation, driven by stress concentration, rotation, and poor rock quality in shear zones in CSA Mine in Australia [291].

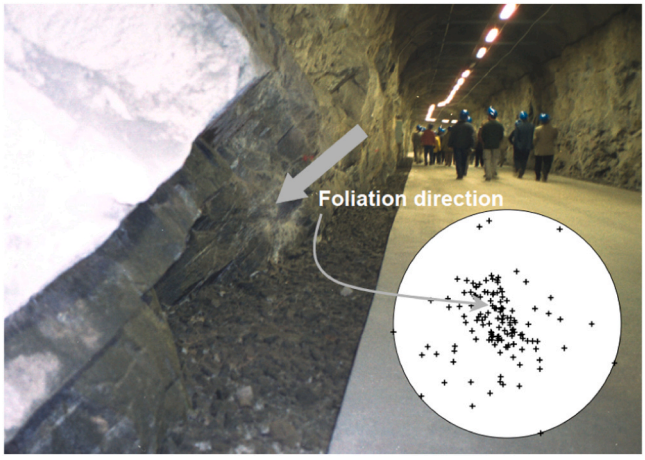

Fig. 28. The foliated rock mass in Olkiluoto (Finland) resulted in fractures aligning with the planar fabric [292].

spalling, (3) bedding's bending, (4) cutter failure, and (5) composite. These failures can occur due to various parameters, including bedding, mechanical behavior, environmental factors, etc. Therefore, taking into account the most significant influencing factors when simulating anisotropic rock masses can potentially yield more realistic results despite the complexity involved. Such parameters are presented in Table 8 for FDEM modeling as an example.

Although numerical modeling yields more acceptable results, it may present several challenges, including the selection of boundary conditions, the influence of mesh or zone size, and uncertainties in materials' constitutive models, all of which can lead to misinterpretations of stress redistribution, displacements, and failure localization in the simulated rock masses. A pivotal concern in numerical methodologies is validation, which ought to be performed as conditional verification of the simulation against independent data, rather than as evidence, due to the nonuniqueness inherent in Earth-system models. Moreover, disregarding scale effects further distorts predictions of confinement, strength, and dilatation. To alleviate these potential misinterpretations, employing an iterative model on in-situ stress, displacement, and microseismic data, along with probabilistic or deterministic calibration methods, provides the associated uncertainties in the results, thereby facilitating model verification.

6. Anisotropic rock mass case studies

Classification systems, numerical modeling, and field investigations are utilized to investigate and evaluate the stability of the openings in anisotropic rock masses. Continuous attempts to understand anisotropic behavior are necessary if excavation and support systems are to function adequately under site-specific geology. This section reviews several case studies relevant to the practical application of empirical and numerical modeling methods in anisotropic rock masses.

These cases, as presented in Table 9, encompass a range of geological properties, lithologies, and engineering challenges, illustrating how the various methods are applied in practice. These cases demonstrate that various geological conditions have induced anisotropy in rock masses, which should be considered and addressed accordingly during the project's site investigation and rock mass characterization phases. It can be noticed as examples that the rock mass in Ballarat Underground Gold Mine in Australia has been considered anisotropic due to inter-bedded sandstone, siltstone, shale, and quartz, as shown in Fig. 25 [258] or Westwood Mine in Canada, anisotropy stemming from foliation, as presented in Fig. 26 [290]; in CSA Mine in Australia, it is because of steeply dipping, thinly bedded siltstone, as illustrated in Fig. 27 [291]; in Olkiluoto in Finland, a well-developed, pervasive foliation and lineation created the anisotropy, as shown in Fig. 28 [292]; and so on that complete details of them have been presented in Table 9. Anisotropic rock masses characterization is a critical step towards design data determination of the projects, which can be done by various methods, including (1) geotechnical site investigation, such as core logging [291], borehole-wall images [292], in-situ stress measurement via acoustic emissions [293] and via Hydraulic fracturing [280], laser scanning [294], terrestrial laser scanning (TLS) for fractures and foliations mapping [295]; (2) experimental tests, such as point load test [290], and pull-off tests [295]; (3) classification systems, such as RMR_{14}, Q and GSI [295]. However, as discussed earlier, most classification systems have been developed for isotropic rock masses, which poses a significant challenge when applied to anisotropic rock masses. Nevertheless, several projects worldwide have utilized this classification.

Numerical modeling plays an important role and has a high capacity in improving the success of rock engineering projects in anisotropic rock masses for the design purposes of the openings before the excavation is started or during the excavation, as discussed earlier. Various numerical models have been utilized in different projects worldwide; for example, FLAC3D is used in mines like Ballarat (see Fig. 25d) [258], CSA Mine [291], or the FEM-based simulation framework of COMSOL, utilized in Shirengou Iron Ore Mine in China (see Fig. 29) [296]; or DEM-based modeling via UDEC and 3DEC in Westwood (Fig. 26b) [290] and in La Ronde and Lapa mines in Canada [297] to deal with anisotropic deformation and special calibration programs to avoid misrepresenting material properties.

The findings from the Olkiluoto project [292] highlight that a special classification must be used to describe the intensity and nature of foliation and understand the excavation-disturbed zone, the Shirenogou mine [296] illustrates how fracture networks and joint orientations strongly affect damage zones, adding weight to the concept that stability analyses need to quantify anisotropy strictly. The Monte Seco Tunnel case [295] emphasizes the value of high-resolution mapping methods such as TLS and DFN modeling in properly characterizing rock mass behavior and predicting failure mechanisms. Additionally, anisotropy profoundly influences mechanical behavior, as observed in the La Ronde and Lapa mines [297], where foliation orientation directly controls strength and deformation properties. This geological complexity and induced stress relationship mandate the development of adaptive mitigation strategies, including reinforcement techniques, redirection of

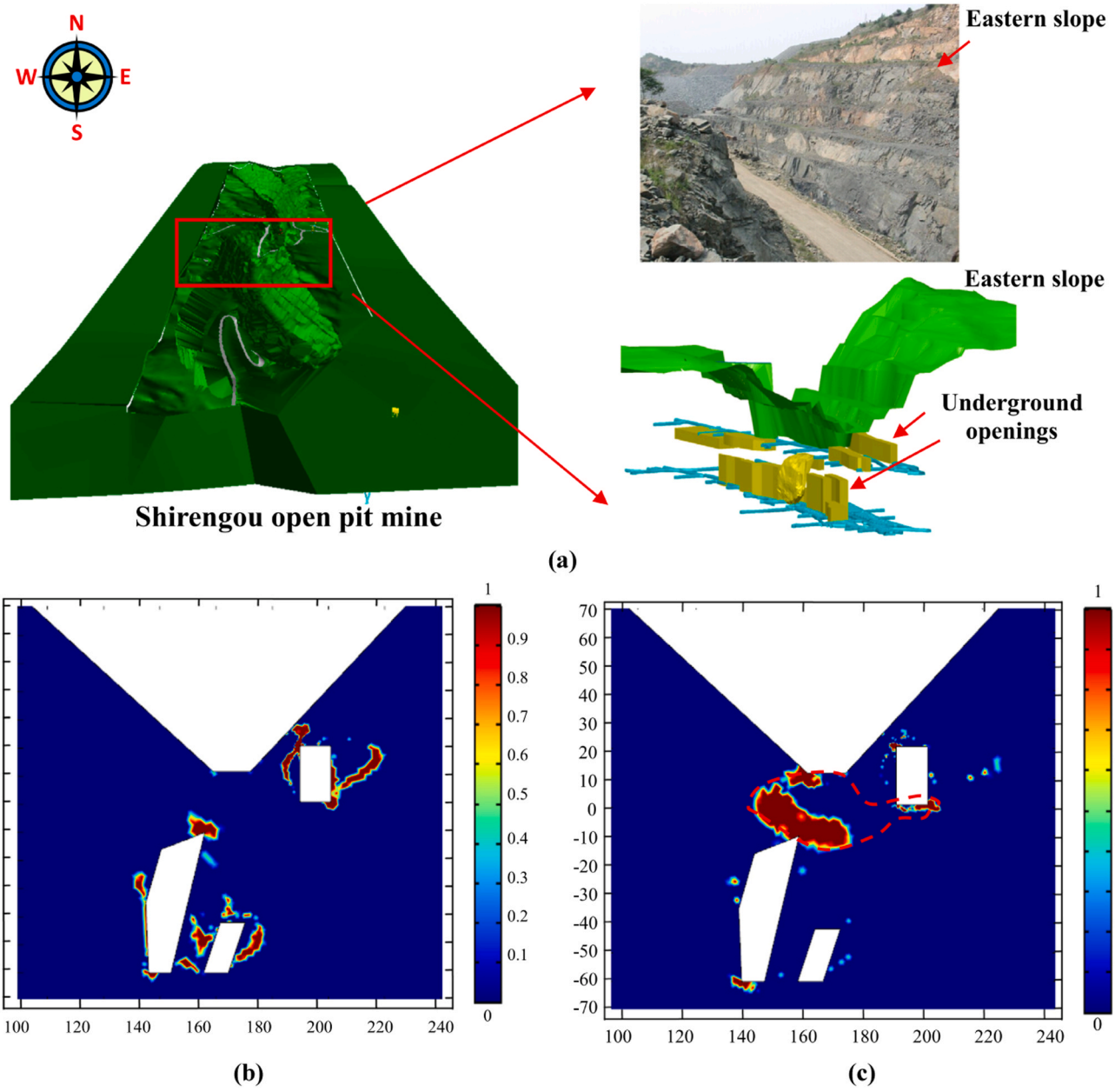

Fig. 29. Shirenogou Iron Ore Mine in China: (a) open pit and underground openings, China; (b) damage zone in isotropic condition; and (c) damage zone in anisotropic condition [296].

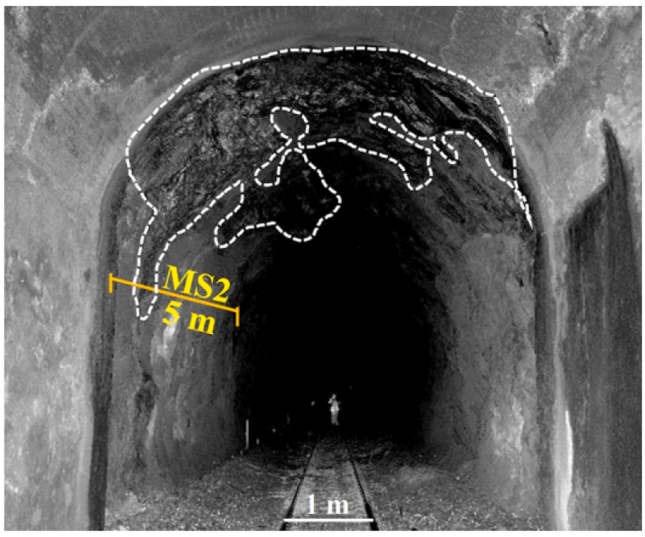

Fig. 30. Influence of foliation planes and wet rock faces on the stability and structural behavior of the Monte Seco Tunnel in Brazil [295].

drifts, and modifying ground support, as illustrated in the dynamic approach employed at the Agnew Gold Mine to manage ground deformation [293]. (Figs. 30–34)

7. Conclusion

The mechanical behaviors of anisotropic rock masses mainly depend on their inherent structural properties, which often govern their strength and deformations and should be considered in engineering design applications. Structural features such as foliation, bedding planes, and fractures introduce directional dependencies that render isotropic models of rock mass classifications unsuitable under these conditions.

The directional variations displayed in metamorphic, sedimentary, and igneous rocks, as well as the presence of secondary features such as faults and shear zones, further complicate stress distribution and failure modes. The directional dependence observed is due to an intrinsic geological property trend that together controls the strength, deformability, and permeability of the rock mass. These characteristics make anisotropy a constitutive problem in geotechnical engineering because they dictate subsurface systems' stability and failure mechanisms. The metamorphic rocks exhibit an intense anisotropic nature because of the

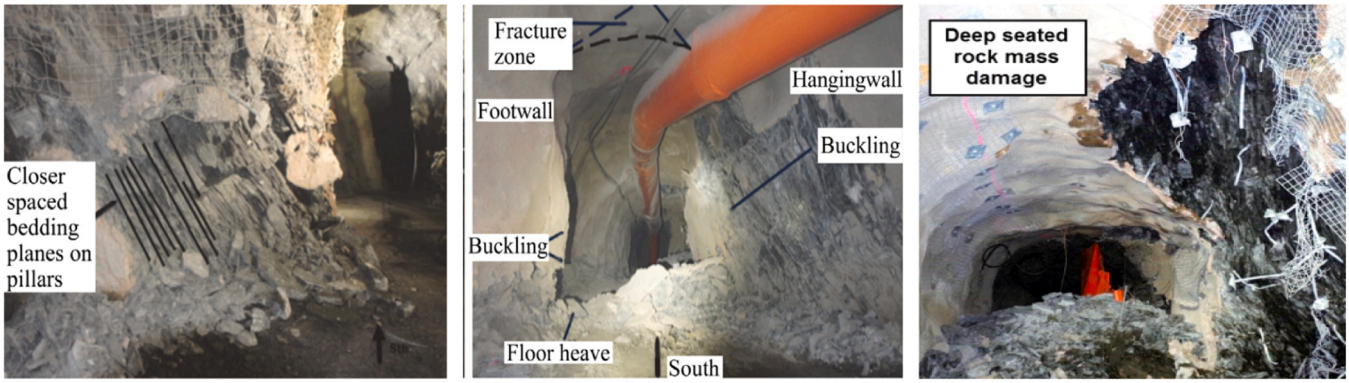

Fig. 31. Typical foliated structures in the Agnew Gold Mine in Australia: (a) footwall pillar; (b) access drive at a depth of 1200 m; and (c) rock mass damage [293].

Fig. 32. Squeezing conditions in La Ronde and Lapa mines in Canada: (a) pronounced squeezing, 2550 m depth; and (b) pronounced squeezing, 1790 m depth [297].

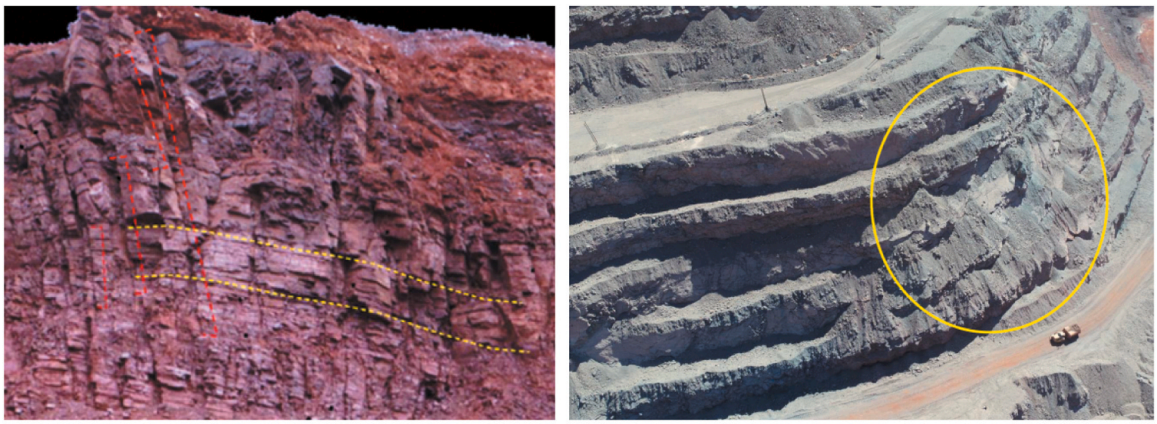

(a) (b)

Fig. 33. Design sector in the northern part of Sishen Mine in South Africa: (a) discontinuity persistence measurements; and (b) planar failure on bedding planes [294].

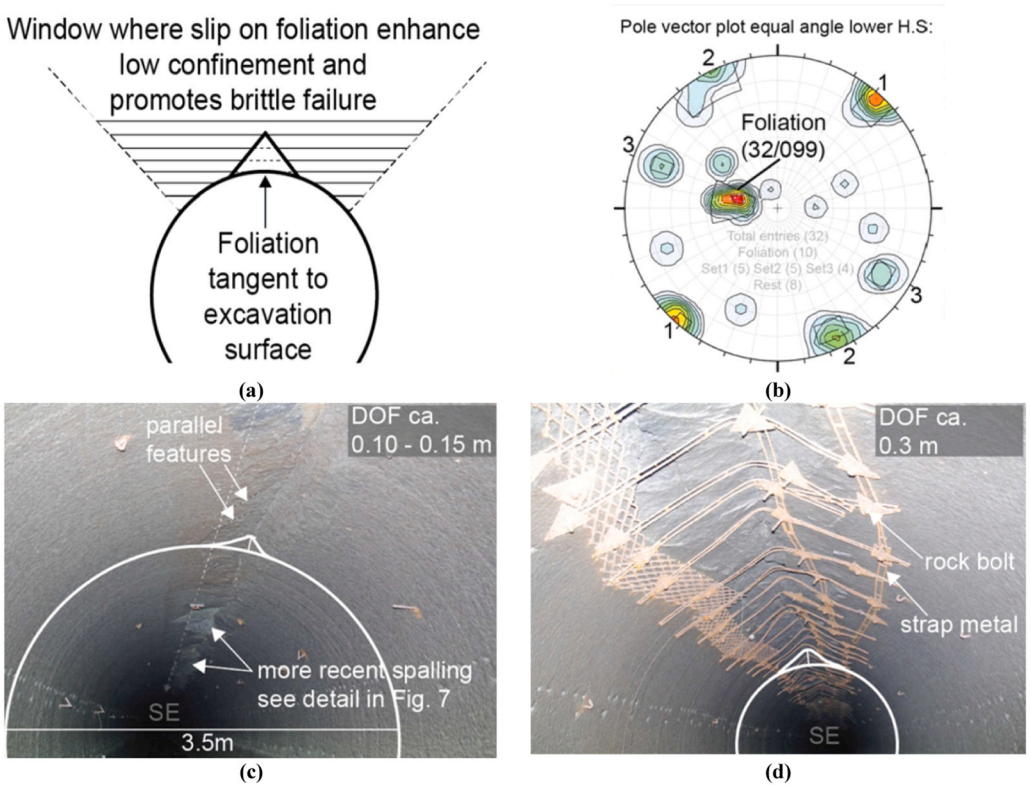

Fig. 34. Failure in tunnel boring machine (TBM)-excavating tunnel in Norway in anisotropic rock mass: (a) development of a V-shaped notch where the foliation is tangent to the excavation surface; (b) mapped dip/dip direction of foliation and fracture sets; (c) parallel features may be related to extensional fractures propagating parallel to the direction of r-max and perpendicular to the foliation strike; and (d) the angle between compression and dip of foliation in the crown lies within the range of intermediate angles [280].

mineral orientation under high-stress conditions. The sedimentary rocks, however, are anisotropic because of the formation of bedding planes and stratification. Igneous rocks may be anisotropic due to the dynamics of magma flow, the process of crystallization, and the effects of subsequent weathering. Classical isotropic model procedures often overlook the complexities of anisotropic rock masses, leading to discrepancies in stress estimation, stability analyses, and engineering design. Therefore, incorporating anisotropic features into classification systems, laboratory testing, and numerical analysis is necessary to enhance predictive models and optimize excavation designs.

Experimental and numerical studies confirm that the dip angle of the surrounding layered rock has a significant influence on deformation patterns. The mechanical behavior of rocks under anisotropic conditions can be assessed through basic rock mechanics laboratory tests, including UCS, TCS, BTS, and direct shear experiments. These tests should be conducted on samples containing different β angles between the loading direction and the weakness planes to reveal the anisotropic characteristics of varying rock parameters, such as compressive or tensile strength, the modulus of elasticity, and shear behavior. The results of such tests determine the excavation strike for the planes of weakness and help assess the impact of anisotropy on the stability and potential supporting systems required for the openings. Previously, it has been shown that in both UCS and TCS tests, the minimum strength may take place between $\beta = 30^{\circ}$ and $\beta = 45^{\circ}$. In comparison, its maximum value occurs

at $\beta = 0^\circ$ and $\beta = 90^\circ$, indicating the shear failure of rock under anisotropic conditions along the foliation with an angle of 30–45 degrees. Unlike the compression strength, no consensus or general conclusion exists for the tensile and shear strengths of anisotropic rocks, and there is a need for further research on these critical properties.

In addition to revealing the general failure behavior of the anisotropic rocks, the tests' results can be used to determine the design data, which would be used in the potential numerical simulations with various computations, such as FEM, DEM, FDEM, etc. The numerical modeling of anisotropic rocks, which involves simulating their tensile and shear strength properties, is not a standard or apparent methodology due to the inherent complexity of anisotropy. However, since the anisotropy characteristic plays a critical role in the stability of underground openings, especially deep ones, extensive research is needed to develop straightforward standardization for numerical simulations. Based on such simulations, this will help save project finances and avoid potential damage and instabilities.

RMCS evolved from early load-based approaches, such as Terzaghi's classification, to more comprehensive systems, including the RMR and Q-System, considering parameters like rock strength, stress conditions, and discontinuities. In underground engineering applications for direct design, Q-System and RMR are widely used to evaluate rock mass quality and inform the decision-making process for support system requirements. Under complex geological conditions, indirect design tools such as the GSI (Hoek–Brown failure criterion) can be utilized to estimate rock mass parameters. ARMR supplies anisotropy-related parameters in rock mass ratings to account for the influence of anisotropy on failure and stress processes and, therefore, is more suitable for anisotropic conditions.

The case studies demonstrate how rock mass anisotropy affects stability, emphasizing its importance as a key determinant of rock mass behavior and excavation design. The presented examples highlight the need for a combination of site investigation, advanced numerical modeling methods, and experimental confirmation to properly evaluate anisotropic rock mass characterization and response properly, enabling informed design decisions and preventing potential damage or collapse in underground openings. Notwithstanding, there is a substantial demand for establishing characterization, classification, and design methods and standards for the anisotropic rock masses.

CRediT authorship contribution statement

Ebrahim Ghorbani: Writing – review & editing, Writing – original draft, Visualization, Investigation. **Marjan Shahinfar:** Writing – original draft, Visualization, Investigation. **Abbas Taheri:** Writing – review & editing, Supervision.

Funding

This study is funded by the Natural Sciences and Engineering Research Council of Canada (NSERC) Alliance grant, project ALLRP 597619 – 24.

Declaration of Competing Interest

The authors declare that they have no known competing financial interests or personal relationships that could have appeared to influence the work reported in this paper. The author Abbas Taheri is a Guest Editor for Deep Resources Engineering and was not involved in the editorial review or the decision to publish this article.

References

[1] Z.T. Bieniawski, Engineering Rock Mass Classifications: A Complete Manual for Engineers and Geologists in Mining, Civil, and Petroleum Engineering, John Wiley & Sons, 1989.
[2] E. Hoek, E.T. Brown, Empirical strength criterion for rock masses, J. Geotech. Eng. Div. 106 (9) (1980) 1013–1035.
[3] A. Palmstrøm, Characterizing rock masses by the RMi for use in practical rock engineering: Part 1: the development of the rock mass index (RMi), Tunn. Undergr. Space Technol. 11 (2) (1996) 175–188.
[4] M. Sari, Determination of representative elementary volume (REV) for jointed rock masses exhibiting scale-dependent behavior: A numerical investigation, Int. J. GeoEng. 12 (1) (2021) 34.
[5] P. Egger, Engineering problems caused by the anisotropic behaviour of the rock mass. in Mechanical Behavior of Anisotropic Solids/Comportment Méchanique des Solides Anisotropes: Proceedings of the Euromech Colloquium 115 Villard-de-Lans, June 19–22, 1979/Colloque Euromech 115 Villard-de-Lans, 19–22 juin 1979, Springer, 1982, pp. 887–900.
[6] B. Amadei, Importance of anisotropy when estimating and measuring in situ stresses in rock, in: International journal of rock mechanics and mining sciences & geomechanics abstracts, 33, Elsevier, 1996, pp. 293–325.
[7] N. Barton, E. Quadros, Anisotropy is everywhere, to see, to measure, and to model, Rock Mech. Rock Eng. 48 (4) (2015) 1323–1339.
[8] S.M. Abbas, H. Konietzky, Rock mass classification systems, Introd. Geomech. 9 (2017) 1–48.
[9] G.H. Erharter, P.J. Unterlaß, N. Radončić, et al., Challenges and Opportunities of Data Driven Advance Classification of Hard Rock TBMs, 2024.
[10] J. Taboada, L. Alejano, F. Bastante, et al., Total exploitation of an ornamental granite quarry, Mater. De. ConstrucciÓN. 55 (279) (2005) 67–78.
[11] M. Rettighieri, J. Triclot, E. Mathieu, et al., Difficulties associated with high convergences during excavation of the saint martin la porte access adit, Proc. Int. Congr. (2008) 395–404.
[12] R. Bewick, P. Kaiser, Influence of rock mass anisotropy on tunnel stability, Proceedings of the 3rd CANUS Rock Mechanics Symposium, 1 (2009).
[13] C. Zhang, X.-T. Feng, H. Zhou, Estimation of in situ stress along deep tunnels buried in complex geological conditions, Int. J. Rock Mech. Min. Sci. 52 (2012) 139–162.
[14] P. Sha, F. Wu, Q. Guo, Anisotropic deformation in muzhailing railway tunnel, gansu, China. ISRM SINOROCK, ISRM, 2013.
[15] D.-P. Xu, X.-T. Feng, D.-F. Chen, et al., Constitutive representation and damage degree index for the layered rock mass excavation response in underground openings, Tunn. Undergr. Space Technol. 64 (2017) 133–145.
[16] C. Saroglou, S. Qi, S. Guo, et al., ARMR, a new classification system for the rating of anisotropic rock masses, Bull. Eng. Geol. Environ. 78 (2019) 3611–3626.
[17] M. Sandy, G. Sharrock, J. Albrecht, et al., Managing the transition from low stress to high stress conditions. Proceedings Second Australasian Ground Control in Mining Conference, 2010, pp. 23–24.
[18] M. Nasseri, K. Rao, T. Ramamurthy, Anisotropic strength and deformational behavior of himalayan schists, Int. J. Rock Mech. Min. Sci. 40 (1) (2003) 3–23.
[19] S. Wang, S. Sloan, C. Tang, et al., Numerical simulation of the failure mechanism of circular tunnels in transversely isotropic rock masses, Tunn. Undergr. Space Technol. 32 (2012) 231–244.
[20] Y.M. Tien, M.C. Kuo, C.H. Juang, An experimental investigation of the failure mechanism of simulated transversely isotropic rocks, Int. J. Rock Mech. Min. Sci. 43 (8) (2006) 1163–1181.
[21] Y.-F. Chen, K. Wei, W. Liu, et al., Experimental characterization and micromechanical modelling of anisotropic slates, Rock Mech. Rock Eng. 49 (2016) 3541–3557.
[22] P. Sha, S.Y. Gao, Y.W. Zhao, et al., Anisotropic failure in foliated rock tunnels: Comparison between deformational behavior and confined pressure, in: IOP Conference Series: Earth and Environmental Science, IOP Publishing, 2020 052018.
[23] F. Oka, S. Kimoto, H. Kobayashi, et al., Anisotropic behavior of soft sedimentary rock and a constitutive model, Soils Found. 42 (5) (2002) 59–70.
[24] Y. Togashi, M. Kikumoto, K. Tani, An experimental method to determine the elastic properties of transversely isotropic rocks by a single triaxial test, Rock Mech. Rock Eng. 50 (2017) 1–15.
[25] T.-H. Yang, W.-H. Shi, P.-T. Wang, et al., Numerical simulation on slope stability analysis considering anisotropic properties of layered fractured rocks: A case study, Arab. J. Geosci. 8 (2015) 5413–5421.
[26] Y. Jin, J.B. Yuan, B. Hou, et al., Analysis of the vertical borehole stability in anisotropic rock formations, J. Pet. Explor. Prod. Technol. 2 (2012) 197–207.
[27] E.Z. Latjai, Structural model tests to investigate fracture propagation in discontinuous rocks, Atl. Geol. 2 (4) (1966) 168–170.
[28] H. Wagner, Deep mining: A rock engineering challenge, Rock Mech. Rock Eng. 52 (2019) 1417–1446.
[29] W. Ortlepp, T. Stacey, Rockburst mechanisms in tunnels and shafts, Tunn. Undergr. Space Technol. 9 (1) (1994) 59–65.
[30] G. Firdaus, M. Prasad, J. Behura, A novel anisotropy template for an improved interpretation of elastic anisotropy data, Sci. Rep. 13 (1) (2023) 16160.
[31] C.M. Sayers, Simplified anisotropy parameters for transversely isotropic sedimentary rocks, Geophysics 60 (6) (1995) 1933–1935.
[32] B.H. Brady, E.T. Brown, Rock mechanics: For underground mining, Springer science & business media, 2006.
[33] A. Palmstrom, RMi-a rock mass characterization system for rock engineering purposes. na, 1995.
[34] E. Hoek, Structurally controlled instability in underground excavations. in ARMA US Rock Mechanics/Geomechanics Symposium, ARMA, 1977 pp. ARMA-77-0362.
[35] S.D. Priest, Discontinuity analysis for rock engineering, Springer Science & Business Media, 1993.

[36] H.I. Chaminé, M.J. Afonso, L. Ramos, et al., Scanline sampling techniques for rock engineering surveys: Insights from intrinsic geologic variability and uncertainty. Engineering geology for society and territory-volume 6: applied geology for major engineering projects, Springer, 2015, pp. 357–361.
[37] M. Heap. "Columnar jointed lavas at Antuco volcano." ⟨https://x.com/LDR_Strasbourg/status/1866100537202184463⟩ (accessed.
[38] C. Estrada. "Metamorphic Rocks." ⟨https://open.maricopa.edu/hazards/chapter/3-5-metamorphic-rocks/⟩ (accessed 2025).
[39] A. Jacobsen. "Folded rock beds - Durdle Door." ⟨https://www.flickr.com/photos/30139221⟩@N04/3115772346/ (accessed.
[40] Y. Luo, H. Xie, L. Ren, et al., Linear elastic fracture mechanics characterization of an anisotropic shale, Sci. Rep. 8 (1) (2018) 8505.
[41] W. Ernst, Petrochemical study of regional/contact metamorphism in metaclastic strata of the central White-Inyo range, eastern california, Geol. Soc. Am. Bull. 108 (12) (1996) 1528–1548.
[42] S. Haldar, J. Tišljar, Metamorphic rocks, Introd. Mineral. Petrol. (2014) 269–289.
[43] A.S. Stepanov, A review of the geochemical changes occurring during metamorphic devolatilization of metasedimentary rocks, Chem. Geol. 568 (2021) 120080.
[44] K.E. Ashton, A.D. Leclair, Foliate: A useful term to complement the textural classification of foliated metamorphic rocks, Can. J. Earth Sci. 27 (8) (1990) 1095–1097.
[45] C.W. Passchier, R.A. Trouw, Microtectonics, Springer Science & Business Media, 2005.
[46] B.E. Hobbs, W.D. Means, P.F. Williams, An outline of structural geology (1976).
[47] C. Wilson, I.A. Bell, Deformation of biotite and muscovite: Optical microstructure, Tectonophysics 58 (1-2) (1979) 179–200.
[48] R. Vernon, V. Williams, W. D'arcy, Grain-size reduction and foliation development in a deformed granitoid batholith, Tectonophysics 92 (1-3) (1983) 123–145.
[49] L.B. Goodwin, H.-R. Wenk, Intracrystalline folding and cataclasis in biotite of the santa rosa mylonite zone: HVEM and TEM observations, Tectonophysics 172 (3-4) (1990) 201–214.
[50] Y. Kanaori, S.-I. Kawakami, K. Yairi, Microstructure of deformed biotite defining foliation in cataclasite zones in granite, central Japan, J. Struct. Geol. 13 (7) (1991) 777–785.
[51] V. Kusbach, M. Machek, Z. Roxerová, et al., Localization effect on AMS fabric revealed by microstructural evidence across small-scale shear zone in marble, Sci. Rep. 9 (1) (2019) 17483.
[52] M.H. Bagheripour, R. Rahgozar, H. Pashnesaz, et al., A complement to Hoek-Brown failure criterion for strength prediction in anisotropic rock, Geomech. Eng. 3 (1) (2011) 61–81.
[53] H.-R. Wenk, R. Yu, V. Cárdenes, et al., Fabric and anisotropy of slates: From classical studies to new results, J. Struct. Geol. 138 (2020) 104066.
[54] S. Álvarez Arias, J. Gómez Barreiro, I. Palomeras, et al., Quantitative texture analysis of slates: An insight into slate's elastic properties and their contribution to the understanding of seismic wave reflections in anisotropic materials, 2022.
[55] B. Deline, R. Harris, K. Tefend, Laboratory Manual for Introductory Geology, University System of Georgia, University Press of North Georgia, 2015.
[56] C. Van Hise, Deformation of rocks.: III. Cleavage and fissility, J. Geol. 4 (4) (1896) 449–483.
[57] R. Ajalloeian, G.R. Lashkaripour, Strength anisotropies in mudrocks, Bull. Eng. Geol. Environ. 59 (2000) 195–199.
[58] R. Ewy, Mechanical Anisotropy of Gas Shales and Claystones, in: Fourth EAGE Shale Workshop, 2014, European Association of Geoscientists & Engineers, 2014, pp. 1–5.
[59] H. Jia, S. Ding, F. Zi, et al., Development of anisotropy in sandstone subjected to repeated frost action, Rock Mech. Rock Eng. 54 (2021) 1863–1874.
[60] S. Horne, A statistical review of mudrock elastic anisotropy, Geophys. Prospect. 61 (4) (2013) 817–826.
[61] M. Garagon, T. Çan, Predicting the strength anisotropy in uniaxial compression of some laminated sandstones using multivariate regression analysis, Mater. Struct. 43 (4) (2010) 509–517.
[62] X. Zhang, J. Yang, B. Liu, Experimental Study on Anisotropic Strength Properties of Sandstone. ISRM SINOROCK, ISRM, 2009.
[63] B.E. Hornby, L.M. Schwartz, J.A. Hudson, Anisotropic effective-medium modeling of the elastic properties of shales, Geophysics 59 (10) (1994) 1570–1583.
[64] H. Saroglou, Engineering behaviour of anisotropic and heterogeneous layered rocks, Proc. Iaeg Conf. Glob. View Eng. Geol. Environ. (2013) 721–731.
[65] A. Taheri, K. Tani, Use of down-hole triaxial apparatus to estimate the mechanical properties of heterogeneous mudstone, Int. J. Rock Mech. Min. Sci. 45 (8) (2008) 1390–1402.
[66] S. Valcke, M. Casey, G. Lloyd, et al., Lattice preferred orientation and seismic anisotropy in sedimentary rocks, Geophys. J. Int. 166 (2) (2006) 652–666.
[67] Y. Matsukura, K. Hashizume, C. Oguchi, Effect of microstructure and weathering on the strength anisotropy of porous rhyolite, Eng. Geol. 63 (1-2) (2002) 39–47.
[68] E. Wahlstrom, Tunneling in rock, Elsevier, 2012.
[69] R. Hargraves, D. Johnson, C. Chan, Distribution anisotropy: The cause of AMS in igneous rocks? Geophys. Res. Lett. 18 (12) (1991) 2193–2196.
[70] N. Ndari, S. Bijaksana, B. Nurhandoko, et al., Measurements combination of elastic anisotropy and anisotropy of magnetic susceptibility on case study in igneous rock of lava flow type from ijen volcanic complex, east java, in: in IOP Conference Series: Earth and Environmental Science, IOP Publishing, 2019 012017.
[71] N. Zamani, G.W. Heij, E.C. Ferré, et al., High-Velocity slip and thermal decomposition of carbonates: Example from the heart mountain slide ultracataclasites, Wyoming, p. e2022JB026185, J. Geophys. Res. Solid Earth 128 (5) (2023). p. e2022JB026185.
[72] F. a S. Nasseri, Mahdi, "ONKALO POSE Experiment - Integrated Analyses of True-Triaxial Tests," 2019. [Online]. Available: ⟨https://www.researchgate.net/publication/335452944_ONKALO_POSE_Experiment_-Integrated_Analyses_of_True-Trixial_Tests⟩.
[73] S.-C. Hu, Y.-L. Tan, H. Zhou, et al., Impact of bedding planes on mechanical properties of sandstone, Rock Mech. Rock Eng. 50 (2017) 2243–2251.
[74] J. Petit, Criteria for the sense of movement on fault surfaces in brittle rocks, J. Struct. Geol. 9 (5-6) (1987) 597–608.
[75] S. Sun, H. Sun, Y. Wang, et al., Effect of the combination characteristics of rock structural plane on the stability of a rock-mass slope, Bull. Eng. Geol. Environ. 73 (2014) 987–995.
[76] C. Ambrosi, G.B. Crosta, Valley shape influence on deformation mechanisms of rock slopes, Geol. Soc. Lond. Spec. Publ. 351 (1) (2011) 215–233.
[77] P. Gattinoni, M. Consonni, V. Francani, et al., Tunnelling in landslide areas connected to deep seated gravitational deformations: An example in central Alps (Northern Italy), Tunn. Undergr. Space Technol. 93 (2019) 103100.
[78] F. Huang, C.Z. Wu, P.P. Ni, et al., Experimental analysis of progressive failure behavior of rock tunnel with a fault zone using non-contact DIC technique, Int. J. Rock Mech. Min. Sci. 132 (2020) 104355.
[79] K. Willis, G.A. Houseman, L. Evans, et al., Strain localization by shear heating and the development of lithospheric shear zones, Tectonophysics 764 (2019) 62–76.
[80] E. Honea, A.M. Johnson, A theory of concentric, kink and sinusoidal folding and of monoclinal flexuring of compressible, elastic multilayers: IV. Development of sinusoidal and kink folds in multilayers confined by rigid boundaries, Tectonophysics 30 (3-4) (1976) 197–239.
[81] P.J. Hudleston, L. Lan, Information from fold shapes, J. Struct. Geol. 15 (3-5) (1993) 253–264.
[82] J.L. Roberts, The formation of similar folds by inhomogeneous plastic strain, with reference to the fourth phase of deformation affecting the dalradian rocks in the southwest highlands of scotland, J. Geol. 74 (6) (1966) 831–855.
[83] H.-B. Mühlhaus, F. Dufour, L. Moresi, et al., A director theory for visco-elastic folding instabilities in multilayered rock, Int. J. Solids Struct. 39 (13-14) (2002) 3675–3691.
[84] R. Smith, Unified theory of the onset of folding, boudinage, and mullion structure, Geol. Soc. Am. Bull. 86 (11) (1975) 1601–1609.
[85] M. Ghaedi Ghalini, M. Bahaaddini, M. Amiri Hossaini, Estimation of in-situ block size distribution in jointed rock masses using combined photogrammetry and discrete fracture network, J. Min. Environ. 13 (1) (2022) 175–184.
[86] P. Lu, J.-P. Latham, Developments in the assessment of in-situ block size distributions of rock masses, Rock Mech. Rock Eng. 32 (1999) 29–49.
[87] M. Elmouttie, G. Poropat, A method to estimate in situ block size distribution, Rock Mech. Rock Eng. 45 (3) (2012) 401–407.
[88] W.R. Dearman, Engineering Geological Mapping, Elsevier, 2013.
[89] A. Vakili, J. Albrecht, M. Sandy, Rock strength anisotropy and its importance in underground geotechnical design, Proc. AusRock (2014) 167–180.
[90] T. Li, C. Ma, M. Zhu, et al., Geomechanical types and mechanical analyses of rockbursts, Eng. Geol. 222 (2017) 72–83.
[91] C.F. Lee, S.J. Wang, Z.F. Yang, Geotechnical aspects of rock tunnelling in China, Tunn. Undergr. Space Technol. 11 (4) (1996) 445–454.
[92] C. Zhang, X.-T. Feng, H. Zhou, et al., Case histories of four extremely intense rockbursts in deep tunnels, Rock Mech. Rock Eng. 45 (2012) 275–288.
[93] G. Khanlari, B. Rafiei, Y. Abdilor, An experimental investigation of the Brazilian tensile strength and failure patterns of laminated sandstones, Rock Mech. Rock Eng. 48 (2015) 843–852.
[94] D. Fereidooni, G.R. Khanlari, M. Heidari, et al., Assessment of inherent anisotropy and confining pressure influences on mechanical behavior of anisotropic foliated rocks under triaxial compression, Rock Mech. Rock Eng. 49 (2016) 2155–2163.
[95] Q. Zhang, Hydromechanical modeling of solid deformation and fluid flow in the transversely isotropic fissured rocks, Comput. Geotech. 128 (2020) 103812.
[96] H. Moomivand, H. Moomivand, R. Nikrouz, et al., Development of a new empirical relation to assess P-wave velocity anisotropy of rocks, Geotech. Geol. Eng. 40 (2022) 1537–1550.
[97] X. Tan, H. Konietzky, T. Frühwirt, et al., Brazilian tests on transversely isotropic rocks: Laboratory testing and numerical simulations, Rock Mech. Rock Eng. 48 (2015) 1341–1351.
[98] P. Wang, T. Yang, J. Zhou, Slope failure analysis considering anisotropic characteristics of foliated rock masses, Arab. J. Geosci. 11 (2018) 1–15.
[99] M. Ju, J. Li, J. Li, et al., Loading rate effects on anisotropy and crack propagation of weak bedding plane-rich rocks, Eng. Fract. Mech. 230 (2020) 106983.
[100] S. Aswad, D.E. Wahyuwibowo, N.F. Qaidahiyani, et al., Study on influence of joint orientation on rock engineering properties for mining and infrastructure design, in: IOP Conference Series: Earth and Environmental Science, IOP Publishing, 2020 012001.
[101] Z. Bieniawski, Determining rock mass deformability: Experience from case histories, in: International journal of rock mechanics and mining sciences & geomechanics abstracts, 15, Elsevier, 1978, pp. 237–247.

[102] H. Kim, J.-W. Cho, I. Song, et al., Anisotropy of elastic moduli, P-wave velocities, and thermal conductivities of Asan Gneiss, Boryeong Shale, and Yeoncheon Schist in Korea, Eng. Geol. 147 (2012) 68–77.
[103] G.R. Khanlari, M. Heidari, A.-A. Sepahi-Gero, et al., Determination of geotechnical properties of anisotropic rocks using some index tests, Geotech. Test. J. 37 (2) (2014) 242–254.
[104] S. Zhong, S.-Y. Zuo, L. Mao, et al., Mechanism of anisotropic characteristics of layered limestone and a constitutive model for different bedding angles based on a Brazilian tensile test, Arab. J. Geosci. 13 (2020) 1–9.
[105] C. Jaeger, Rock mechanics and engineering, Cambridge University Press, 1979.
[106] T. Ramamurthy, G.V. Rao, J. Singh, A strength criterion for anisotropic rocks. in Fifth Australia-New Zealand Conference on Geomechanics: Prediction Versus Performance; Preprints of Papers, Institution of Engineers, Australia Barton, ACT, 1988, pp. 253–257.
[107] F. Donath, Strength variation and deformational behavior in anisotropic rock, State Stress Earth's. Crust 281 (1964).
[108] E. Hock, Brittle failure of rock. Rock Mechanics in Engineering Practice, Wiley, *New York, NY*, 1968, pp. 97–124.
[109] E. Deklotz, J. Brown, O. Stemler, Anisotropy of a schistose gneiss. in ISRM Congress, ISRM, 1966 pp. ISRM-1CONGRESS-1966-079.
[110] F.G. Horino, M.L. Ellickson, A method for estimating strength of rock containing planes of weakness. US Department of Interior, Bureau of Mines, 1970.
[111] K. Akai, The failure surface of isotropic and anisotropic rocks under multiaxial stresses, Jour. Soc. Mater. Sci. Jpn. 20 (1971) 122–128.
[112] D. Allirot, Evaluation of mechanical properties of a stratified rock under confining pressure, Proc. 4th Cong. ISRM Montreux 1 (1979) 15–22.
[113] C. Pomeroy, D. Hobbs, A. Mahmoud, The effect of weakness-plane orientation on the fracture of barnsley hards by triaxial compression, Int. J. Rock Mech. Min. Sci. Geomech. Abstr. 8 (1971) 227–238.
[114] M. Behrestaghi, K.S. Rao, T. Ramamurthy, Engineering geological and geotechnical responses of schistose rocks from dam project areas in India, Eng. Geol. 44 (1-4) (1996) 183–201.
[115] H. Saroglou, P. Marinos, G. Tsiambaos, The anisotropic nature of selected metamorphic rocks from Greece, J. South. Afr. Inst. Min. Metall. 104 (4) (2004) 217–222.
[116] K. Goshtasbi, M. Ahmadi, J. Seyedi, Anisotropic strength behaviour of slates in the Sirjan-Sanadaj zone, J. South. Afr. Inst. Min. Metall. 106 (1) (2006) 71–75.
[117] D. Li, L.N.Y. Wong, G. Liu, et al., Influence of water content and anisotropy on the strength and deformability of low porosity meta-sedimentary rocks under triaxial compression, Eng. Geol. 126 (2012) 46–66.
[118] H. Song, Y. Jiang, D. Elsworth, et al., Scale effects and strength anisotropy in coal, Int. J. Coal Geol. 195 (2018) 37–46.
[119] J.L. Pinto, Deformability of schistous rocks. ISRM Congress, ISRM, 1970 pp. ISRM-2CONGRESS-1970-067.
[120] S. Read, N. Perrin, I. Brown, Measurement and analysis of laboratory strength and deformability characteristics of schistose rock. Isrm Congress, ISRM, 1987 pp. ISRM-6CONGRESS-1987-043.
[121] M. Kwaśniewski, H. Nguyen, Experimental studies on anisotropy of time-dependent behaviour of bedded rocks. Proceedings of the International Symposium on Engineering in Complex Rock Formations, Elsevier, 1988, pp. 325–337.
[122] O. Saeidi, V. Rasouli, R.G. Vaneghi, et al., A modified failure criterion for transversely isotropic rocks, Geosci. Front. 5 (2) (2014) 215–225.
[123] H. Saroglou, G. Tsiambaos, A modified Hoek–Brown failure criterion for anisotropic intact rock, Int. J. Rock Mech. Min. Sci. 45 (2) (2008) 223–234.
[124] X.-P. Zhang, L.N.Y. Wong, S.-J. Wang, et al., Engineering properties of quartz mica schist, Eng. Geol. 121 (3-4) (2011) 135–149.
[125] F.A. Villalobos, P.A. Rodríguez, M. Vera, Study of the anisotropic elastic response of a foliated phyllite, Proc. Inst. Civ. Eng. Geotech. Eng. 175 (5) (2022) 539–548.
[126] R. Berenbaum, I. Brodie, The tensile strength of coal, J. Inst. Fuel 32 (222) (1959) 320–326.
[127] P. Chamberlain, E. Van Eeckhout, E. Podnieks, Four factors influencing observed rock properties. Soil Specimen Preparation for Laboratory Testing, ASTM International, 1976.
[128] G. Barla, N. Innaurato, Indirect tensile testing of anisotropic rocks, Rock Mech. 5 (1973) 215–230.
[129] N.D.J. Simpson, An analysis of tensile strength, fracture initiation and propagation in anisotropic rock (gas shale) using Brazilian tests equipped with high speed video and acoustic emission, Institutt for petroleumsteknologi og anvendt geofysikk, 2013.
[130] S. Mighani, C. Sondergeld, C. Rai, Observations of tensile fracturing of anisotropic rocks. Society of petroleum engineers, SPE J 21 (4) (2016) 1289–1301.
[131] T. Ma, N. Peng, Z. Zhu, et al., Brazilian tensile strength of anisotropic rocks: Review and new insights, Energies 11 (2) (2018) 304.
[132] J. Kundu, B. Mahanta, K. Sarkar, et al., The effect of lineation on anisotropy in dry and saturated himalayan schistose rock under Brazilian test conditions, Rock Mech. Rock Eng. 51 (2018) 5–21.
[133] A. Alencar, M. Muñiz-Menéndez, I. Pérez-Rey, et al., An experimental study of tensile stress and deformation in an anisotropic rock, in: IOP Conference Series: Earth and Environmental Science, IOP Publishing, 2024 012010.
[134] Y. Abdi, Investigation of the strength behavior and failure modes of layered sedimentary rocks under Brazilian test conditions, Int. J. GeoEng. 15 (1) (2024), https://doi.org/10.1186/s40703-024-00208-2.
[135] A. Tavallali, A. Vervoort, Effect of layer orientation on the failure of layered sandstone under Brazilian test conditions, Int. J. Rock Mech. Min. Sci. 47 (2) (2010) 313–322.
[136] S. Liu, S. Chen, F. Yu, et al., Anisotropic properties study of chlorite schist, Rock Soil Mech. 33 (12) (2012) 3616–3623.
[137] C.-S. Chen, E. Pan, B. Amadei, Determination of deformability and tensile strength of anisotropic rock using Brazilian tests, Int. J. Rock Mech. Min. Sci. 35 (1) (1998) 43–61.
[138] M. Cai, P. Kaiser, Numerical simulation of the Brazilian test and the tensile strength of anisotropic rocks and rocks with pre-existing cracks, Int. J. Rock Mech. Min. Sci. 41 (2004) 478–483.
[139] A. Vervoort, K.-B. Min, H. Konietzky, et al., Failure of transversely isotropic rock under Brazilian test conditions, Int. J. Rock Mech. Min. Sci. 70 (2014) 343–352.
[140] A. Ghazvinian, R.G. Vaneghi, M. Hadei, et al., Shear behavior of inherently anisotropic rocks, Int. J. Rock Mech. Min. Sci. 61 (2013) 96–110.
[141] P. Wang, F. Ren, S. Miao, et al., Evaluation of the anisotropy and directionality of a jointed rock mass under numerical direct shear tests, Eng. Geol. 225 (2017) 29–41.
[142] P. Liu, Q.S. Liu, P.H. Deng, et al., Anisotropic shearing mechanism of kangding slate: Experimental investigation and numerical analysis, J. Rock Mech. Geotech. Eng. 16 (5) (2024) 1487–1504.
[143] Z. Zheng, Z.P. Ma, J.H. Qi, et al., Multi-directional disturbance effect of shear mechanical behaviors and fracturing mechanisms of rockmass intermittent structural plane under true triaxial shear test, Int. J. Min. Sci. Technol. 35 (6) (2025) 933–960.
[144] Z. Zheng, R.H. Li, H. Zheng, et al., Static-disturbance shear properties and failure mechanisms of karst limestone under different hydrochemical corrosions, Eng. Geol. 353 (2025) 108124.
[145] Y.-K. Lee, S. Pietruszczak, Application of critical plane approach to the prediction of strength anisotropy in transversely isotropic rock masses, Int. J. Rock Mech. Min. Sci. 45 (4) (2008) 513–523.
[146] N. Bar, C. Saroglou, The ARMR classification system and the modified Hoek-Brown failure criterion compared to directional shear strength models for anisotropic rock masses, Period. Polytech. Civ. Eng. 64 (1) (2020) 14–19.
[147] S.-F. Guo, S.-W. Qi, C. Saroglou, A-BQ, a classification system for anisotropic rock mass based on China national standard, J. Cent. South Univ. 27 (10) (2020) 3090–3102.
[148] E. Skretting, G.H. Erharter, J.K.Y. Chiu, Virtual reality based uncertainty assessment of rock mass characterization of tunnel faces. ISRM Congress, ISRM, 2023 pp. ISRM-15CONGRESS-2023-149.
[149] N. Bar, L. Borgatti, D. Donati, et al., Classification of natural and engineered rock slopes using UAV photogrammetry for assessing stability. ISRM EUROCK, ISRM, 2021 pp. ISRM-EUROCK-2021-042.
[150] K. Terzaghi, Theor. Soil Mech. (1943).
[151] H. Lauffer, Classification for tunnel construction, Geol. und Bauwes. 24 (1) (1958) 46–51.
[152] D. Deere, The rock quality designation (RQD) index in practice. in Rock classification systems for engineering purposes, ASTM International, 1988.
[153] H. Tanaka, Introduction of Geology for Civil Engineers, Sankaidou, Japan, 1964.
[154] I. Hansagi, Numerical determination of mechanical properties of rock and of rock masses, Int. J. Rock Mech. Min. Sci. Geomech. Abstr. 2 (1965) 219–223.
[155] G.E. Wickham, H.R. Tiedemann, E.H. Skinner, Support determinations based on geologic predictions, N. Am. Rapid Excav. Tunn. Conf. Proc. 1 (1972).
[156] Z. Bieniawski, Engineering classification of jointed rock masses, Civ. Eng. = Siviele Ing. 1973 (12) (1973) 335–343.
[157] N. Barton, R. Lien, J. Lunde, Engineering classification of rock masses for the design of tunnel support, Rock Mech. 6 (1974) 189–236.
[158] J. Jakubec, D.H. Laubscher, The MRMR rock mass rating classification system in mining practice. Proceedings of the 3rd international conference and exhibition on mass mining, Brisbane, Australia, 2000, pp. 413–421.
[159] D. Laubscher, Geomechanics classification of jointed rock masses: Mining applications, Inst. Min. Metall. Trans. Sect. A 86 (1977).
[160] P. Pells, D. Douglas, B. Rodway, et al., Des. Load. Found. shale sandstone Syd. Reg. (1978).
[161] M. Selby, A rock mass strength classification for geomorphic purpose: with tests from Antarctica and New Zealand, Zeit Geomorph. NF 24 (1980) 31–51.
[162] M. Romana, New adjustment ratings for application of bieniawski classification to slopes. Proceedings of the international symposium on role of rock mechanics, Zacatecas, Mexico, 1985, pp. 49–53.
[163] E.C. Robertson, Thermal properties of rocks, US Geol. Surv. (1988) 2331. -1258.
[164] Y. Chan, K. Ho, W. Pun, A new marble rock mass classification system for the interpretation of karst morphology in Hong Kong, HKIE Trans. 1 (2) (1994) 1–12.
[165] R. Goel, J. Jethwa, A. Paithankar, Indian experiences with q and RMR systems, Tunn. Undergr. Space Technol. 10 (1) (1995) 97–109.
[166] C. Mark, G. Molinda, Evaluating roof control in underground coal mines with the coal mine roof rating, Int. J. Rock Mech. Min. Sci. Geomech. Abstr. 8 (32) (1995) 417A.

[167] Z. Chen, Recent Developments in Slope Stability Analysis. ISRM Congress, ISRM, 1995 pp. ISRM-8CONGRESS-1995-196.
[168] A. Palmström, B. Strömme, The rock mass index (RMÐ applied in rock mechanics and rock engineering, J. Rock Mech. Tunn. Technol. 11 (1996) 1–40.
[169] E. Unal, Modified rock mass classification: M-RMR system, Milest. Rock Eng. (1996).
[170] E. Hoek, E.T. Brown, Practical estimates of rock mass strength, Int. J. Rock Mech. Min. Sci. 34 (8) (1997) 1165–1186.
[171] Y. Lin, An introduction of the Chinese standard for engineering classification of rock masses (GB50218-94), Adv. Rock Mech. (1998) 317–327.
[172] B.T. Benumof, G.B. Griggs, The dependence of seacliff erosion rates on cliff material properties and physical processes: San Diego county, California, Shore Beach 67 (4) (1999) 29–41.
[173] R. Hack, An evaluation of slope stability classification. ISRM EUROCK, ISRM, 2002 pp. ISRM-EUROCK-2002-001.
[174] D. Walker, I. De Bruyn, Geotechnical blockiness index: A systematic geotechnical mapping method for underground and open pit mines. Proceedings of the 7th Australia–New Zealand Young Geotechnical Professionals Conference, Australian Geomechanics Society, Sydney, 2006.
[175] R. Tomás, J. Delgado, J.B. Serón, Modification of slope mass rating (SMR) by continuous functions, Int. J. Rock Mech. Min. Sci. 44 (7) (2007) 1062–1069.
[176] A. Taheri, K. Tani, Assessment of the stability of rock slopes by the slope stability rating classification system, Rock Mech. Rock Eng. 43 (2010) 321–333.
[177] Ö. Aydan, R. Ulusay, N. Tokashiki, A new rock mass quality rating system: Rock mass quality rating (RMQR) and its application to the estimation of geomechanical characteristics of rock masses, Rock Mech. Rock Eng. 47 (2014) 1255–1276.
[178] N. Barton, N. Bar, Introducing the Q-slope method and its intended use within civil and mining engineering projects. ISRM EUROCK, ISRM, 2015 pp. ISRM-EUROCK-2015-026.
[179] A. McQuillan, I. Canbulat, D. Payne, et al., New risk assessment methodology for coal mine excavated slopes, Int. J. Min. Sci. Technol. 28 (4) (2018) 583–592.
[180] H. Bineshian, I-System: Index of Ground-Structure; a comprehensive indexing system for Ground-Structure behaviour; classification and characterization, JOEG XLIV (2019) 73–109.
[181] V. Maazallahi, A. Majdi, Directional rock mass rating (DRMR) for anisotropic rock mass characterization, Bull. Eng. Geol. Environ. 80 (2021) 4471–4499.
[182] M. Rezaei, S. Latifi, Development of a new empirical relation between RMR and Q rock mass classification systems, Iran. J. Eng. Geol. 12 (2) (2018) 100–103.
[183] Y. Chang, L. Chang, F. Ren, Strength anisotropy of jointed rock slope considering mining damage: A numerical analysis method, Geomat. Nat. Hazards Risk 11 (1) (2020) 2587–2614.
[184] V. Marinos, P. Marinos, E. Hoek, The geological strength index: Applications and limitations, Bull. Eng. Geol. Environ. 64 (2005) 55–65.
[185] K.-S. Kang, N.-L. Hu, C.-S. Sin, et al., Determination of the mechanical parameters of rock mass based on a GSI system and displacement back analysis, J. Geophys. Eng. 14 (4) (2017) 939–948.
[186] H. Sonmez, R. Ulusay, Modifications to the geological strength index (GSI) and their applicability to stability of slopes, Int. J. Rock Mech. Min. Sci. 36 (6) (1999) 743–760.
[187] G.L. Morelli, Variability of the GSI index estimated from different quantitative methods, Geotech. Geol. Eng. 33 (4) (2015) 983–995.
[188] B.-H. Kim, R. Peterson, T. Katsaga, et al., Estimation of rock block size distribution for determination of geological strength index (GSI) using discrete fracture networks (DFNs), Min. Technol. 124 (3) (2015) 203–211.
[189] S. Narimani, S.M. Davarpanah, N. Bar, et al., Geological strength index relationships with the Q-System and Q-Slope, Sustainability 15 (14) (2023) 11233.
[190] B. Yang, D. Elmo, Why engineers should not attempt to quantify GSI, Geosciences 12 (11) (2022) 417.
[191] E. Hoek, E. Brown, The Hoek–Brown failure criterion and GSI–2018 edition, J. Rock Mech. Geotech. Eng. 11 (3) (2019) 445–463.
[192] S. Hussian, N. Mohammad, Z.U. Rehman, et al., Review of the geological strength index (GSI) as an empirical classification and rock mass property estimation tool: Origination, modifications, applications, and limitations, Adv. Civ. Eng. 2020 (1) (2020) 6471837.
[193] J. Shen, Z. Shu, M. Cai, et al., A shear strength model for anisotropic blocky rock masses with persistent joints, Int. J. Rock Mech. Min. Sci. 134 (2020) 104430.
[194] J. Ambrose , Failure of anisotropic shales under triaxial stress conditions, 2014.
[195] Q. Qin, K. Li, M. Li, et al., An anisotropic failure criterion for jointed rocks under triaxial stress conditions, Rock Mech. Rock Eng. 57 (2024) 1–18.
[196] M. Singh, N.K. Samadhiya, A. Kumar, et al., A nonlinear criterion for triaxial strength of inherently anisotropic rocks, Rock Mech. Rock Eng. 48 (2015) 1387–1405.
[197] M. Asadi, M.H. Bagheripour, Modified criteria for sliding and non-sliding failure of anisotropic jointed rocks, Int. J. Rock Mech. Min. Sci. 73 (2015) 95–101.
[198] J. Tunsakul, P. Jongpradist, W. Kongkitkul, et al., Investigation of failure behavior of continuous rock mass around cavern under high internal pressure, Tunn. Undergr. Space Technol. 34 (2013) 110–123.
[199] S. Pietruszczak, Z. Mroz, On failure criteria for anisotropic cohesive-frictional materials, Int. J. Numer. Anal. Methods Geomech. 25 (5) (2001) 509–524.
[200] E. Mammoliti, F. Di Stefano, D. Fronzi, et al., A machine learning approach to extract rock mass discontinuity orientation and spacing, from laser scanner point clouds, Remote Sens. 14 (10) (2022) 2365.
[201] X. Shi, X. Yang, Y. Meng, et al., Modified Hoek–Brown failure criterion for anisotropic rocks, Environ. Earth Sci. 75 (2016) 1–11.
[202] L. Zhang, F.J. Niu, M.H. Liu, et al., Fracture characteristics and anisotropic strength criterion of bedded sandstone, Front. Earth Sci. 10 (2022) 879332.
[203] R.V. Mises, Mechanik der plastischen Formänderung von kristallen, ZAMM-J. Appl. Math. Mech. Z. F. üR. Angew. Math. und Mech. 8 (3) (1928) 161–185.
[204] R. Hill, A theory of the yielding and plastic flow of anisotropic metals, Proc. R. Soc. Lond. Ser. A. Math. Phys. Sci. 193 (1033) (1948) 281–297.
[205] W. Olszak, W. Urbanowski, The plastic potential and the generalized distortion energy in the theory of non-homogeneous anisotropic elastic-plastic bodies, Arch. Mech. Stos. 8 (4) (1956) 671–694.
[206] S.A.F. Murrell, The effect of triaxial stress systems on the strength of rocks at atmospheric temperatures, Geophys. J. Int. 10 (3) (1965) 231–281.
[207] I. Goldenblat, V. Kopnov, A generalized theory of plastic flow of anisotropic metals, Stroit. Mekhanika 307 (1966) 319.
[208] J. Boehler, A. Sawczuk, On yielding of oriented solids, Acta Mech. 27 (1) (1977) 185–204.
[209] S.W. Tsai, E.M. Wu, A general theory of strength for anisotropic materials, J. Compos. Mater. 5 (1) (1971) 58–80.
[210] W.G. Pariseau, Plasticity theory for anisotropic rocks and soil. ARMA US Rock Mechanics/Geomechanics Symposium, ARMA, 1968 pp. ARMA-68-0267.
[211] Y. Dafalias, Issues on the constitutive formulation at large elastoplastic deformations, part 1: Kinematics, Acta Mech. 69 (1) (1987) 119–138.
[212] R. Nova, G. Sacchi, A generalized failure condition for orthotropic solids. in Mechanical Behavior of Anisotropic Solids/Comportment Méchanique des Solides Anisotropes: Proceedings of the Euromech Colloquium 115 Villard-de-Lans, June 19–22, 1979/Colloque Euromech 115 Villard-de-Lans, 19–22 juin 1979, Springer, 1979, pp. 623–641.
[213] R. Nova, The failure of transversely isotropic rocks in triaxial compression, Int. J. Rock Mech. Min. Sci. Geomech. Abstr. 17 (1980) 325–332.
[214] J. Boehler, J. Raclin, Ecrouissage anisotrope des matériaux orthotropes prédéformés, 1982.
[215] O. Cazacu, N. Cristescu, A paraboloid failure surface for transversely isotropic materials, Mech. Mater. 31 (6) (1999) 381–393.
[216] Z. Mróz, J. Maciejewski, Critical plane approach to analysis of failure criteria for anisotropic geomaterials. Bifurcations, instabilities and degradations in geomaterials, Springer, 2011, pp. 69–89.
[217] A. Casagrande, Shear failure of anisotropic materials, Proc. Boston Soc. Civ. Engrs 31 (1944) 74–87.
[218] J. Jaeger, Shear failure of anistropic rocks, Geol. Mag. 97 (1) (1960) 65–72.
[219] R. McLamore, K. Gray, The mechanical behavior of anisotropic sedimentary rocks, (1967).
[220] M.B. Smith, J.B. Cheatham Jr, An anisotropic compacting yield condition applied to porous limestone, Int. J. Rock Mech. Min. Sci. Geomech. Abstr. 17 (1980) 159–165.
[221] H.A. Ashour, A compressive strength criterion for anisotropic rock materials, Can. Geotech. J. 25 (2) (1988) 233–237.
[222] D.-Q. Zhou, X.-S. Liu, L. Qi, Strength criteria anisotropic rocks and experimental studies, (1992).
[223] S. Singh, Relationship among fatigue strength, mean grain size and compressive strength of a rock, Rock Mech. Rock Eng. 21 (4) (1988) 271–276.
[224] Y.M. Tien, M.C. Kuo, A failure criterion for transversely isotropic rocks, Int. J. Rock Mech. Min. Sci. 38 (3) (2001) 399–412.
[225] R.P. Tiwari, K. Rao, Response of an anisotropic rock mass under polyaxial stress state, J. Mater. Civ. Eng. 19 (5) (2007) 393–403.
[226] L. Zhang, H. Zhu, Three-dimensional Hoek-Brown strength criterion for rocks, J. Geotech. Geoenviron. Eng. 133 (9) (2007) 1128–1135.
[227] Y.-K. Lee, S. Pietruszczak, B.-H. Choi, Failure criteria for rocks based on smooth approximations to Mohr–Coulomb and Hoek–Brown failure functions, Int. J. Rock Mech. Min. Sci. 56 (2012) 146–160.
[228] Jaeger, Shear failure of transversely isotropic rock, Geol. Mag. 97 (1960) 65–72.
[229] J. Walsh, W. Brace, A fracture criterion for brittle anisotropic rock, J. Geophys. Res. 69 (16) (1964) 3449–3456.
[230] C. Smith, M. Gilbert, Application of discontinuity layout optimization to plane plasticity problems, Proc. R. Soc. A Math. Phys. Eng. Sci. 463 (2086) (2007) 2461–2484.
[231] T. Backers, Applications of fracture mechanics numerical modelling in rock engineering, First Break 28 (3) (2010), https://doi.org/10.3997/1365-2397.2010008.
[232] R. Pramanik, D. Deb, SPH procedures for modeling multiple intersecting discontinuities in geomaterial, Int. J. Numer. Anal. Methods Geomech. 39 (4) (2015) 343–367.
[233] J. Pei, H.H. Einstein, A.J. Whittle, The normal stress space and its application to constructing a new failure criterion for cross-anisotropic geomaterials, Int. J. Rock Mech. Min. Sci. 106 (2018) 364–373.
[234] M. Pouragha, R. Wan, M. Eghbalian, Critical plane analysis for interpreting experimental results on anisotropic rocks, Acta Geotech. 14 (2019) 1215–1225.
[235] P.-Z. Pan, F. Yan, X.-T. Feng, et al., Modeling of an excavation-induced rock fracturing process from continuity to discontinuity, Eng. Anal. Bound. Elem. 106 (2019) 286–299.
[236] J.-C. Zhang, S.-H. Zhou, Z.-N. Lin, et al., Using the Pietruszczak-Mroz anisotropic failure criterion to model the strength of stratified rocks, Int. J. Rock Mech. Min. Sci. 130 (2020) 104312.
[237] E. Hoek, Fracture of anisotropic rock, J. South. Afr. Inst. Min. Metall. 64 (10) (1964) 501–518.
[238] E. Hoek, Strength of jointed rock masses, Geotechnique 33 (3) (1983) 187–223.
[239] B. Ladanyi, G. Archambault, Evaluation of shear strength of a jointed rock mass. Proceedings of the 24th International Geological Congress, 1972, pp. 249–270.

[240] Z.T. Bieniawski, Estimating the strength of rock materials, J. South. Afr. Inst. Min. Metall. 74 (8) (1974) 312–320.
[241] R. Yoshinaka, T. Yamabe, A strength criterion of rocks and rock masses. in ISRM International Symposium, ISRM, 1981 pp. ISRM-IS-1981-099.
[242] A. Ghosh, J.J. Daemen, Fractal characteristics of rock discontinuities, Eng. Geol. 34 (1-2) (1993) 1–9.
[243] B. Gong, S. Wang, S.W. Sloan, et al., Modelling rock failure with a novel continuous to discontinuous method, Rock Mech. Rock Eng. 52 (2019) 3183–3195.
[244] P. Fortsakis, K. Nikas, V. Marinos, et al., Anisotropic behaviour of stratified rock masses in tunnelling, Eng. Geol. 141 (2012) 74–83.
[245] M. Diederichs, P. Kaiser, Stability of large excavations in laminated hard rock masses: The voussoir analogue revisited, Int. J. Rock Mech. Min. Sci. 36 (1) (1999) 97–117.
[246] D. Bakun-Mazor, Y.H. Hatzor, W.S. Dershowitz, Modeling mechanical layering effects on stability of underground openings in jointed sedimentary rocks, Int. J. Rock Mech. Min. Sci. 46 (2) (2009) 262–271.
[247] C. Martin, P. Kaiser, D. McCreath, Hoek-Brown parameters for predicting the depth of brittle failure around tunnels, Can. Geotech. J. 36 (1) (1999) 136–151.
[248] T.M. Vu, J. Sulem, D. Subrin, et al., Semi-analytical solution for stresses and displacements in a tunnel excavated in transversely isotropic formation with non-linear behavior, Rock Mech. Rock Eng. 46 (2013) 213–229.
[249] O.P. Vitali, T.B. Celestino, A. Bobet, Analytical solution for a deep circular tunnel in anisotropic ground and anisotropic geostatic stresses, Rock Mech. Rock Eng. 53 (2020) 3859–3884.
[250] Z. Zhang, Y. Sun, Analytical solution for a deep tunnel with arbitrary cross section in a transversely isotropic rock mass, Int. J. Rock Mech. Min. Sci. 48 (8) (2011) 1359–1363.
[251] H. Tran Manh, J. Sulem, D. Subrin, et al., Anisotropic time-dependent modeling of tunnel excavation in squeezing ground, Rock Mech. Rock Eng. 48 (2015) 2301–2317.
[252] H. Tran Manh, J. Sulem, D. Subrin, A closed-form solution for tunnels with arbitrary cross section excavated in elastic anisotropic ground, Rock Mech. Rock Eng. 48 (2015) 277–288.
[253] A. Bobet, Lined circular tunnels in elastic transversely anisotropic rock at depth, Rock Mech. Rock Eng. 44 (2011) 149–167.
[254] Z. Chen, C. He, G. Xu, et al., Supporting mechanism and mechanical behavior of a double primary support method for tunnels in broken phyllite under high geo-stress: A case study, Bull. Eng. Geol. Environ. 78 (2019) 5253–5267.
[255] R.P. Bewick, Effects of anisotropic rock mass characteristics on excavation stability, Masters Abstr. Int. 47 (3) (2008).
[256] P. Małkowski, The impact of the physical model selection and rock mass stratification on the results of numerical calculations of the state of rock mass deformation around the roadways, Tunn. Undergr. Space Technol. 50 (2015) 365–375.
[257] P. Yadav, S. Sharan, Numerical investigation of squeezing in underground hard rock mines, Rock Mech. Rock Eng. 52 (2019) 1211–1229.
[258] B. Sainsbury, D. Sainsbury, Practical use of the ubiquitous-joint constitutive model for the simulation of anisotropic rock masses, Rock Mech. Rock Eng. 50 (2017) 1507–1528.
[259] E. Karatela, A. Taheri, Three-dimensional hydro-mechanical model of borehole in fractured rock mass using discrete element method, J. Nat. Gas. Sci. Eng. 53 (2018) 263–275.
[260] Z. Zheng, S.X. Li, Q. Zhang, et al., True triaxial test and DEM simulation of rock mechanical behaviors, meso-cracking mechanism and precursor subject to underground excavation disturbance, Eng. Geol. 337 (2024) 107567.
[261] A. Li, N. Xu, F. Dai, et al., Stability analysis and failure mechanism of the steeply inclined bedded rock masses surrounding a large underground opening, Tunn. Undergr. Space Technol. 77 (2018) 45–58.
[262] A. Li, F. Dai, N. Xu, et al., Analysis of a complex flexural toppling failure of large underground caverns in layered rock masses, Rock Mech. Rock Eng. 52 (2019) 3157–3181.
[263] F. Gao, D. Stead, H. Kang, Numerical simulation of squeezing failure in a coal mine roadway due to mining-induced stresses, Rock Mech. Rock Eng. 48 (2015) 1635–1645.
[264] K. Duan, C. Kwok, Evolution of stress-induced borehole breakout in inherently anisotropic rock: Insights from discrete element modeling, J. Geophys. Res. Solid Earth 121 (4) (2016) 2361–2381.
[265] X. Liu, Y. Deng, B. Zou, Implementation of a constitutive model for anisotropic rocks based on modified lade failure criterion, Sci. Rep. 13 (1) (2023) 3210.
[266] M. Saadat, A. Taheri, A cohesive discrete element based approach to characterizing the shear behavior of cohesive soil and clay-infilled rock joints, Comput. Geotech. 114 (2019) 103109.
[267] Z. Zheng, H. Tang, Q. Zhang, et al., True triaxial test and PFC3D-GBM simulation study on mechanical properties and fracture evolution mechanisms of rock under high stresses, Comput. Geotech. 154 (2023) 105136.
[268] Y. Jiang, B. Li, Y. Yamashita, Simulation of cracking near a large underground cavern in a discontinuous rock mass using the expanded distinct element method, Int. J. Rock Mech. Min. Sci. 46 (1) (2009) 97–106.
[269] M. Tsesarsky, Y.H. Hatzor, Tunnel roof deflection in blocky rock masses as a function of joint spacing and friction–a parametric study using discontinuous deformation analysis (DDA), Tunn. Undergr. Space Technol. 21 (1) (2006) 29–45.
[270] P. Jia, C. Tang, Numerical study on failure mechanism of tunnel in jointed rock mass, Tunn. Undergr. Space Technol. 23 (5) (2008) 500–507.
[271] A. Lisjak, B.S. Tatone, G. Grasselli, et al., Numerical modelling of the anisotropic mechanical behaviour of opalinus clay at the laboratory-scale using fem/dem, Rock Mech. Rock Eng. 47 (2014) 187–206.
[272] A. Lisjak, D. Figi, G. Grasselli, Fracture development around deep underground excavations: Insights from FDEM modelling, J. Rock Mech. Geotech. Eng. 6 (6) (2014) 493–505.
[273] A. Lisjak, B.S.A. Tatone, O.K. Mahabadi, et al., Hybrid finite-discrete element simulation of the EDZ formation and mechanical sealing process around a microtunnel in opalinus clay, Rock Mech. Rock Eng. 49 (2016) 1849–1873.
[274] J. Coggan, F. Gao, D. Stead, et al., Numerical modelling of the effects of weak immediate roof lithology on coal mine roadway stability, Int. J. Coal Geol. 90 (2012) 100–109.
[275] K. Kim, J. Rutqvist, J. Birkholzer, Lattice modeling of excavation damage in argillaceous clay formations: Influence of deformation and strength anisotropy, Tunn. Undergr. Space Technol. 98 (2020) 103196.
[276] B. Karimi-Khajelangi, M. Noorian-Bidgoli, Numerical study of the effect of rock anisotropy on stresses around an opening located in the fractured rock mass, J. Pet. Sci. Eng. 208 (2022) 109593.
[277] M.N. Bidgoli, L. Jing, Anisotropy of strength and deformability of fractured rocks, J. Rock Mech. Geotech. Eng. 6 (2) (2014) 156–164.
[278] Z. Sun, D. Zhang, A. Li, et al., Model test and numerical analysis for the face failure mechanism of large cross-section tunnels under different ground conditions, Tunn. Undergr. Space Technol. 130 (2022) 104735.
[279] G. Armand, F. Leveau, C. Nussbaum, et al., Geometry and properties of the excavation-induced fractures at the Meuse/Haute-Marne URL drifts, Rock Mech. Rock Eng. 47 (1) (2014) 21–41.
[280] Ø. Dammyr, Prediction of brittle failure for TBM tunnels in anisotropic rock: a case study from Northern Norway, Rock Mech. Rock Eng. 49 (2016) 2131–2153.
[281] J. Ha, B.S. Tatone, G.M. Gaspari, et al., Simulating tunnel support integrity using FEM and FDEM based on laboratory test data, Tunn. Undergr. Space Technol. 111 (2021) 103848.
[282] A. Lisjak, G. Grasselli, T. Vietor, Continuum–discontinuum analysis of failure mechanisms around unsupported circular excavations in anisotropic clay shales, Int. J. Rock Mech. Min. Sci. 65 (2014) 96–115.
[283] W. Wang, Q. Liu, H. Ma, et al., Numerical analysis of material modeling rock reinforcement in 2D FDEM and parameter study, Comput. Geotech. 126 (2020) 103767.
[284] P. Deng, Q. Liu, X. Huang, et al., FDEM numerical modeling of failure mechanisms of anisotropic rock masses around deep tunnels, Comput. Geotech. 142 (2022) 104535.
[285] L. Jing, O. Stephansson, Fundamentals of Discrete Element Methods for Rock Engineering: Theory and Applications, Elsevier, 2007.
[286] N. Moussaei, M. Sharifzadeh, K. Sahriar, et al., A new classification of failure mechanisms at tunnels in stratified rock masses through physical and numerical modeling, Tunn. Undergr. Space Technol. 91 (2019) 103017.
[287] L.R. Alejano, J. Taboada, F. García-Bastante, et al., Multi-approach back-analysis of a roof bed collapse in a mining room excavated in stratified rock, Int. J. Rock Mech. Min. Sci. 45 (6) (2008) 899–913.
[288] E. Karampinos, J. Hadjigeorgiou, J. Hazzard, et al., Discrete element modelling of the buckling phenomenon in deep hard rock mines, Int. J. Rock Mech. Min. Sci. 80 (2015) 346–356.
[289] P. Deng, Q. Liu, X. Huang, et al., Sensitivity analysis of fracture energies for the combined finite-discrete element method (FDEM), Eng. Fract. Mech. 251 (2021) 107793.
[290] L. Bouzeran, M. Pierce, P. Andrieux, et al., Accounting for rock mass heterogeneity and buckling mechanisms in the study of excavation performance in foliated ground at westwood mine. Deep Mining 2019: Proceedings of the Ninth International Conference on Deep and High Stress Mining, The Southern African Institute of Mining and Metallurgy, 2019, pp. 29–44.
[291] G. Sharrock, B. Chapula, Anisotropic rock mass behaviour in high-displacement ground at CSA mine, J. South. Afr. Inst. Min. Metall. 120 (1) (2020) 57–66.
[292] A.G. Milnes, J. Hudson, L. Wikström, et al., Foliation: Geological background, rock mechanics significance, and preliminary investigations at olkiluoto, Posiva Oy (2006).
[293] C. Moulding, R. Stephenson, B. Barsanti, et al., Managing the onset of accelerated deformation in capital development at agnew gold mine. Deep Mining 2017: Proceedings of the Eighth International Conference on Deep and High Stress Mining, Australian Centre for Geomechanics, 2017, pp. 937–948.

[294] M. Bester, T. Stacey, T. Russell, Synthetic rock mass modelling and geotechnical mapping: An open pit mine case study in anisotropic rock, Int. J. Min. Reclam. Environ. 35 (5) (2021) 356–378.
[295] P.P. Cacciari, M.M. Futai, The influence of fresh and weathered rock foliation on the stability of the monte seco tunnel, Rock Mech. Rock Eng. 54 (2021) 537–558.
[296] T.H. Yang, P.T. Wang, T. Xu, et al., Anisotropic characteristics of jointed rock mass: A case study at Shirengou iron ore mine in China, Tunn. Undergr. Space Technol. 48 (2015) 129–139.
[297] E. Karampinos, J. Hadjigeorgiou, P. Turcotte, et al., Empirical and numerical investigation on the behaviour of foliated rock masses under high stress conditions. Deep Mining 2014: Proceedings of the Seventh International Conference on Deep and High Stress Mining, Australian Centre for Geomechanics, 2014, pp. 345–361.
[298] M. Pierce, Numerical Modeling of Rock Mass Weakening, Bulking and Softening Associated with Cave Mining. ARMA e-newsletter," ed: ARMA publications committee, spring, 2013.

Abbas Taheri is a Tenured Associate Professor at the Robert M. Buchan Department of Mining at Queen's University in Kingston, Canada, where he holds the Chair in Mine Design. Abbas has over 20 years of industry, research, and teaching experience in geotechnical engineering, rock mechanics, and mining engineering.